Digit formation during embryonic development of bats and mice

Ash Parker

Dissertation presented for the degree:
Master of Science

In the Department:
Molecular and Cell Biology

University of Cape Town

November 2017

Supervisors:
Prof. Nicola Illing and Dr Dorit Hockman

Plagiarism declaration

I, Ash Parker, know the meaning of plagiarism and declare that all of the work in the dissertation, save for that which is properly acknowledged, is my own.

Signed:
Date: 3 November 2017

Dedicated to:

Emma Woodrow

Who loved bats and was so excited about the prospects of my project.

Acknowledgements

I would like to thank my supervisors, Prof. Nicola Illing and Dr. Dorit Hockman, for their guidance, support and input into the work involved in this thesis. I would also like to thank all my current and past lab members in the Evo-devo Lab for their advice, patience, support and entertainment. Special thanks to Rafe Lyall, Dorit Hockman, Stephen Schlebusch and Luke Hannan for general assistance in the field of Bioinformatics. I am also grateful to all those who assisted on bat field trips and made them exceptionally enjoyable. Thanks must also be given to Morea Petersen and Faezah Davids whose help and advice was greatly appreciated in the work involved in this project.

I am grateful to the National Research Fund for awarding me the Scarce Skills scholarship and to RSG McKay of the National Institute of Neurological Disorders kindly donated Ψ2 packaging for cell lines.

I would like to say a big thank you to my mom, who is always supportive and proud of me no matter what I do. Finally, I am so grateful to TJ Nhundu who has put up with long detailed explanations of this project, sat with me over work-filled weekends and nights, helped out on bat field trips and pushed me to do my best.

Table of contents

List of illustrations

Figures:

Tables:

Abbreviations

Acan (gene)	Aggrecan
Autopod	Hand or foot
BMP (gene)	Bone morphogen protein
Bmpr (gene)	BMP receptor
Bp	Base pairs
ChIP-seq	Chromatin immunoprecipitation sequencing
Chondrogenesis	The early stages of endochondral bone formation in which a cartilage template is formed prior to ossification of the bone
Col2a1 (gene)	Collagen 2a1
CS	Carollia stage – a developmental staging system developed by Cretekos et al (2005) on the short-tailed fruit bat, *Carollia perspicillata*.
DAP	Days after plating
E	Embryonic days – a developmental staging system in mouse
Env (gene)	Envelope protein in viruses
evo-devo	Evolutionary development
Fgf8 (gene)	Fibroblast growth factor 8
FL	Forelimb
Gag (gene)	Group Antigens; polyprotein in viruses
Genome + Sox9	The *M natalensis* annotated genome from Eckalbar et al. (2016) with an additional annotation for the Sox9 gene.
H&E	Haematoxylin and eosin
HL	Hind limb
IPA	Ingenuity pathway analysis
LPR (gene)	Lipoprotein receptor-related protein
Meis2 (gene)	Meis homeobox 2
Miniopterus natalensis	Bat species used in this study and Eckalbar et al. (2016)

Miniopterus shreibersii	Bat species used in the RNA-seq by Wang et al. (2014)
MIQE	Minimum Information for Publication of Quantitative Real-Time PCR Experiments
MLV	Murine leukaemia virus
PNA	Peanut agglutinin
Pol (gene)	Reverse transcriptase in viruses
RNA-seq	RNA sequencing
Shh (gene	Sonic hedgehog
Sox (gene family)	Sex-determining region on the Y chromosome
Stylopod	Upper arm or leg
SV40 Tag	Simian virus 40 large T antigen
VSV-G	Vesicular stomatitis Indiana virus - glycoprotein
Wnt (gene family)	Combine gene name for orthologues wingless (*Drosophila*) and Intergration-1 (*Mus*)
Zeugopod	Lower arm or leg

Abstract

The evolution of a strikingly elongated and webbed forelimb (FL) in bats, which contrasts with a small, free-toed hindlimb (HL), has seen extensive research into bat wing development in an effort to determine the molecular mechanism driving limb development. A recent RNA-seq and ChIP-seq study carried out on *Miniopterus natalensis* showed differences in FL and HL activity for several genetic pathways known to be involved in bone formation during key bat development stages CS15-CS17. In this project the prediction made from the literature and the RNA-seq results was that the observed decreased Wnt/β-catenin signalling and increased BMP signalling in the bat FL may lead to elevated levels of *Sox9* expression, and larger fields of mesenchymal condensations. This was tested by annotating *Sox9* in the *M. natalensis* genome to further analyse the expression levels and associated ChIP-seq data. In addition the behaviour of condensing mesenchymal cells during bat and mouse limb development was observed by visualising the various stages of chondrogenesis, using H&E and PNA stains. In addition the RNA-seq study found 3000 genes to be differentially expressed. Thus, the project also set out to create an immortalised bat autopod cell line to facilitate future testing and predictions.

The *Sox9* gene was successfully annotated and revealed to not be differentially expressed between FL and HL as predicted. However, downstream targets of *Sox9* were further inspected as potential ideas for further investigation. The histological stains provided a set of data characterising mesenchymal condensation in both mouse and bat stages, revealing many interesting features such as the non-specific binding behaviours of PNA prior to digit formation. In addition, quantitative results demonstrated the bat FL digits are already longer than the HL digits at CS16. Cell line work established a working protocol for the storage, dissociation and plating of bat primary cells that retain their bat limb expression identity. Mouse cells were successfully immortalised and a cell line was established from a HL digit cell. This project has facilitated further studies in understanding extreme digit elongation in the bat FL autopod during development.

Chapter 1:

Comparative limb development in bats and mice: digit formation

1.1 Introduction

The process of limb development has been used for decades as an exemplar system on which to study organ patterning and the mechanisms of embryonic development (Zuniga 2015, Rodrigues et al. 2017). That is, studying limb development provides an understanding of how a ball of undifferentiated embryonic cells undergoes the necessary changes to produce a complex individual made up of cell systems that carry out extremely different functions. The advantage of limb development studies is that this external organ is able to endure genetic manipulation and malformation without fatal harm to the embryo under study. An extension of this work is that these studies have allowed insight into the evolutionary differences during development that have led to the large phenotypic diversity seen across tetrapod limbs (Zuniga 2015).

The generic tetrapod limb consists of the stylopod (upper arm or leg), zeugopod (lower arm or leg) and autopod (hand or foot) (Figure 1.1 A). Due to varying evolutionary pressures, these elements – typically the autopod – vary in length or shape to aid animals in locomotion, among other activities, in their different environments (Mariani and Martin 2003, Hall 2008) (Figure 1.1 B). For example the fusion and enlargement in the zeugopod of the mole improving digging abilities (Bickelmann et al. 2012) and the relative enlargement of the autopod and robustness of the two proximal elements in the whale to produce a fin for swimming (Bejder and Hall 2002) (Figure 1.1 B). Development of these limb elements has been extensively studied in mice and chicken embryos (reviewed in Petit et al. (2017)). However, to further our understanding of limb diversity and gain insight into the molecular mechanisms that lead to adaptation of limbs, research needs to focus on limb development of other morphologically diverse species.

A relatively recent field of work, evolutionary development biology, or 'evo-devo', does just that. In this field researchers study the embryological development of a non-model organism in light of what is known in model organisms, such as mouse or chick (Heffer and Pick 2013). This allows researchers to pin point molecular development changes that have led to the adapted phenotype or function in the non-model species. These studies are possible due to a

number of important factors. For one there is evidence to suggest vertebrates possess a developmental genetic toolkit (Carroll 2008, Zeller et al. 2009). This is a highly conserved collection of genes that control development, the majority of which are transcription factors involved in regulating expression of genes coding for body structure (Carroll 2008). Among the most important toolkit genes is the *Hox* cluster, transcription factors which play an important role in segmentation and body plan, for example specifying from where on the body limbs will grow and then the patterning of the stylopod, zeugopod and autopod within the limb (Carroll 2008).

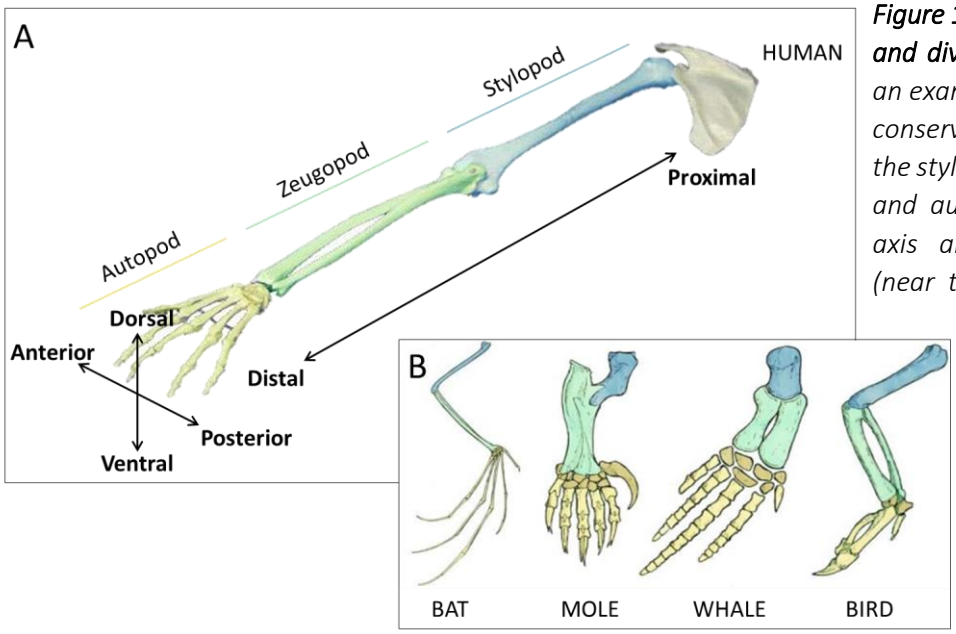

Figure 1.1: Tetrapod limb morphology and diversity. A: The human arm as an example of the basic layout of the conserved tetrapod limb containing the stylopod (blue), zeugopod (green) and autopod (yellow). The relevant axis are displayed with proximal (near to the body), distal away from the body), anterior (thumb –side of the limb), posterior (pinky-side of the limb), ventral (palm side of the hand) and dorsal (top of the hand). B: The morphological variation seen in these three elements across tetrapods.

Initially it was thought that morphological difference arose due to non-synonymous changes in the coding sequence of homologous development genes, affecting which amino acid is coded for and potentially the function of a protein (King and Wilson 1975). However in 1975 a study tried to correlate the phylogenetic genetic distance in coding regions between chimpanzees and humans to the phenotypic differences and found that when looking at coding regions alone, the genetic distances were too small to account for the vast organismal differences (King and Wilson 1975). Currently it is suggested that it is alterations in the regulatory regions, DNA sequences that bind enhancers, activators or repressors, that control the expression of these conserved toolkit genes and ultimately lead to phenotypic variation (Myers 2007). Specifically, changes in the temporal and spatial expression of the conserved

genes during development allow these genes to perform new or additional functions, thus facilitating the ability of organisms to adapt to diverse environments (Carroll 2008, Lories et al. 2013).

Limb diversification can thus be studied via an evo-devo approach by looking at the expression patterns of well-known development genes in a phenotypically extreme limb. Based on knowledge gained from a 'normal' limb, usually belonging to a model organism, researchers can gain insight into what molecular mechanisms may be causing the extreme phenotype. Bats are useful candidates for such studies (Cretekos et al. 2001). These mammals have evolved a highly adapted forelimb (FL) autopod that has undergone elongation in digits II to V and retained the webbing between these digits (Figure 1.2 A). This is in contrast to the bat hindlimb (HL) autopod which possess five free toes of equal length (Figure 1.2 B) and is more similar in proportion to the limbs of mice. Mouse digits however are not all equal in length with digit I and V being smaller on both autopods and in addition the autopod is slightly elongated in the

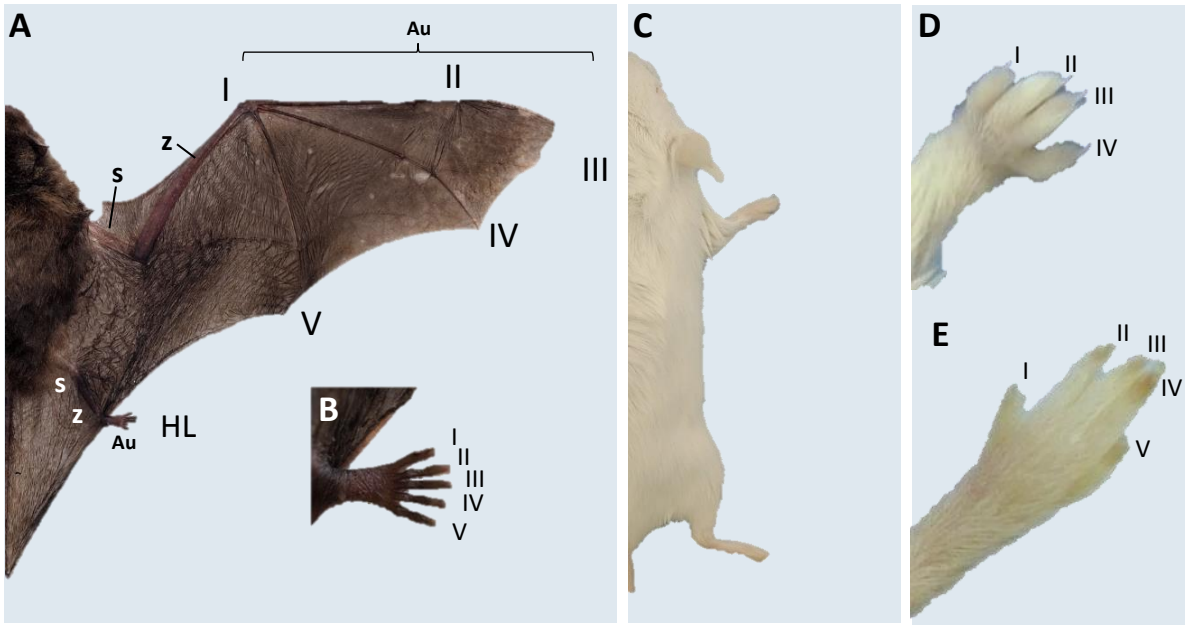

Figure 1.2: Limb anatomy of the Natal long-fingered bat (Miniopterus natalensis*) and mouse (*Mus musculus*). **A**: Dorsal view of a female adult* M. natalensis *illustrating the size and morphological differences between the forelimb (FL) and the hindlimb (HL). The stylopod (S), zeugopod (Z) and autopod (Au) are all longer in the FL. The most exaggerated difference is seen in the autopods with drastic elongation of the FL digits (II-V) connected by an interdigital membrane (webbing). Digit I (thumb) of the FL is not connected to webbing and is similar in length to the five short digits in the HL. **B**: Dorsal close-up of the HL indicating the five free digits of equal length. **C:** Dorsal view of adult* M. musculus *to show the similarity in size between FL and HL. **D** & **E**: a close up of* M. musculus *FL (D) in which digit V is hidden and HL (E) to show similarity in digit length between the autopods as well as to the HL of* M. natalensis *(B). Images are not to scale. Bat images were taken by Dorit Hockman.*

HL compared to FL (Figure 1.2 C, D & E). The bat HL provides the researcher with a biological evolutionary 'control' with which to compare molecular mechanisms responsible for the adaptions in the FL (Cretekos et al. 2001, Eckalbar et al. 2016). Comparing the ontogeny of bat limbs to that of the mouse can provide insight into the modifications that were necessary for the evolution of powered flight in the ancestral bat (Hockman et al. 2009).

1.2 Comparison of mouse and bat limb development

A detailed comparison of mouse and bat limb development can be found in Hockman et al. (2009). However a brief overview of key differences will be discussed. The initial stages of limb formation are uniform across tetrapod species. The FL bud appears first in both mice and bats at equivalent stages E9.5 and Carollia Stage (CS) 12 (not shown), respectively, with the HL lagging a stage behind, emerging at E10 and CS13 respectively (Hockman et al. 2009) (Figure 1.3 B & D). The limbs start as a bulge of undifferentiated mesenchymal cells on either side of the embryo which then expands. At CS14 the bat FL begins to differ from that of the mouse at the equivalent stage, E11.5, with the wing membranes on the FL autopod becoming evident (Figure 1.3 E & G). While the mouse FL autopod begins to expand symmetrically at E12.5 (Figure 1.3 K), the bat FL expands asymmetrically along the anterior-posterior axis, with greater expansion on the posterior edge visible at CS15 (Figure 1.3 I). The bat and mouse HL are asymmetrical domes at CS14 and E11.5 respectively, with slight elongation on the posterior side (Figure 1.3 F & H). By CS15 however the bat HL has formed a smooth-edged symmetrical paddle shape (Figure 1.3 J) while the equivalent stage mouse HL has slight scalloping on the edges of the paddle (Figure 1.3 L) (Hockman et al. 2009).

At stage CS16 the bat FL thumb becomes easily distinguished from the rest of the digits as interdigital tissue between the thumb and digit II begins to recede (Figure 1.3 M). Digit formation is also apparent in both CS16 bat and E13 mouse FL as the tissue is thicker dorso-ventrally in regions containing precursor digits (Figure 1.3 M & O). The bat HL at this stage expands in an anterior-posterior direction, which is not seen in the equivalent mouse HL (Figure 1.3 N & P). The smoothness of the HL edge is lost as slight scalloping is seen where the interdigital tissue begins to recede (Figure 1.3 N). This is more apparent in the mouse HL at this stage (Figure 1.3 P). In both mouse E13.5 limbs and the bat CS17 HL interdigital regression has progressed substantially while this is not seen in the bat CS17 FL, with exception to the tissue separating digit I and II (Figure 1.3 Q, R, S & T). The retained webbing in the CS17 bat FL appears

to be thinner than the digit regions and slightly scalloped. Digits II-IV in the bat have clear joints where digits are bent, causing the bat FL to form a cup shape (Figure 1.3 Q). The bat HL digits are noticeably all equal in length compared to the mouse HL. In the mouse HL digits II-IV are longer than I and V (Figure 1.3 R & T) (Hockman et al. 2009).

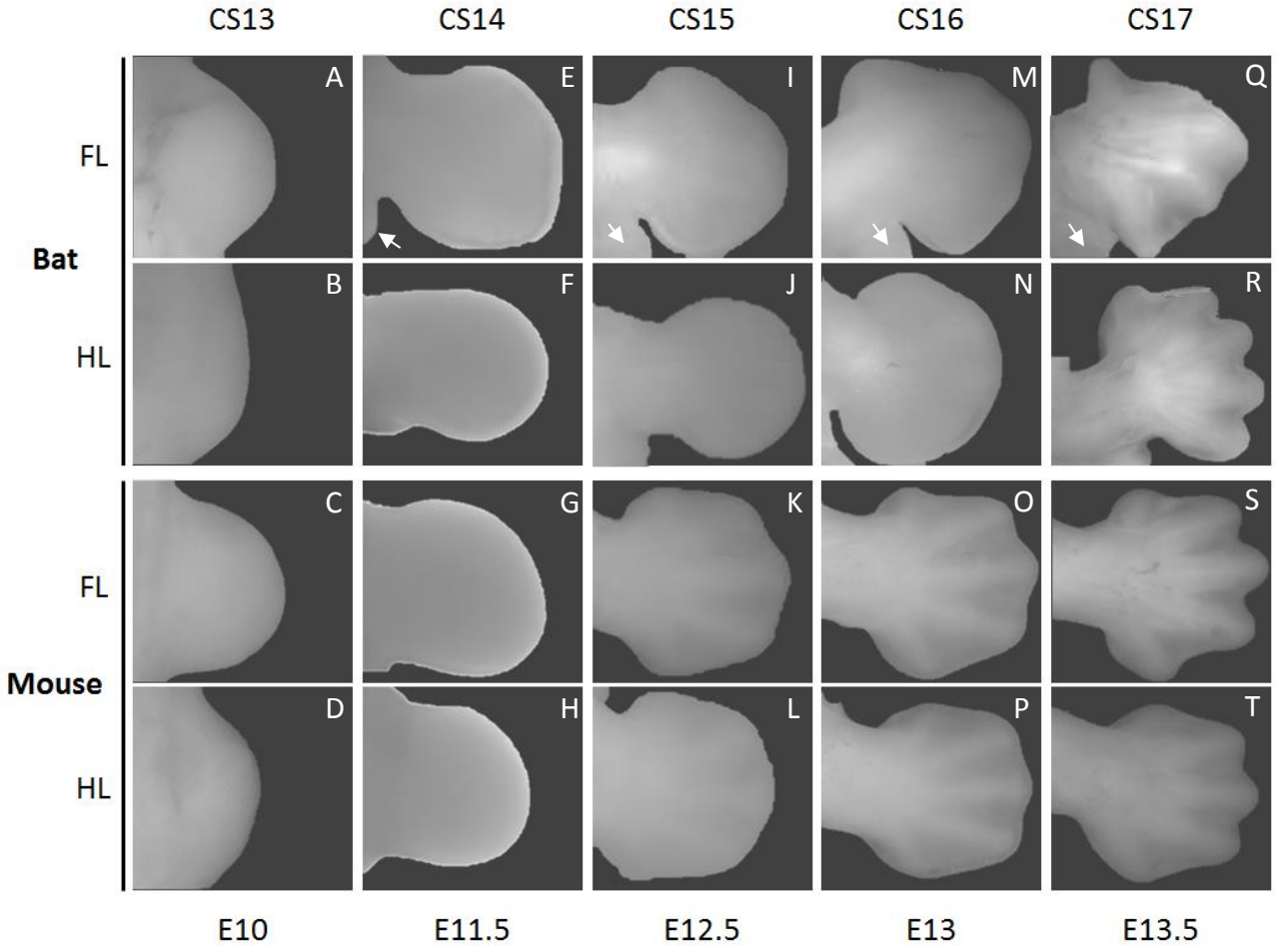

Figure 1.3: The progression of limb development in M. natalensis ***embryos (CS13 to CS17) compared to equivalently staged mouse embryos (E10 to E13.5).*** *A, E, I, M and Q:* M. natalensis *forelimbs. White arrow indicates developing wing membrane between FL autopod and HL. B, F, J, N and R:* M. natalensis *hindlimbs. C, G, K, O and S: Mouse forelimbs. D, H, L, P and T: Mouse hindlimbs. The embryonic day (E) of mouse development is indicated along the bottom, while the stage of bat development (CS) based on Hockman et al. (2009) and Cretekos et al. (2005) is indicated along the top. All panels show the dorsal surface of the limb with anterior toward top and proximal at left, views are not to scale. Images were compiled and adapted from Hockman et al. (2009) and Mason (2016).*

The uniquely elongated digits and retained interdigital webbing in the bat FL can already be seen at these early stages of development. This project will focus specifically on the evolutionary development of these elongated digits. In order to compare digit formation

between bats and mice it is important to understand the process of endochondral bone formation, a process which leads to the formation most skeletal elements in tetrapods.

1.3 Tetrapod digit formation

Wrists, ankles and digits are the elements that distinguish the tetrapod limb from the ancestral fin (Shubin et al. 2006). These elements are housed in the autopod, which is both temporally last to form and the most distal of the three elements (Tamura et al. 2008). The limb initially starts out as a protrusion of undifferentiated mesenchymal cells. This protrusion begins to take a paddle-like shape with the formation of the stylopod and zeugopod making up the shaft of the paddle. The autopod extends in the posterior-anterior direction prior to digit formation, forming what would be the blade of the paddle. Adult digits are made of endochondral bone tissue which means the skeletal template is first established as intermediate cartilage elements, formed during a process called chondrogenesis (Tamura et al. 2008). Chondrogenesis takes place along a multistep pathway involving differentiation and proliferation of cells, the basic steps of which are displayed in Figure 1.4.

In the autopod the first stage of chondrogenesis is marked by condensation of the undifferentiated mesenchymal cells where the digits will form (Figure 1.4 IA - B). This involves uniform mesenchymal cells forming aggregates through cell-cell interactions mediated by adhesion molecules such as N-cadherin and Tenascin-C (Hall and Miyake 2000, Goldring et al. 2006). These aggregated mesenchymal cells then differentiate into immature chondrocytes (Figure 1.4 IC) which proliferate, extending the proximal-distal outgrowth of the digit zone (Akiyama et al. 2002, Goldring et al. 2006). At the centre of the digit zone the proliferating chondrocytes flatten and stack as they differentiate into columnar chondrocytes (Figure 1.4 ID) (Akiyama et al. 2002).

The columnar chondrocytes at the centre of the digit zone further differentiate into hypertrophic chondrocytes, which are larger in size than chondrocytes (Lefebvre and Bhattaram 2016). Subsequently these hypertrophic chondrocytes will apoptose. The gaps left behind by the apoptosed hypertrophic chondrocytes will be replaced by osteoblasts (bone cells) in a zone termed the ossification centre at the middle of the developing digit shaft (Kozhemyakina et al. 2015).

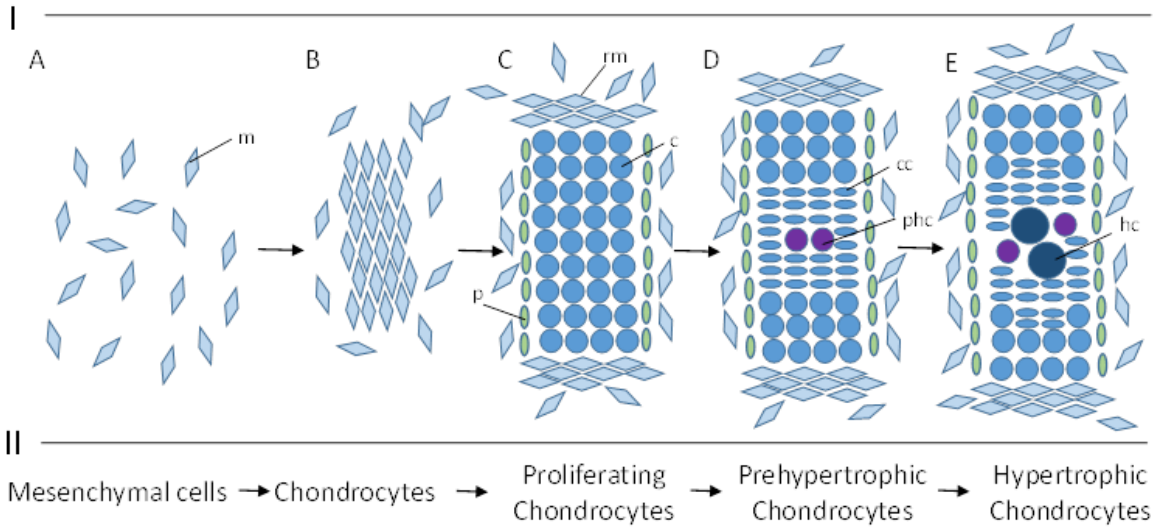

Figure 1.4: The process of chondrogenesis in the limb. *I) Schematic representation of a digit forming* ***A****: The limb bud is made up of undifferentiated mesenchymal cells (m).* ***B****: The first sign of chondrogenesis is the condensation of the mesenchymal cells when bones will later form.* ***C****: The condensed mesenchymal cells differentiate into chondrocytes (c) while mesenchymal cells continue to be recruited at the ends of the shaft (rm). The cells at the boundary of the cartilage template form the perichondrium (p).* ***D:*** *Starting at the centre of the cartilage shaft, chondrocytes proliferate and stack in columns forming the columnar chondrocytes (cc). These proliferating chondrocytes differentiate into pre-hypertrophic chondrocytes (phc).* ***E:*** *Pre-hypertrophic chondrocytes further differentiate into hypertrophic chondrocytes (hc) which will soon apoptose, leaving gaps for osteoblasts to come in and replace the cartilage with bone.* ***II****) The pathway of differentiation from mesenchymal cell to hypertrophic chondrocyte*

Another important group of cells involved in digit development is the perichondrium which surrounds the cartilage template during chondrogenesis (Rooney and Archer 1992) (Figure 1.4 IC). This sheath of cells plays an important role in ensuring longitudinal growth of the digit fields in a proximal-distal direction (Alvarez et al. 2001). The perichondrium is formed from the outer condensed mesenchymal cells that initially remain undifferentiated once columnar chondrocytes appear. These cells also separate the cartilage template from the surrounding mesenchymal cells. This however is not seen on proximal or distal ends of the cartilage shaft. The ends of the shaft are capped with a bulbous end that continues to recruit mesenchymal cells which aggregate (Figure 1.4 IC, D & E) and subsequently follow the same differentiation patterns as previous described, extending the digit zone along the proximal-distal axis (Rooney and Archer 1992, Kronenberg 2003).

Since a large proportion of these studies have been done on mice, a lot is known about the timing of these events in mouse limb development. Bats on the other hand have been studied

less thoroughly. However, with the use of a cartilage staining agent, Alcian blue, some information on chondrogenesis in the later stages of development has been revealed (Steedman 1950). In bats, Alcian blue is absent in the FL and HL autopods until CS16 when the cartilaginous condensations appear (Sears et al. 2006, Hockman et al. 2008). A study reported that the rapid elongation of bat FL digits can only be seen until CS20 (Sears et al. 2006). However more recent studies reveal that pre-ossified bat FL digits II-V are longer than digit I as early as CS16, in contrast to the digits of a stage E12.5 mouse FL, where digits I and V are the shortest and digit III is the longest (Cretekos et al. 2005, Hockman et al. 2008, Sohaskey et al. 2008). It thus appears that the unique patterning for wing development in the bat has already started during the process of digit formation as differences are already seen in the cartilage templates.

It would be interesting to observe if any differences can be seen in the developing bat wing prior to the differentiation of mesenchymal cells into chondrocytes. In order to look at the process of specifying cells as digit or interdigit, a thorough understanding of the genetic factors involved in initiating the cell fates in the autopod needs to be discussed.

1.3.1 *Specifying digit fields*

The partitioning of the mesenchymal cells into a digital and interdigital fate has been hypothesised to be under control of a Turing reaction-diffusion model (Raspopovic et al. 2014). This model explains the interaction of a diffusible activator and inhibitor to form a periodic digit-interdigit pattern along the posterior-anterior plane (Gierer and Meinhardt 1972). Three players have been implicated in this model, namely the BMP pathway, Wnt/β-catenin pathway and a master transcription factor, Sox9 (Raspopovic et al. 2014), all of which I will discuss in detail.

1.3.1.1 BMP Pathway

Bone morphogenic proteins (BMPs) are members of the transforming growth factor (TGF) β superfamily and transduce signals by binding to one of three cell surface receptors: Bmpr1a, Bmpr1b or ActR1. This binding causes phosphorylation of intracellular transcription regulators, Smads, allowing them to translocate into the nucleus, where they regulate gene expression (Shi and Massagué 2003).

Decades of research has revealed that the BMP pathway is essential for regulating mesenchymal condensations (Barna and Niswander 2007) as well as cell differentiation from a mesenchymal cell all the way through to hypertrophic chondrocyte (Roark and Greer 1994). This was demonstrated through conditional gene knockouts and overexpression of the various BMP pathway players at different stages during chondrogenesis, both *in vitro* and *in vivo*. Mis-expression of BMP-2 and -4 can lead to ectopic chondrogenesis (Duprez et al. 1996) while almost all conditional knockouts of the pathway components lead to the absence in expression of chondrogenesis markers *in vitro* and severe chondrodysplasia *in vivo (Kawakami et al. 1996, Yoon et al. 2005, Retting et al. 2009)*. In addition to this, the Smad1 protein has been shown to bind to key transcription factors, Sox6 and Sox5, which are in part responsible for the expression of the key chondrogenic markers such as *Collagen (col) 2a1*, and *Aggrecan* (Nordin and LaBonne 2014).

The initial expression of *Sox9*, the master transcription factor of chondrogenesis, is dependant of the BMP pathway via ligands binding to Bmpr1a and Bmpr1b which are functionally redundant (Yoon et al. 2005). Knockout studies of these cell receptor genes simultaneously reveal a lack of *Sox9* as well as *Sox5* and *Sox6* expression in mesenchymal condensations. These mesenchymal cells do not differentiate into chondrocytes, thus inhibiting further progression of chondrogenesis.

1.3.1.2 Wnt/β-catenin Pathway

Wnt proteins were first described as a murine proto-oncogene called *Intergration-1 (Int1)* in 1982 (Nusse and Varmus 1982). Later it was learnt that *Int1* was an orthologue of a previously discovered gene in *Drosophila*, called *wingless*, which plays a crucial role in segment polarity during embryonic development (Nüsslein-Volhard and Wieschaus 1980, Rijsewijk et al. 1987). This gene is now known to be part of a highly conserved group of signalling ligands known as Wnt, with 19 members found in the genomes of mouse and human (Clevers and Nusse 2012, Lories et al. 2013).

Wnts bind to cell surface receptors and create a signalling cascade via a number of different pathways. The Wnt/β-catenin or canonical Wnt pathway is the best described (Figure 1.5) (Lories et al. 2013). In this pathway, typically a Wnt ligand will bind to a cell surface receptor from the Frizzled (Fzd) family to activate the cascade (reviewed in Kretzschmar and Clevers (2017)). If the Wnt ligand is tethered to an inhibitor of the pathway, such as Secreted frizzled-related protein (sFRP) or Wnt inhibiting factor 1 (WIF-1), the pathway is not activated. In this case, the key mediator of the canonical pathway, β-catenin, will be sequestered into a destruction complex leading to phosphorylation, ubiquitination and proteasomal disintegration within the cytoplasm. However when a Wnt ligand interacts with Fzd, it results in the phosphorylation of a co-receptor, lipoprotein receptor-related protein (LRP) 5/6 which recruits a cytoplasmic protein, Dishevelled (Dsh). Dsh tethers the destruction complex to the membrane bound phosphorylated LPR 5/6, freeing β-catenin which is then able to accumulate and translocate into the nucleus (Li et al. 2012).

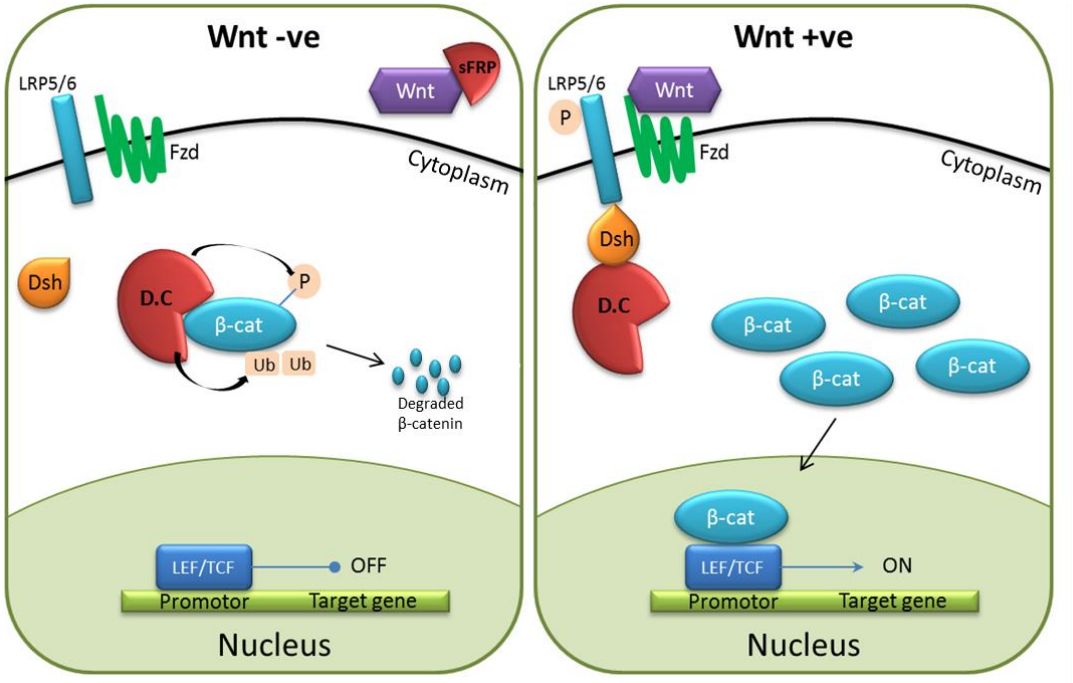

Figure 1.5: Canonical Wnt/β-catenin pathway. *Wnt signalling pathway is shown in the absence of Wnt ("Wnt –ve") and the presence of Wnt ("Wnt +ve"). When Wnt ligands are tethered to an inhibitor such as sFRP, the destruction complex (D.C) phosphorylates and ubiquitinates β-catenin (β-cat), being therefore destroyed by the proteasome before it can enter the nucleus. In this case the DNA-binding proteins LEF/TCF do not transactivate target genes. In the Wnt positive cascade, Wnt binds to Fzd resulting in the phosphorylation LRP5/6. A cytoplasmic protein, Dsh tethers the D.C to LRP5/6 by binding to both proteins. As a result β-catenin is free to accumulate and enter the nucleus where it binds to LEF/TCF proteins, activating transcription of target genes.*

Once in the nucleus, β-catenin binds to the N-terminus of DNA-binding proteins of the LEF/TCF family which then governs the transcriptional activity of a number of genes such as *cMyc*, *Cyclin D1* and *Axin2* to name a few (Reya and Clevers 2005, Clevers 2006, Lories et al. 2013). Many of these downstream genes are important in skeletal growth and maintenance (Lories et al. 2013). For example the Wnt/β-catenin pathway prevents cartilage formation in the autopod via suppression of the master transcription factor, *Sox9*, which initiates and maintains many of the earlier processes of chondrogenesis.

1.3.1.3 Sox9

Sox9 belongs to a family of transcription factors that bind to the minor groove of DNA via a DNA-binding domain termed the HMG-box (High mobility group). There are 20 Sox genes present in humans and mice, all of which play very different roles in development (Bowles et al. 2000). Sox9 specifically has been implicated in male sexual development as well as chondrogenesis, this specific role will be further discussed.

Sox9 is reported to be one of the earliest markers of digit formation (Lefebvre et al. 2001) with many studies having demonstrated its indispensable role in the initiation of mesenchymal cells aggregating into digit precursors via conditional knockout and ectopic expression studies (Bi et al. 1999, Chimal-Monroy et al. 2003, Diederichs et al. 2016). *Sox9* expression has also been found in E11.5 mouse embryo autopod prior to any visible signs of digit formation (Kawakami et al. 2006). It continues to be expressed and play a vital role through all stages of early chondrogenesis, thus making it an appropriate marker of chondrogenic tissue (Bi et al. 1999, Raspopovic et al. 2014).

This master transcription factor of digit formation features a potent transactivation domain (Lefebvre et al. 2001) with which it first targets transactivation of *Sox6* and a longer version of *Sox5* (*L-Sox5*) by binding to their promotor regions (Lefebvre et al. 2001, Akiyama et al. 2002). These two *Sox* genes contain the same HMG domain as with all Sox proteins however both lack a transcription activation domain, present in Sox9 (Smits et al. 2001). Together L-Sox5, Sox6 and Sox9 directly activate key cartilage matrix genes such as *Col2a1, Col9a2, Col11a2* and *Aggrecan*, and initiate the differentiation of mesenchymal cells to chondrocytes (De Crombrugghe et al. 2000, Lefebvre et al. 2001, Barna and Niswander 2007).

Once chondrocytes are present, the *Sox* trio maintains chondrocytes in a proliferative state as well as preventing further differentiation of these chondrocytes into hypertrophic chondrocytes. This was illustrated in a study by Akiyama et al. (2002) that used cre/loxp recombinant mouse embryos to knockout *Sox9* after mesenchymal condensations had been formed. The results were that new mesenchymal cells did not undergo overt differentiation into chondrocytes, further proliferation of chondrocytes was grossly inhibited and joint formation was defective. It has been demonstrated that while Sox9 is essential for these aforementioned functions, Sox6 and L-Sox5 have redundant functions in chondrogenesis, however these two proteins greatly enhance expression of Sox9 target genes (Lefebvre et al. 2001, Akiyama et al. 2002, Lefebvre and Bhattaram 2016). A rapid decrease in *Sox9* expression and simultaneously *Sox6* and *L-sox5*, is seen when chondrocytes further differentiate into a hypertrophic chondrocyte (Lefebvre et al. 2001, Akiyama et al. 2002).

Regulation of *Sox9* is also relatively well studied. It was briefly discussed that activation of the *Sox9* transcription factor is dependent on Bmpr1a and Bmpr1b, the two redundant cell surface receptors of the BMP pathway (Yoon et al. 2005). Also previously mentioned is that *Sox9* is inhibited by the Wnt/β-catenin pathway. Some Wnt ligands excreted from the ectoderm of the autopod have a relatively short range in cell signalling. Thus they bind to the surface of cells on the limb periphery, allowing β-catenin to indirectly induce irreversible methylation and repressive chromatin marks (H3K27me3) over the *Sox9* promoter, rendering this this gene transcriptionally inactive (Kumar and Lassar 2014). Sox9 expression is then restricted to the centre of the developing autopod initially (Solursh 1984).

1.3.1.4 Interaction of the three players

In digit development, a Turing model, based on the interactions between BMP/Sox9/Wnt (BSW), predicts the periodic formation of five alternating digit/interdigital regions (Raspopovic et al. 2014). This model was built by first identifying candidate growth factors that were differentially expressed between Sox9 positive and Sox9 negative primary cell cultures prepared from embryonic mouse autopods. Genes from both Wnt and BMP pathways were differentially expressed between Sox9 positive and negative cells. Microarray analysis of these FACS sorted cells revealed that the BMP ligand, *Bmp2*, was expressed out of phase with *Sox9* in all stages of digit patterning. However analysis of the signalling activity of the BMP pathway

was looked at using Smad protein phosphorylation (indicating active Smad) which showed complete in-phase signalling with *Sox9* expression, supporting the positive effect of BMP signalling on *Sox9* activation (Pan et al. 2008). Although the Wnt ligands themselves did not show differential expression in Sox9 positive and negative cells, downstream targets including *Axin* and *LEF1* were expressed in Sox9 negative cells. In agreement with this observation, antibodies that recognize de-phosphorylated (active) β-catenin were used to analyse the signalling effects of the Wnt/β-catenin pathway and showed complete out of phase expression with *Sox9* in microarray data. The authors stated that Sox9 was also required for the Turing network, and not just a downstream effector. This was concluded as previous studies had shown that *Sox9* knockouts resulted in the loss of expression of all genes that reflect a digital or interdigital pattern, such as *Bmp2*, *Chordin* and *Noggin* (Akiyama et al. 2002). The contrasting actions of the BMP activator and Wnt inhibitor pathways ultimately sets up the alternating rays of pre-digit and pre-interdigital cells (Raspopovic et al. 2014)

1.4 Methods of genetic analysis in bat limbs

Many of the earliest studies on bat wing development took a candidate gene approach based on what is known about mouse/chick autopod development. Researchers saw whether they could identify genes with novel spatial and temporal patterns of expression during bat wing development. There are two strategies to studying the genes involved in limb development. The majority of studies on bat limb development have adopted the candidate gene approach in which the expression and function of a selected gene is characterised as it is known to be involved in the limb development of a mouse or chick. This approach was the primary focus for many years and has successfully revealed significant differences in gene expression patterns during bat and mouse development, as well as between bat FL and HL development, for genes such as *Shh*, *Fgf8* (Weatherbee et al. 2006, Hockman et al. 2008), *Prrx1* (Cretekos et al. 2008), and *Bmp2* (Sears et al. 2006) among others. The disadvantage of this approach is that there are so many genes involved in limb development that not only would this approach require time and money, but many genes will be thoroughly examined only to show no differentiation at all. Other criticisms are that some of the techniques, such as *in situ,* are not quantitative and require the use of many embryos.

The development of technologies such as microarrays and high throughput sequencing has meant that differential gene expression analysis can be used to identify multiple genes

important for bat wing development, rather than limiting analysis to one gene at a time. It is then possible to compare results across conditions, such as comparing bat FL gene expression to that of the mouse, to detect significant differences in gene expression, potentially exposing previously unexamined genes involved in limb development. This approach has recently been applied to analyse limb development in two microbat species from the genus *Miniopterus* (Wang et al. 2014, Eckalbar et al. 2016, Mason 2016).

In the more recent study, focussing on *Miniopterus natalensis*, the researchers performed a RNA sequencing (RNA-seq) study in order to compare gene expression levels between the developing FL and HL tissue across consecutive stages CS15, CS16 and CS17 (Figure 1.6). The regulatory elements were looked at in parallel through ChIP sequencing (ChIP-seq). Antibodies for both H3K27ac were used to look at areas of open chromatin (Lindblad-Toh et al. 2011) and H3K27me3 were used to analyse repressed regions of DNA (Barski et al. 2007). The aforementioned stages were selected as the bat FL at CS15 greatly expands in an anterior-posterior direction while the HL does not expand to the same degree, creating a relatively large difference in the limbs' appearances (Hockman et al. 2009, Gill 2016) (see Figure 1.3). The following stages further separate the two limbs morphologically and have previously shown unique expression patterns of key developmental genes such as *Shh* and *Fgf8 (Weatherbee et al. 2006, Hockman et al. 2008)*.

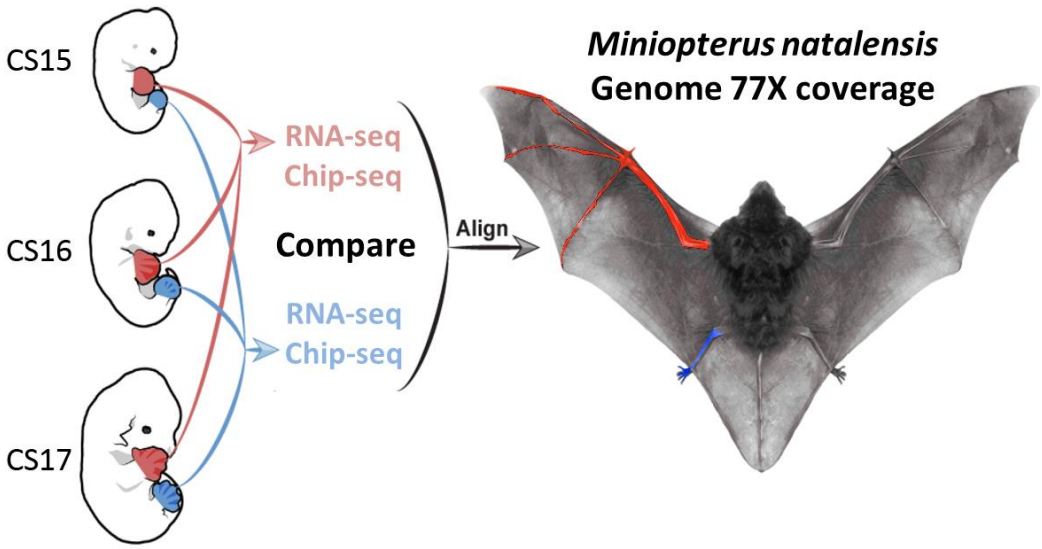

***Figure 1.6: Eckalbar et al. (2016) experimental design**. Three* M. natalensis *developmental stages (CS15, CS16 and CS17) forelimb (red) and hindlimb (blue) autopods were analysed by RNA-seq and ChIP-seq (H3K27ac, H3K27me3). Data was aligned to the* M. natalensis *genome, allowing for annotation of the genes. Figure adapted from Eckalbar et al. (2016).*

The transcriptomes for the FL and HL at the three stages of development were annotated using the *M. natalensis* genome which was assembled de novo (Eckalbar et al. 2016). The study identified 2952 genes that were differentially expressed between HL and FL across the three stages. However genes typically don't act in isolation and it is far more robust to determine the overall expression behaviour on whole gene pathways. Thus Ingenuity Pathway Analysis (IPA) was performed using the RNA-seq data, comparing FL and HL transcriptomes during stages of bat limb development. A number of signalling pathways were identified as differentially activated between bat FL and HL autopods. Among the top 10 IPA canonical pathways were a number of those known to play a role in chondrogenesis, such as BMP signalling which was found to be upregulated in the earlier stages of development observed. This signalling pathway showed higher expression in the FL with the two *BmpR1* cell surface receptors as well as several *Smad* protein transcripts significantly upregulated in the FL compared to the HL. The HL showed upregulation of two repressor genes *Bmp3* and *Gremlin1* at CS15 and CS17.

In addition the Wnt/β-catenin pathway was found to be supressed in the FL compared to the HL at CS15 and CS16. Multiple repressors of the pathway, *sFRP*, *Dickkopf Wnt signalling inhibitors (Dkk)* and *WIF* were upregulated in the FL of the bats across the three studied stages. A Wnt cell surface receptor, *Fzd 10*, was found to be significantly upregulated in the developing HL of the bats (Eckalbar et al. 2016). As mentioned previously, both the Wnt/β-catenin and BMP pathway are involved in the initial patterning of digit and interdigital regions during mesenchymal condensation via interaction and regulation of the master transcription factor, *Sox9* (Raspopovic et al. 2014).

1.5 Aims and objectives

A prediction made from the literature and the RNA-seq results from Eckalbar et al. (2016) was that the observed increase in BMP signalling and decreased Wnt/β-catenin signalling in the bat FL autopod may lead to elevated levels of *Sox9* expression in this limb, and larger fields of mesenchymal condensations. My project focused on testing this hypothesis, as well as establishing an immortalised cell line from limb tissue to be used as a tool for future functional studies.

These objectives were achieved in three parts. The first part investigated the genome and RNA-seq results for *Sox9* expression patterns in *M. natalensis*. This involved annotating the *Sox9*

locus and drawing conclusions about the *Sox9* expression by rerunning the differential expression analysis between FL and HL across CS15, CS16 and CS17. The second part of the project focussed on establishing the mesenchymal cell behaviour patterns during both bat and mouse autopod development. This was achieved through a series of histological stains of whole autopod sections. Last, I have work towards establishing an immortalised cell line of both bat and mouse developing autopod cells in which future functional experiments and biochemical assays can be done, without the need to capture new bat embryos.

Chapter 2:

Characterising the role of Sox9 in *M. natalensis* limb development

2.1 Introduction

Sox9 plays an indispensable role in the initiation and maintenance of digit formation in tetrapod development. Specifically, Sox9 has been implicated as one of the three key players interacting in the reaction-diffusion Turing-like model proposed to initiate digit-interdigit fate of autopod cells as described in Chapter 1 (Raspopovic et al. 2014). Once mesenchymal cells have undergone condensation, Sox9 along with its downstream paralogues, L-Sox5 and Sox6, directly binds to and actives cartilage and differentiation markers as reviewed in Lefebvre and Bhattaram (2010). This *Sox* trio is highly expressed in all chondrocytes before the cells undergo hypertrophy (Lefebvre et al. 2001).

Akiyama et al. (2002) showed that embryos, in which *Sox9* was deleted after the condensation of mesenchymal cells, displayed severe chondrodysplasia. Most cells remained as condensed mesenchymal cells and did not undergo differentiation into chondrocytes. Chondrocyte proliferation was severely inhibited and prearticulation was defective. It has also been shown that changes in timing or rate of gene expression during development can lead to physiological changes, such as alterations in the size and shape of the effected organ in the adult organism (Blanco et al. 1998, Bickelmann et al. 2012). This process is termed developmental penetrance (Richardson 1999). *Sox9* heterochrony has been implicated as the cause for developmental penetrance in the Talpid mole (*Talpa occidentalis*) which, in its adult form, has two enlarged and robust FLs used for digging, in contrast to smaller HLs. A study showed that in this mole species, *Sox9* was expressed earlier during the development of the FLs in comparison to the HLs. This temporal difference in *Sox9* expression was not seen in a shrew species (*Cryptotis parva*) in the same order as the Talpid moles or in mouse limb development, with both mouse and shrew having similar sized FLs and HLs (Bickelmann et al. 2012).

Given the important role of Sox9 in digit formation and the hypothesised role it plays to contribute to the adult FL phenotype of the Talpid mole, it is plausible that developmental *Sox9* expression may play an important role in the elongation of the adult bat FL digits. As mentioned

in Chapter 1.4, Eckalbar et al. (2016) recently performed an RNA-seq study which aided in the annotation of the *M. natalensis* genome. The RNA-seq study explored the differences in gene expression profiles between the FL and HL during three stages of development in the bat: CS15, CS16 and CS17. These stages are ideal to analyse the process of digit development, and thus *Sox9* expression, as CS15 is the stage at which mesenchymal cells begin to condense prior to differentiation into chondrocytes at CS16 (refer to Figure 1.3). Further differentiation of chondrocytes occurs at CS17, with the chondrocyte hypertrophy starting at the centre of the medial cartilage element, where *Sox9* expression is then expected to cease (Lefebvre et al. 2001).

However, it became apparent when looking for *Sox9* expression in the *M. natalensis* RNA-seq dataset that *Sox9* had not been annotated correctly in the *M. natalensis* genome assembly, thus there were no results for its expression. There are several reasons why *Sox9* may not have been annotated in the genome assembly, however to hypothesise the cause, an understanding of the annotation procedure is required. The *M. natalensis* genome was annotated using three sources of gene coding sequence: 1) the *M. natalensis* developing limb transcriptome used for the RNA-seq study (Eckallbar et al. 2016), 2) a transcriptome from lungs, brain and liver of the bat species, *Myotis brandtii* (Seim et al. 2013), and 3) all known mouse protein sequences from the RefSeq protein database in NCBI (Pruitt et al. 2006). Thus one possible, yet improbable, scenario for the lack of annotation could be that *Sox9* was not expressed in any of the tissues used for the transcriptome assembly from both bat species and that the *M. natalensis* Sox9 protein has poor conservation across species, thus did not align to the mouse Sox9 protein sequence. A more likely reason is that sequencing or assembly errors occurred at the position of the *Sox9* locus that resulted in regions of unknown sequence. This would be seen as a series of 'N's' in the genome assembly where sequence information is missing. If significant regions of the exons at the *Sox9* locus consisted of unknown sequence then neither the bat transcripts nor the mouse protein sequence would align with the required identity coverage to be included in the genome annotation.

As a result of this missing annotation, it is not possible to analyse Sox9 expression and it is also not possible to analyse the available ChIP-seq data for *Sox9* (Eckalbar et al. 2016) as the positional information of the locus is unknown. Thus, it is important to correct the annotation of the *Sox9* locus in the *M. natalensis* genome to facilitate further analysis of this essential

development gene. Despite the lack of a correct annotation for the *Sox9* locus, the genes involved in *Sox9* regulation as well as its downstream effectors may be analysed to determine whether there is indirect evidence of differential expression of *Sox9* between the developing bat FL and HL.

As discussed in Chapter 1, *Sox9*, as part of the Turing-like model (Raspopovic et al. 2014), is positively regulated by the BMP signalling pathway and inhibited by the Wnt/β-catenin pathway (Solursh 1984, Chimal-Monroy et al. 2003, Yoon et al. 2005, Raspopovic et al. 2014). Eckalbar et al. (2016) found that the BMP signalling pathway was significantly upregulated in the bat FL compared to the HL from CS15 through to CS17. In particular the two redundant cell surface receptors *Bmpr1a* and *Bmpr1b*, which have been previously proposed to play a role in *Sox9* upregulation (Yoon et al. 2005), were upregulated in the FL at CS15. *Bmpr1b* continued to be upregulated at CS16 (Eckalbar et al. 2016). Furthermore, several Wnt/β-catenin pathway suppressors were upregulated in the FL across all stages such as *Sfrp2/3*, *Sostdc1*, *Dkk2/3*, *Wif1* and *Cdh2*. In addition, *Sox6* and *Aggrecan,* downstream targets of Sox9, were both found to be significantly upregulated at CS15 and CS16. These observations suggests that *Sox9* signalling may be upregulated in the FL at CS15 and CS16 in developing bat embryos and that this differential expression may be in part responsible for the great elongation of digits seen in the adult bat wing.

Another research group, (Wang et al. 2014), published an RNA-seq study on the developing FL and HL of a closely related bat species, *Miniopterus Schreibersii*. While my study and the Eckalbar et al. (2016) study analysed three biological replicates for each of the three distinct stages of development (CS15, CS16 and CS17), Wang et al. (2014) pooled the limbs of eight embryos of varying stages (two CS15 (FL only), one CS16 and five CS17). Additionally, they separated interdigital tissue from digital tissue in the FL and HL pools (Figure 2.1). This strategy may be an advantage in the context of *Sox9* expression analysis, as *Sox9* is only expressed in the digital regions of the developing limb (Kawakami et al. 2006, Raspopovic et al. 2014) and thus it may be more informative to analyse *Sox9* expression in the digital tissue alone.

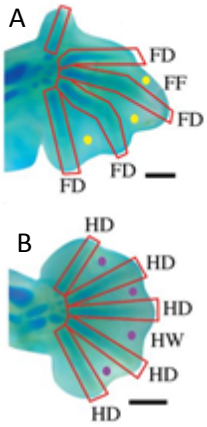

Figure 2.1: Tissue separation for RNA-seq study on Miniopterus schreibersii ***bat forelimb and hindlimb.*** *A study by Wang et al. (2014) separated out different tissue types in the forelimb (**A**) and hindlimb (**B**) of CS17, CS16 and CS15. A dorsal view of the CS17 autopod is shown, with distal on the left and anterior at the top. FD: the four most posterior forelimb digits; FF (yellow dots): interdigital tissues between FD forelimb digits; HD: hindlimb digits; HW (purple dots): interdigital tissues between hindlimb digits. Adapted from Wang et al. (2014).*

In this study, I located the *Sox9* locus in the *M. natalensis* genome and discovered large regions of missing sequence in the *Sox9* coding region. I use a combination of methods, including targeted cross-species genome alignments and analysis of the *M. natalensis* limb transcriptome assembly, to fill in the missing sequence in the *Sox9* exons. I then repeated the differential expression analysis conducted by Eckalbar et al. (2016) to determine the levels of *Sox9* at the three stages of limb development. I compared my expression results to those found by in Wang et al. (2014) in digit and interdigit tissue of both FL and HL. In addition I analysed the ChIP-seq datasets generated by Eckalbar et al. (2016) for H3K27ac (open chromatin; Rada-Iglesias et al. (2011) and Creyghton et al. (2010)) and H3K27me3 (closed chromatin; Barski et al. (2007)) marks around the *Sox9* locus. Finally, I analysed all available RNA-seq and ChIP-seq datasets for eight other genes that are either closely linked to *Sox9* expression or well-studied in a limb development context. The justification for the analysis of each gene is described below.

The first two genes, *Tbx5* and *Tbx4*, are the well-characterised tetrapod FL and HL markers respectively (Rodriguez-Esteban et al. 1999). The genes are expected to be expressed at high levels throughout the respective limbs. The gene loci should display an enrichment of H3K27ac marks compared to H3K27me3 in the FL for *Tbx5* and HL for *Tbx4* (Gibson-Brown et al. 1996, Wang et al. 2010). The Hox genes, *Hoxd11* and *Hoxd13*, are key limb patterning genes (Davis and Capecchi 1996). *Hoxd13* is important for specifying the autopod region of the developing limb and is expected to be expressed at similar levels in the FL and HL and should be associated with open chromatin marks in both limbs. *Hoxd11* however was reported to have significantly upregulated expression in the developing bat FL compared to the HL, a pattern that is not seen in mice (Wang et al. 2014). Thus it is expected that there will be a greater enrichment of

H3K27ac marks compared to H3K27me3 at the *Hoxd11* locus in the FL compared to the HL. The last three genes analysed are all downstream targets of Sox9 whose expression is likely to be affected the most in the event of *Sox9* differential expression. These include *L-Sox5*, *Sox6* and *Col2a1* (Lefebvre et al. 2001, Smits et al. 2001). If the hypothesis holds true that *Sox9* is upregulated in the developing bat FL in response to greater activation by the BMP signalling pathway and a decrease in repression by the Wnt/β-catenin pathway, then *Sox6*, *L-Sox5* and *Col2a1* are likely to display a similar expression profile to that of *Sox9*.

2.2 Methods and materials

2.2.1 *Locating* Sox9 *in the* M. natalensis *genome*

The mouse and human *Sox9* gene loci were aligned to the an early version of the *M. natalensis* genome assembly (prior to clean up of contigs smaller than 500bp) using BLASTn (v2.2.29+; Altschul et al. (1990)). The alignments to scaffold 212 were investigated to pinpoint the putative *Sox9* locus in the *M. natalensis* genome, using the integrative genomics viewer (igv; v2.3.32; Robinson et al. (2011).

To support the proposed position of *Sox9* on scaffold 212, neighbouring genes in the mouse genome were aligned to the *M. natalensis* genome using BLASTn. In addition, the closest annotation to the putative *Sox9* locus in *M. natalensis* genome assembly was *SLC39a11*. An Ensembl Genome Browser (Hubbard et al. (2002); www.ensembl.org) search was used to determine the location of this gene relative to *Sox9* in both the mouse and human genome assemblies.

The mouse and human *Sox9* mRNA transcripts were aligned to their respective genomes using BLASTn to determine the intron/exon boundaries in each species. With this information, the sequence placement for contig 29352585, which had been excluded during assembly and annotation of the *M. natalensis* genome, was determined on scaffold 212. The *M. natalensis Sox9* exons were then mapped onto scaffold 212 of the *M. natalensis* genome assembly along with the surrounding sequence gaps using the human and mouse *Sox9* gene annotations.

2.2.2 *Filling in the missing* Sox9 *sequence*

In order to fill in the missing sequence information at the proposed *Sox9* locus in the *M. natalensis* genome, the transcriptome information for *Sox9* was extracted for the same

species. To do this, the mouse *Sox9* mRNA sequence was aligned to the *M. natalensis* limb transcriptome assembly generated by Eckalbar et al. (2016) using BLASTn. All resulting transcripts that with close to 100% alignment and had e-values lower than $1e^{-147}$ were aligned to the *M. natalensis* genome to determine if they aligned to scaffolds other than 212 and thus likely represent paralogues of the *Sox9* gene. Transcripts not associated with other scaffolds were then manually aligned to each other as well as to the *Sox9* locus in the *M. natalensis* genome and mouse *Sox9* mRNA using Mega5.2 (Tamura et al. 2011).

A gap remaining on the 5' end of the first exon of the *Sox9* locus was filled using PCR followed by Sanger sequencing. *M. natalensis* genomic DNA to be used in the PCR was extracted from the same adult male skin that was used for the sequencing of the *M. natalensis* genome (Eckalbar et al. 2016). 600 mg of tissue was crushed into digestible pieces in liquid nitrogen. Ground pieces were suspended in 10 ml digestion buffer[1] at 65°C overnight with gentle shaking. DNA was extracted by adding 600 ml 1:1:1 phenol: chloroform: isoamyl alcohol and centrifuging at 1700 g for 10 minutes in a Qiagen 4-15C centrifuge (Sigma 14425). The top layer (±200 ml) was transferred to a new tube with 100 µl ammonium acetate and 400 µl 100% ethanol after which a stringy precipitate (DNA) was seen. The tube was centrifuged at 1700 g for 2 minutes to pellet the DNA, which was then washed in 70% ethanol and air dried. To solubilise the DNA, the pellet was resuspended in TE buffer[2] and shaken at 65°C for 2 hours before long term storage at -20°C. The quantity was reported at 329.8 ng/µl with an A260/A280 of 1.88 and A260/A230 of 1.71 using a nanodrop (ND-1000 spectrophotometer). A gel electrophoresis (Supp. Fig. 2.1 A) shows that extracted DNA was intact due to the solid band present as opposed to a smear which would suggest it was degraded.

PCR primers that flanked the sequencing gap were designed in PearlPrimer (v1.1.21; Marshalll (2004)) (Sox9CF-5' GAACTTGTCCTCTTCGGTCTC; Sox9CR-5' TGACATTAGGAGAGTACGGCA) and assessed for primer dimers in Oligo Analyser 3.1 (https://www.idtdna.com/calc/analyzer). Each 25 µl PCR reaction contained 0.3 µM forward- and reverse-primers, 1 x KapaTaq HiFi Ready Mix (Lasec DKAPKK2601PRO) and 2 ng genomic DNA. A "no template" control which excluded the genomic DNA was also run. Primers specific to the *Tatabox binding like protein 1* (*Tbpl1*) locus, which have been previously shown to produce a 3000 bp band (Mason et al. 2015), were

[1] 100 mM NaCl, 10mM Tris Cl pH8, 25 mM EDTA pH 8, 0.5% SDS, 0.1 mg/ml proteinase K

[2] 10 mM Tris, 1 mM EDTA at pH8 acidified with HCl

used as a positive control. The PCR reaction cycle conditions (95°C for 3 minutes, 30 cycles of 98°C for 20 seconds, 63.5°C for 15 seconds, 72°C for 40 seconds and then a single cycle of 72°C for 2 minutes) were optimised to produce a single clear band of 900 bp (Supp. Fig. 2.1 B). The PCR product was extracted from a gel using Wizard® SV Gel and PCR Clean-Up System (Promega, A9282) according to manufacturer's guidelines and sequenced using the PCR primers at the Central Analytical Facility (Stellenbosch University).

The forward and reverse sequences were aligned to the mouse genome using BLAT in Ensembl Genome Browser (Kent 2002) to ensure the correct genes were sequenced. Mega5.2 was used to trim sequences with poor sequencing quality and create one continuous DNA sequence called 'Gap C'. Gap C was then manually aligned in Mega5.2 to a *M. natalensis* genome extract containing Sox9, along with the *Sox9* transcripts obtained from the limb transcriptome assembly and the Contig from an early draft of the genome assembly (Figure 2.2). Coding sequence (blue lines in Figure 2.2) was identified via either the transcriptome transcripts or alignment of *M. natalensis* DNA to the mouse mRNA. In two cases, once at the 5' end of Gap C (red line in Figure 2.2 C) and at the 3' end of the *M. natalensis* genome extract (red patterns in Figure 2.2. A), manual alignment between *M. natalensis* DNA and mouse mRNA was no longer possible. For these sequences, BLASTn was used to search online databases and determine whether or not they aligned to the *Sox9* gene in the mouse genome.

A consensus sequence of all known DNA sequence for *M. natalensis* at the *Sox9* locus was assembled from the accumulated *M .natalensis* sequence data describe above. This consensus sequence was added to the end of the *M. natalensis* genome and given the gene ID Mnat.G.24240. The new *Sox9* locus was given the same name as the original incomplete locus on scaffold 212 to ensure that the RNA-seq reads that mapped to each locus could be combined for later analysis. The new genome was termed "Genome + Sox9."

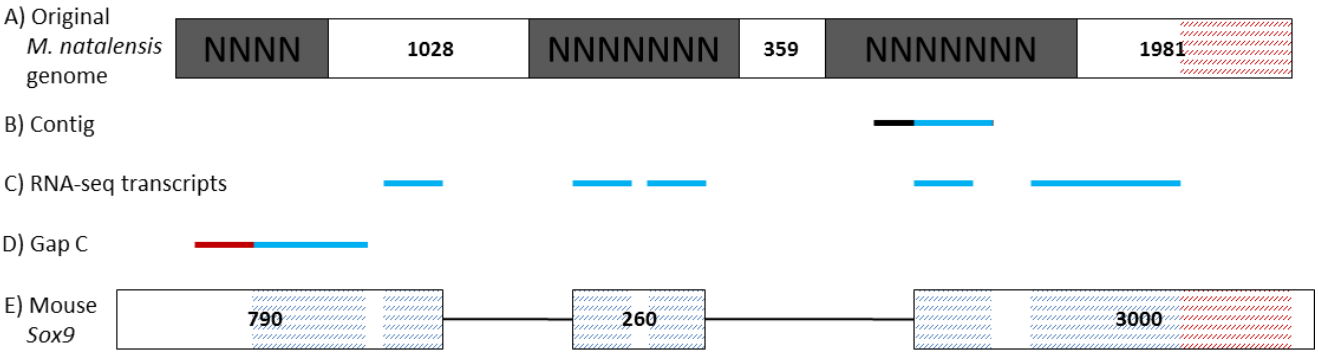

***Figure 2.2: Filling in the gaps of the* Sox9 *locus in* M. natalensis.** *The putative* Sox9 *locus was extracted from scaffold 212 of the* M. natalensis *genome (**A**). Grey blocks with "N" represent regions of missing sequence information while white blocks are regions of known sequence with lengths in base pairs (bp). This locus was aligned in Mega5.2 to a contig from an early draft of the* M. natalensis *genome assembly (**B**), RNA-seq transcripts likely coding for* M. natalensis Sox9 *mRNA (**C**), the gDNA Sanger sequence for Gap C (**D**) and the mouse* Sox9 *exons (**E**). White boxes in E represent exons with their length in bp. The bold black line in B represents noncoding* M. natalensis *sequence. Blue solid lines represent* M. natalensis *coding sequence while blue – patterned regions in the mouse mRNA (E) shows manual alignment to the* M. natalensis *coding sequences. Red-patterned sequence region indicates program alignment with lower coverage alignment between mouse mRNA (E) and* M. natalensis *genome extract (A). Solid red line in D represents sequence with low stringency alignment to* Sox9 *promotor in mouse (not shown).*

2.2.3 *Obtaining new RNA-seq read counts*

The RNA-seq reads from the FL and HL of three biological replicates across three embryological stages (CS15, CS16 and CS17) (Eckalbar et al. 2016) were aligned to the genome + Sox9 using the splice-aware sequence aligner, Tophat2 (v2.0.13; Kim et al. (2013)). The accepted hits were sorted by name using Samtools (v1.3.1) and a read count matrix generated using Htseq_count (v.0.6.0; Anders et al. (2015)) with the mode "intersection-nonempty".

2.2.3.1 Principle Component Analysis (PCA) and Differential expression analysis

PCA and Differential expression analysis was conducted using *DESeq2* (v1.8.1; (Love et al. 2014)) in R studio (Studio 2012) as described in the *DESeq2* RNA-seq workflow tutorial (Love et al. 2015). For PCA, the read count matrix generated in section 2.2.3 was filtered to remove genes with no read counts and rlog transformed. A PCA plot was produced from the rlog-transformed values using the plotPCA command. Differential expression analysis was conducted on the untransformed read count matrix from this study as well as the read count

matrix from Eckalbar et al. (2016) (not containing a Sox9 annotation). The generalised linear mode (GLM) used for the differential expression was as follows:

design = ~ Stage + Limb + Stage:Limb

Normalised read counts were plotted for the following genes: *Tbx5*, *Tbx4*, *Hoxd11*, *Hoxd13*, *Hoxd12*, *Evx2*, *Sox9*, *Sox6*, *Sox5* and *Col2a1*. Genes with an adjusted p-value equal to or less than 0.01 were considered significantly differentially expressed (as described in Eckalbar et al. 2016).

2.2.4 *ChIP-seq data mining*

Eckalbar et al. (2016) performed ChIP-seq using antibodies against the chromatin marks H3K27ac and H3K27me3 on stage CS15, CS16 and CS17 FL and HL autopods and conducted peak calling on these datasets using SICER (Zang et al. 2009). I was able to assess the read count information for the 'islands' of peaks called by SICER. For each development stage, limb type and chromatin mark, a 'track' containing the island distributions and associated read counts was aligned to the annotated genome using igv. The read counts for the islands associated with the *Sox9* gene region were summed for each tissue condition separately. The $\log_2$ ratio of H3K27ac (acetylation) to H3K27me3 (methylation) for each tissue condition was calculated and the values for FL and HL were compared at each stage in Excel. A high ratio of acetylation to methylation was assumed to indicate a region of open chromatin (Rada-Iglesias et al. 2011), while a low ratio indicated closed chromatin (Barski et al. 2007). The loci for the list of genes mentioned in Section 2.2.3.1 were also assessed. However because the islands of called peaks are relatively broad they often extend beyond the gene boundary, or in the case of *Hoxd13,* extend over neighbouring genes. It was decided that all islands existing within or partially within a gene would be included in the final read counts and only whole islands were included. Additionally, the region over which island read counts were counted was kept constant between limb and stage samples, unless otherwise specified. As there were only a few genes to be analysed the decision of which islands were included was justified in each case. An example of the justifications can be seen below (Figure 2.3). Justifications for ChIP analysis of the remaining genes is described in Supp. Fig. 2.2.

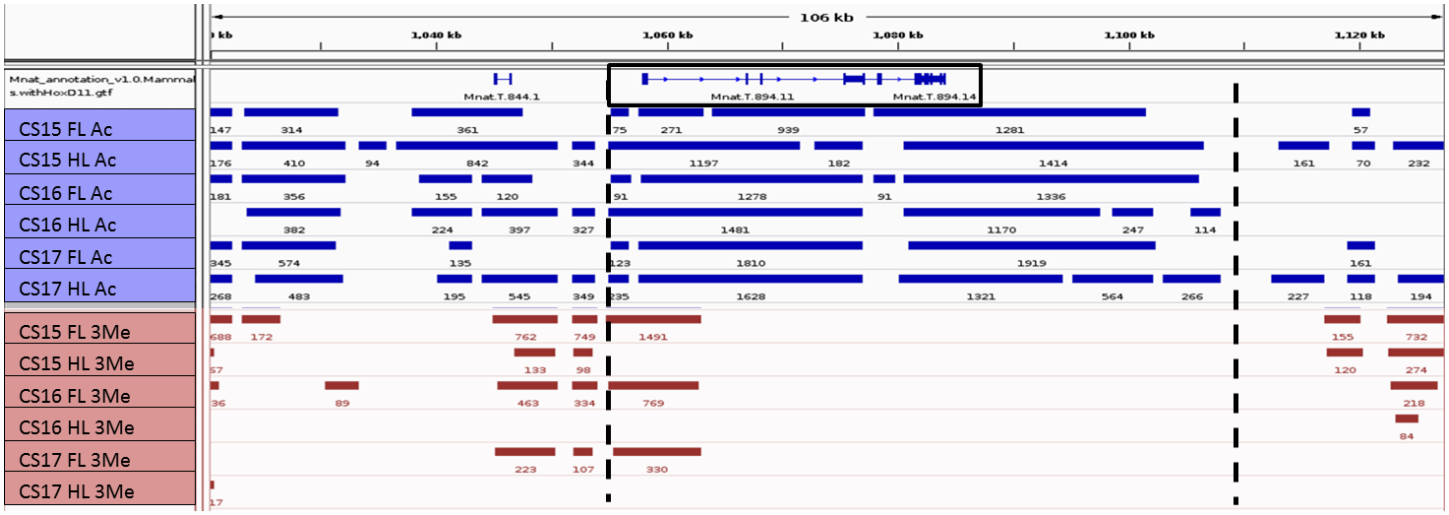

Figure 2.3: ChIP island inclusion demarcation for Tbx4*. The ChIP sequencing read counts and distribution for H3K27 acetylation (Ac, blue) and H3K27 trimethylation (3Me, red) in FL and HL of CS15, CS16 and CS17* M. natalensis *embryos. The black box indicates the* Tbx4 *gene and the dashed lines demarcate the ChIP-seq island distribution included in the comparison for* Tbx4 *ChIP-seq read counts. The justification of the positioning of the dashed lines is that the line on the left and right are in the first break in all ChIP islands that occurs before and after the gene.*

2.2.5 *Wang et al. (2016) RNA-seq data mining*

The normalised read count table and limb transcriptome for the RNA-seq study on *M. schreibersii* (Wang et al. 2014) were downloaded from NCBI Genes expression omnibus (accession number: GSE50699). To identify the *M. schreibersii Sox9* transcripts, the *M. natalensis Sox9* consensus sequence was aligned to the *M. schreibersii* transcriptome. To ensure the consensus of the resulting *M. schreibersii* transcripts was similar to the *M. natalensis Sox9* consensus sequence, the *M. schreibersii* transcripts and *M. natalensis Sox9* consensus sequence were manually aligned in Mega5.2. The putative *M. schreibersii Sox9* transcript ID's were then used to pull out the read counts associated with each transcript from the normalised read count table. These data were analysed in Microsoft Excel and transcript read counts were summed and compared for FL digits, FL interdigits, HL digits and HL interdigits separately. The same procedure performed for *Sox9* was repeated for the list of genes mentioned in section 2.2.3.1, except *Evx2* and *Hoxd12*.

2.3 Results

2.3.1 *Locating and completing the* M. natalensis Sox9 *gene locus*

Cross-species genomic alignment using BLASTn revealed that scaffold 212 of the *M. natalensis* genome assembly was the most promising location for the *Sox9* locus. The mouse *Sox9* gene aligned 5 times with this scaffold with e-values less than $1e^{-50}$, while the human gene when aligned twice with e-values less than $1e^{-150}$ (Supp. Table 2.1). Navigation to the region, 576564 - 581358 on scaffold 212, as determined by the cross-species alignments, revealed three sequencing gaps in the *Sox9* locus of 593 bp, 397 bp and 708 bp (Figure 2.4). The exon/intron boundaries at the *M. natalensis Sox9* locus were determined using a consensus between mouse and human *Sox9* gene structure (Figure 2.4).

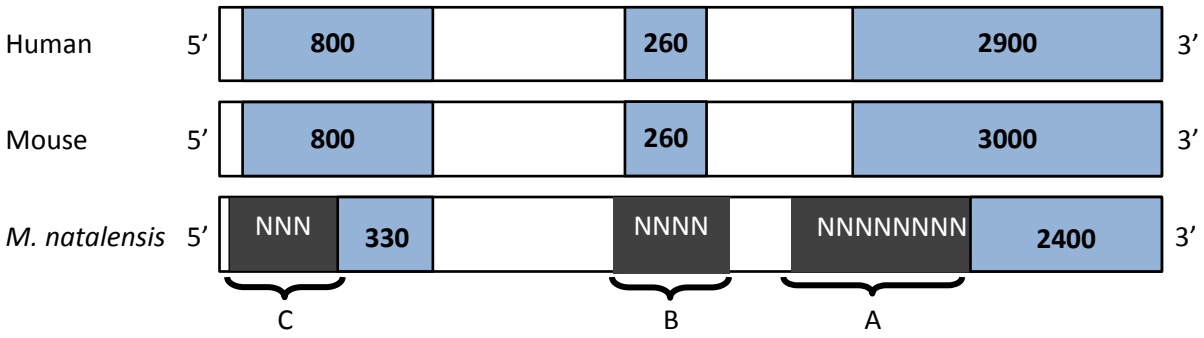

Figure 2.4: The* M. natalensis Sox9 *locus and mapped gaps*. The* Sox9 *exons and their approximate length (bp) are represented by blue blocks. Alignment of the human and mouse* Sox9 *loci to the* M. natalensis *genome revealed two truncated exons and three problematic gaps (in grey). Gap B covers the region potentially coding for the middle exon.*

The predicted location of *Sox9* was supported by gene synteny, as two of the four genes nearby the *Sox9* locus in the mouse genome were located on the same scaffold as the predicted *Sox9* locus in the *M. natalensis* genome (Supp. Table 2.2). The closest annotated gene to the putative *Sox9* locus in *M. natalensis* was *SLC39a11,* which is on the same chromosome as *Sox9* in both the mouse and human genomes.

Gaps at the *Sox9* locus were partially filled in using the Sanger sequence for Gap C, along with the transcripts from the *M. natalensis* transcriptome and the genomic contig that was removed during genome assembly, as depicted in Figure 2.2. The 3' end of Gap C filled in missing information for the first exon, aligning to the first exon of mouse *Sox9*. The 5' end however did not align to the mouse mRNA. An online BLASTn search resulted in a top hit to the mouse Sox9 promotor region. The final size of the first exon was determined to be 491 bp (Figure 2.5).

Through alignment to the mouse *Sox9* mRNA sequence, Gap B sequence was filled by two transcripts from the *M. natalensis* transcriptome with a gap of unknown length between them. Both transcripts aligned with the second exon of the mouse *Sox9*, completing the exon on 5' and 3' ends with a putative final size of 312 bp. The genomic contig consisted mostly of coding information that filled in Gap A, including the third exon's start site. Other than a small gap of an unknown size, the rest of the missing sequence in this exon was completed by transcripts from the *M. natalensis* transcriptome. The total length of known sequence for the third exon was 870 bp (Figure 2.5). The gap between the genomic contig and the transcriptome sequence, using the mouse genome as reference, is likely to be 163 bp in length. Thus the final length of the third exon is estimated at 1030 bp (Figure 2.5).

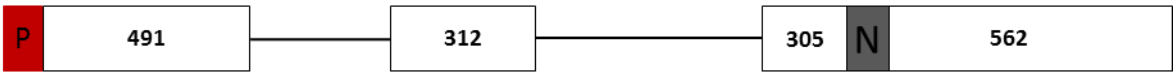

***Figure 2.5: Annotated Sox9 gene in* M. natalensis.** *The* Sox9 *exons (white blocks) and their respective length (bp) as determined in this study using transcriptome data and the mouse* Sox9 *mRNA. The red box labelled "P" represents the putative promotor region of the gene. The grey block labelled "N" represents a region, estimated at 163 bp, of unknown sequence within the third Sox9 exon.*

A consensus sequence of 4613 bp was assembled using all known DNA sequence and estimated sizes of remaining gaps at the *Sox9* locus. This consensus sequence was added to the end of the last scaffold in the *M. natalensis* genome assembly with the gene ID Mnat.G.24240.

2.3.2 *RNA-seq and ChIP-seq analysis*

2.3.2.1 Differential expression analysis of RNA-seq datasets

The RNA-seq reads from the FL and HL of three biological replicates across three embryological stages (CS15, CS16 and CS17) (Eckalbar et al. 2016) were aligned to the *M. natalensis* genome + Sox9. Principal component analysis (PCA) of the resulting read counts showed the expected separation of samples, with principal component 1 (PC1) reflecting the developmental stage and accounting for 40.1% of the variation in the dataset. Principal component 2 (PC2) reflected the limb-type of the sample and accounted for 20.1% of the

variation in the data. Segregation of the samples was similar to the segregation reported by Eckalbar et al (2016) (Figure 2.6).

Differential expression analysis of the RNA-seq reads that were mapped to the updated *M. natalensis* genome, including the Sox9 gene ID, found 2961 genes that were significantly differentially expressed in at least one stage of embryonic development in the forelimb and hindlimb (adjusted p value ≤ 0.01). Of the 2961 significantly differentially expressed genes 1720 showed greater forelimb expression, the remaining 1241 genes showed upregulation in the hindlimb. Of the top 10 genes found in this differential analysis 9 were also in the top 10 of the Eckalbar et al. (2016) differentially expressed genes (Supp. Table 2.3).

2.3.2.2 Analysis of positive control genes

To assess the validity of my methodology for RNA-seq and ChIP-seq analysis, I analysed four genes with well documented expression patterns in tetrapods and bats: *Tbx5*, *Tbx4*, *Hoxd11* and *Hoxd13*. In the two *M. natalensis* RNA-seq datasets [this study and Eckalbar et al. (2016)] the FL marker, *Tbx5*, showed significantly higher expression in the FL compared to the HL across the three stages of development (P=,0.01,n=3) (Figure 2.7 Ai and Aii). In the *M. schreibersii* RNA-seq dataset, the digital tissue had more reads in the FL compared to the HL, while this difference was not seen in the interdigital tissue with similar reads in FL and HL interdigits (Figure 2. 7 Aiii). *The M. natalensis* ChIP-seq data for the *Tbx5* locus showed a greater ratio of acetylation to methylation in the FL compared to the HL across all stages (Figure 2.7 Aiv).

The HL marker, *Tbx4*, showed a pattern that was opposite pattern to *Tbx5*. The *M. natalensis* RNA-seq data excluding the *Sox9* annotation agreed with the differential expression analysis in this study, with a significantly higher *Tbx4* expression in the HL compared to the FL at all three developmental stages (P<0.01, n=3) (Figure 2.7 Bi & Bii). The *M. schreibersii* dataset gave similar results, also showing higher expression in the HL with compared to the FL. The *M. natalensis* ChIP-seq data over the Tbx4 locus showed a consistently high ratio of acetylation to methylation in the HL while a much lower ratio is seen in the FL across the three developmental stages, in line with the RNA-seq datasets.

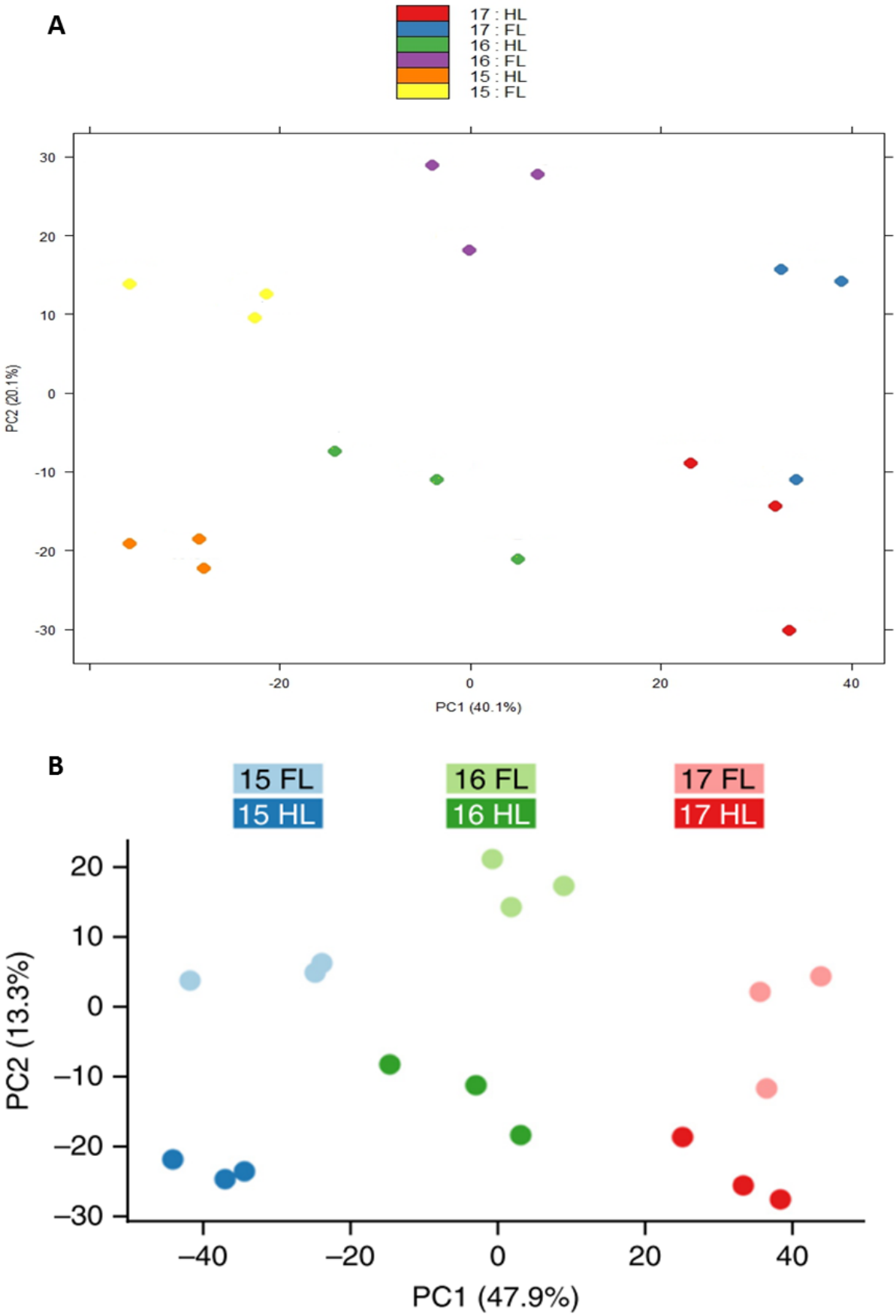

Figure 2.6: Comparison of PCA plots of M. natalensis *genes. A: PCA plot of all* M. natalensis *genes found in this study. B: PCA plot of all* M. natalensis *genes reported by Eckalbar et al. (2016).*

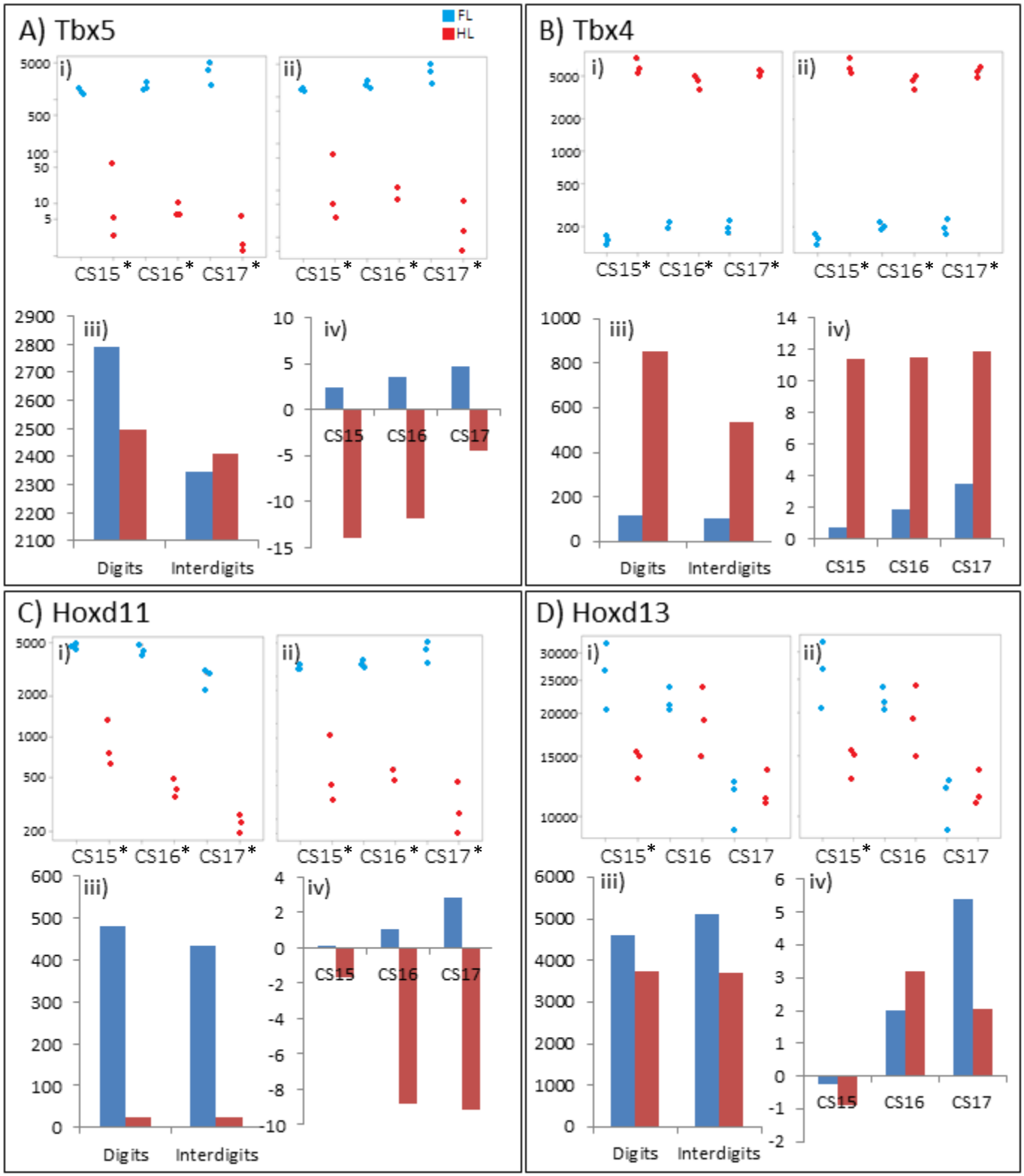

Figure 2.7: ***Expression and chromatin modifications of*** positive control genes analysed ***in developing bat limbs.*** *The same four data sets were used to analyse gene expression and chromatin modifications for four well researched genes* Tbx5 *(A),* Tbx4 *(B),* Hoxd11 *(C) and* Hoxd13 *(D). The four datasets analysed for each gene are:* ***i)*** *The normalised read counts obtained in this study from FL and HL of three* M. natalensis *embryos per stage during early digit formation.* ***ii)*** *The normalised read counts obtained in Eckalbar et al. (2016) from FL and HL of three* M. natalensis *embryos per stage during digit development. In i) and ii) Asterisks shows significant difference between FL and HL at a given stage (p-adjusted < 0.01).* ***iii)*** *The normalised read counts for FL digital tissue, FL interdigital tissue, HL digital tissue and HL interdigital tissue of* M. schreibersii *embryos during stages of early digit formation.* ***iv)*** *The ratio of acetylation to methylation ChIP-seq read counts over the respective gene loci* in M. natalensis *for the same three stages as i) and ii).*

The four data sets for *Hoxd11* were all in agreement (Figure 2.7 C). The two *M. natalensis* RNA-seq dataset analyses revealed that *Hoxd11* was significantly upregulated in the FL compared to the HL at all three stages ($p<0.01$, $n=3$) (Figure 2.7 Ci & Cii). *Hoxd11* in *M. schreibersii* was equally expressed in digit and interdigital tissue. In terms of FL and HL differences, the results were similar to what was found for *M. natalensis,* with 18-fold higher expression in the FL compared to the HL (Figure 2.7 Ciii). The ChIP-seq data for *Hoxd11* supported the RNA-seq results in that at all stages the ratio of acetylation to methylation is much lower in the HL compared to the FL (Figure 2.7 Civ).

The datasets were also in agreement for *Hoxd13* at CS15 (Figure 2.7 Di, ii & iii) in that the two *M. natalensis* RNA-seq datasets showed that *Hoxd13* was significantly upregulated in the FL compared to the HL ($p<0.01$, $n=3$) (Figure 2.7 Di & ii) while the ChIP-seq datasets showed a greater ratio of acetylation to methylation in the FL. The *M. schreibersii* RNA-seq dataset also showed higher expression in the FL compared to the HL (Figure 2.7 Diii). However, in the latter two stages, CS16 and CS17, the *M. natalensis* RNA-seq and ChIP-seq datasets did not completely agree. At CS16, the ratio of acetylation to methylation was higher in the HL than in the FL and at CS17 this ratio was higher in the FL than in the HL, while the RNA-seq data at these stages suggested that FL and HL gene expression levels were very similar to one another. It must be noted that the ChIP-seq peak islands for *Hoxd13* extend to include the locus of two neighbouring genes, *Hoxd12* and *Evx2*. Because I could not be sure which genes the chromatin marks are associated with, the RNA-seq data for these two genes was analysed to determine whether the expression patterns of these two genes more closely mirrored the ChIP-seq data (Supp. Fig. 2.3 A & B). *Hoxd12* expression in the FL was significantly higher than in the HL at CS16 and CS17. This pattern was reflected in the ChIP-seq data at CS17, but not at CS16 where the ratio of acetylation to methylation was lower in the FL that in the HL. Evx2 showed no differential expression or correlation to the ChIP-seq results. These results give me confidence that the RNA-seq and ChIP-seq analyses will be useful in determining the expression of the newly annotated *Sox9* gene if expression differences between FL and HL are extreme.

2.3.2.3 Analysis of *Sox9* and downstream effectors

Differential expression analysis revealed that there was no significant difference in *Sox9* expression between the FL and HL at any of the studied stages of development (CS15: P-adj = 0.72; CS16: P-adj = 0.2; CS17: P-adj = 0.9, n=3) (Figure 2.8 A). Analysis of the *M. schreibersii* RNA-seq datasets revealed 1.7-fold higher levels of *Sox9* in the HL compared to the FL, as well as 2.1-fold higher levels of *Sox9* in the digit zones compared to interdigital tissue. The ratio of acetylation to methylation over the *Sox9* locus was similar for the FL and HL at CS15. At CS16 however, the ratio of acetylation to methylation was high in the HL while the remaining low in the FL. At CS17 the HL ratio dropped to the same level as in the FL.

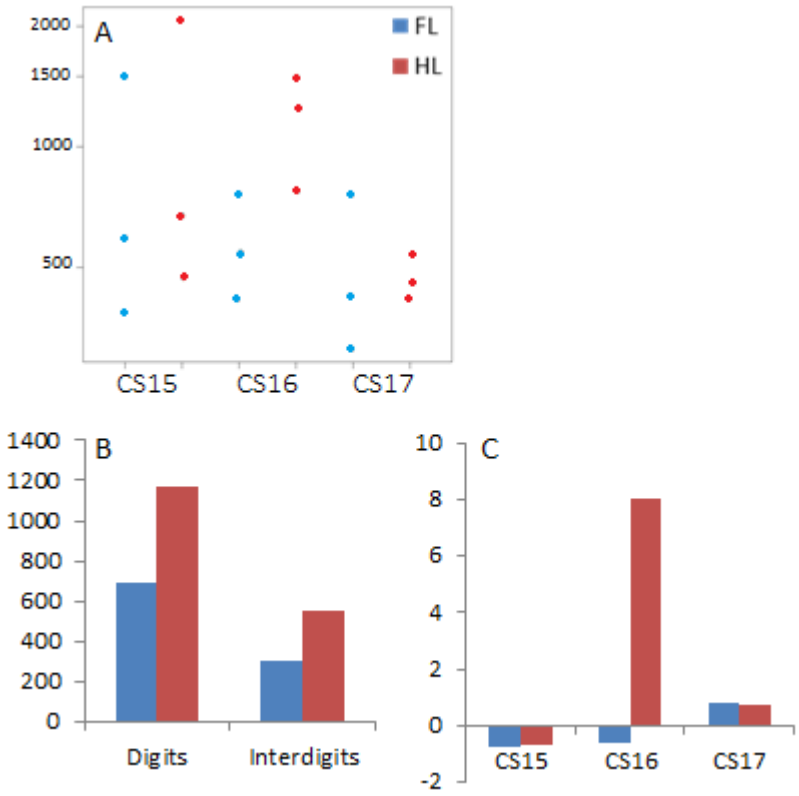

Figure 2.8: Expression and chromatin modifications of* Sox9 *in developing bat limbs. ***A****: The average raw read counts for FL and HL of three* M. natalensis *embryo stages during the early stages of digit formation.* ***B****: The normalised read counts for FL digital tissue, FL interdigital tissue, HL digital tissue and HL interdigital tissue of* M. schreibersii *embryos during early stages of digit formation.* ***C****: the ratio of acetylation to methylation ChIP-seq read counts over the* Sox9 *locus* in M. natalensis *for the same three stages as A.*

Similarly, the downstream targets of Sox9, *L-Sox5* and *Col2a1*, did not show any significant differential expression between FL and HL across the studied stages (Supp. Fig. 2.4 Ai & Bi). The normalised read counts generated in this study using the Genome + Sox9 closely resembled those from the Eckalbar et al. (2016) analysis (Supp. Fig. 2.4 Aii & Bii). The *M. Schreibersii* RNA-seq dataset revealed higher expression of these two genes in the digits compared to interdigits (Supp. Fig. 2.4 Aiii & Biii*). L-Sox5* expression was higher in the HL compared to the FL in both tissue types (Supp. Fig. 2.4 Aiii). *Col2a1* on the other hand showed similar expression levels in

the digits of both limbs and slightly more expression the interdigits of the HL compared to those of the FL (Supp. Fig. 2.4 Biii). In *M. natalensis*, *Sox6* showed significantly higher expression in the FL compared to the HL at CS15 (P-adj=0.009, n=3) (Supp. Fig. 2.4 Ci & Cii). In *M. schreibersii*, *Sox6* was expressed at similar levels in digits and interdigits and showed slightly higher expression in the HL compared to FL (Supp. Fig. 2.4 Ciii).

All three *Sox9* downstream targets had similar ChIP-seq patterns (Supp. Figure 2.4 Aiv, Biv, & Civ). At CS15, the *L-Sox5* locus had a higher ratio of acetylation to methylation in the HL than in the FL. At CS16 the HL ratio increased while the FL ratio slightly decreased. At CS17 the FL increased to match that of the HL, while the HL remained unchanged from CS16. For *Col2a1* at CS15, the ratio of acetylation to methylation was also higher in the HL than in the FL. CS16 displayed the same increase in the HL ratio as in *L-Sox5*. The FL pattern remained relatively unchanged until CS17 where it increased to the same ratio as seen in the HL, with the HL remaining unchanged. The ChIP-seq data for *Sox6* was slightly different to the other Sox9 downstream targets as it started with a slightly higher ratio of acetylation to methylation in the FL compared to the HL. At CS16 however the HL ratio increased, while the FL decreased. At CS17, similar to *L-Sox5* and *Col2a1*, the ratio of acetylation to methylation in the FL levelled out, while the HL ratio remained unchanged.

2.4 Discussion

There is a vast amount of literature on *Sox9* and its crucial role in digit formation is well understood. It is a key marker of the early stages of chondrogenesis and is the master transcription factor that allows for differentiation of mesenchymal cells to chondrocytes (Bi et al. 1999, Goldring et al. 2006, Lefebvre and Bhattaram 2010, Diederichs et al. 2016). It was suggested by Hockman et al. (2009) that differences in the digit length between bat FL and HL begin as early as CS16, when digital mesenchyme condensation is already underway. However, two research groups have proposed that the mechanism of elongation of the FL digits lies in the proliferation of chondrocytes and a larger hypertrophic zones within the digit shafts, only seen at CS20 (Sears et al. 2006, Farnum et al. 2008). In this study, I explored the hypothesis that digit elongation begins earlier, when mesenchymal cells are condensing, and that this process is controlled by *Sox9*.

This hypothesis is supported by evidence that there is significant upregulation of the BMP signalling pathway, which positively regulates *Sox9*, in the FL compared to HL of developing bat embryos, while there is significant downregulation of the *Sox9* inhibitor pathway, the Wnt/β-catenin pathway (Eckalbar et al. 2016). In light of this data, it was expected that *Sox9* would be upregulated in the bat FL. Interrogation of the *M. natalensis* RNA-seq data set published by Eckalbar et al. (2016) lead to the discovery that *Sox9* was not annotated in the genome. Annotation of this locus was essential to further test the hypothesis that *Sox9* plays a role in the development of the extreme limb morphology seen in the bat.

In this study, the *Sox9* locus was identified with a fair amount of confidence. *Sox9* has many paralogues, all of which contain the same HMG domain (Lefebvre et al. 2001) and thus alignment of the mouse and human *Sox9* to multiple *M. natalensis* genome scaffolds was expected. However, scaffold 212 had the lowest e-values for both species and the most alignments to the mouse *Sox9* locus. Confirmation of the locus position was strengthened by gene synteny in mice, half these genes occurred on the same scaffold as the predicted locus in the *M. natalensis* genome. In addition, looking at the converse comparison, the closest gene to the predicted *Sox9* locus was found on the same chromosome as *Sox9* in both humans and mice. Having successfully found the *Sox9* locus it was then apparent why the gene had not been annotated in the *M. natalensis* genome. Three large sequencing gaps in the coding region of the locus would have prevented the transcriptome data and mouse protein data from aligning to the *Sox9* locus.

A contig which was present in an early version of the *M. natalensis* genome assembly, but had been removed to increase the efficiency of the assembly process, showed high sequence similarity to the mouse *Sox9* mRNA and coincided with a region of unknown sequence in the third exon of the *M. natalensis* gene. This sequence, along with several transcripts from the transcriptome assembly, allowed near completion of the second and third exons in the *M. natalensis Sox9* locus. The second exon was at least 50 bp longer than the equivalent exon found in mice and humans, while the third exon was 1900 bp shorter. It is possible that a portion of 3' coding sequence for the third exon is missing due to low sequence similarity to mice and human genes. The unknown sequence that likely contained the 5' end of the first exon was completed using Sanger sequencing. From this information, the first exon was estimated to be 491 bp long compared to approximately 800 bp in mouse and human. The 5'

end of the sequence however aligned to the mouse *Sox9* promotor, thus it is likely that the 5' UTR is substantially smaller in the bats compared to the mouse. The final intron lengths could not be determined as transcripts in exon 2 did not overlap with any previously known sequence and the size of the missing sequence information is unknown. There thus remains unknown sequence before and after exon 2 as well as between the contig and transcript sequence within exon 3. These could be further completed using targeted Sanger sequencing of genomic DNA.

Successfully finding the *Sox9* locus position and filling in the missing coding sequence allowed me to re-analyse the RNA-seq data generated by (Eckalbar et al. 2016). First, it was important to assess whether the differential expression analysis I performed showed similar results to that performed by Eckalbar et al. (2016). I did not expect to see large differences between the analyses of the two datasets as the only difference was the addition of *Sox9* coding sequence. Reanalysis of the RNA-seq data using the updated *M. natalensis* genome containing *Sox9* supported the findings of Eckalbar et al. (2016). The 2952 genes found to be significantly differentially expressed in Eckalbar et al. (2016) were all present in the list of 2961 significantly differentially expressed genes produced in this study. In addition the top 9 differentially expressed genes were the same in both data sets.

In addition to comparing the overall differential expression analysis results, I assessed the expression/chromatin state of four well-characterised limb development genes as positive controls. I first analysed the FL and HL markers, *Tbx5* and *Tbx4* (Rodriguez-Esteban et al. 1999). The low ratio of acetylation to methylation at the *Tbx5* locus in the HL and high ratio in the FL suggested that this locus is closed to transcription machinery in the HL, while it is accessible in the FL. This finding is in line with chromatin ChIP-seq experiments conducted on developing mouse limbs (Cotney et al. 2012). Additionally, *Tbx5* expression was significantly upregulated in the FL across the three stages in *M. natalensi*s. In *M. schreibersii, Tbx5* was expressed at higher levels in the digital tissue of the FL compared to the HL, thus in accordance with the literature it was clearly a FL associated gene (Rodriguez-Esteban et al. 1999). Conversely, the *Tbx4* acetylation to methylation ratios revealed that this locus is hyper-acetylated in the HL when compared the FL, suggesting *Tbx4* is open to transcription in the HL. The RNA-seq data supports this conclusion as *Tbx4* expression is a significantly upregulated in the HL of *M. natalensis* and *M. schreibersii* across all stages and in both digital and interdigital tissue, as expected of the HL marker (Rodriguez-Esteban et al. 1999).

The *Hoxd11* results further support the literature and the link between the ChIP-seq data and RNA-seq data. Wang et al. (2014) reported that *Hoxd11* was upregulated in the *M. schreibersii* FL during limb development when compared to the HL. This is seen in my analysis of the *M. schreibersii* data for both the digit and interdigit tissue. Mason et al. (2015) echoed this finding in *M. natalensis,* showing that this gene is significantly upregulated in the FL across the three key stages of digit formation. My RNA-seq analysis closely resembles that of Mason et al. (2015) and Eckalbar et al. (2016). The ratio of acetylation to methylation at the *Hoxd11* locus shows that while there is slightly higher acetylation in the FL, the *Hoxd11* locus is highly methylated in the HL. Thus, as reflected in the expression studies, *Hoxd11* is silenced in the HL compared to the FL due to the closed chromatin state (Barski et al. 2007).

Thus far all the genes analysed show significant differences in expression between the FL and HL across the three stages and the chromatin state robustly supports these differences in expression. Another gene analysed was *Hoxd13*, which showed significant differential expression at CS15 in the dataset obtained from Eckalbar et al. (2016) but not at CS16 and CS17. This same expression pattern is seen in my RNA-seq analysis and a slight FL upregulation over HL is seen in both tissue types in *M. schreibersii*. The ratio of acetylation to methylation at CS15 is higher in the FL compared to the HL, thus supporting the significantly higher FL expression at this stage. The ChIP-data for CS16 and CS17, however, do not correlate well with the expression patterns seen at these stages. The HL locus is more acetylated than the FL at CS16, yet the FL and HL have very similar *Hoxd13* expression levels. At CS17 the FL is hyper-acetylated compared to the HL while again the expression data suggests equal expression of *Hoxd13* in the FL and HL. It is important to note that the ChIP-seq islands over the *Hoxd13* locus extended over neighbouring genes on both sides. Thus the expression patterns of the genes flanking *Hoxd13* (*Hoxd12* and *Evx2*) were analysed to see if they correlated with the ratio of acetylation to methylation at the *Hoxd13* locus. *Hoxd12* was significantly upregulated in the FL at both CS16 and CS17. This expression pattern does not correlate well with the chromatin state at CS16 but is in accordance with the chromatin state at CS17. Thus, the influence of the chromatin state of neighbouring genes may be able to explain the disaccord between the *Hoxd13* expression and chromatin state at least at CS17.

It is clear that the RNA-seq and ChIP-seq datasets are in agreement when there are significant differences in gene expression between the FL and HL. This suggests that using differential

histone modifications as a proxy for differential gene expression is only reliable when expression differences are extreme for a given gene. Genes that display only subtle differences in expression will not reliably display distinct chromatin marks. Chromatin state data is inherently difficult to interpret. Regions of open or closed chromatin are not only found directly over a gene body but are also located around promotor and enhancer regions (Cotney et al. 2012). Enhancers are difficult to identify due to the large range in distance they can occur from the promotor, such as within the gene's intron to as far reaching at 85 Kb upstream of the gene, as is the case of the wing margin enhancer of the *Drosophila Cut* locus (Blackwood and Kadonaga 1998). The method used in this study to decide on the region in which to count reads associated with chromatin state for a specific gene had drawbacks. This was mainly due to the broad peak ranges or "islands" produced by the SICER peak-calling algorithm used by Eckalbar et al. (2016). Neither enhancers nor promotors could be analysed on their own and it was not possible to create a set rule for which ChIP-seq reads to include that would satisfy all the genes that were analysed. Instead, I chose to minimise bias by taking into account the ChIP-seq read counts for the whole gene locus. As I could not determine the read distribution within an island, I also chose to only include whole islands, even when they overlapped neighbouring genes. The neighbouring gene expression data was then taken into account for analysis, such as with *Hoxd13*. Thus while chromatin modification data can enhance a whole genome study, it is best to analyse the data in combination with other resources, such as RNA-seq data.

The positive controls discussed earlier gave confidence in the RNA-seq analysis methodology used to determine the expression patterns of *Sox9*. Contrary to what was hypothesised, during the early stages of development, when the digit primordia are forming (CS15 and CS16), *Sox9* read counts were higher in the HL compared to the FL. At CS17, *Sox9* read counts decreased for both limbs. This decrease in expression is expected since around CS17 the chondrocytes in the digit shafts likely start differentiating into hypertrophic chondrocytes that no longer express *Sox9* (Lefebvre et al. 2001, Hockman et al. 2009, Eckalbar et al. 2016). Differential expression analysis showed that there was no significant difference in *Sox9* expression between FL and HL across all three developmental stages. Similar results were seen for *M. schreibersii*, as there was higher *Sox9* expression in the HL compared to the FL in both digital and interdigital tissue of *M. schreibersii*. The Wang et al. (2014) RNA-seq study provides additional information as, in both FL and HL, there is higher expression of *Sox9* in the digital

tissue compared to the interdigital tissue. This is expected as *Sox9* is a transcription factor expressed in condensed mesenchymal cells and is often used in studies to visualise early digit formation and morphology (Bi et al. 1999, Lefebvre et al. 2001, Zheng and Cohn 2011, Raspopovic et al. 2014)

The chromatin ChIP-seq dataset for *Sox9* reflects the expression patterns described above. At CS15 and CS17 the chromatin mark patterns are very similar in the FL and HL, which is also true for the expression results. At CS16, the HL is hyper-acetylated in comparison to the FL and suggests that there should be significantly higher *Sox9* expression in the HL than in the FL. Although the HL *Sox9* expression is higher, this difference is not significant. As seen for *Hoxd13*, since there is no significant difference in *Sox9* gene expression between FL and HL, it is unlikely that the chromatin state will provide reliable information regarding gene expression.

With the confidence that the data obtained from the new RNA-seq analysis is accurate, the question now turns to the initial hypothesis. *Sox9* is not differentially expressed between the FL and HL. This contradicts the hypothesis that the combination of an upregulation of the BMP pathway and suppression of Wnt/β-catenin in the FL will lead to the upregulation of *Sox9* in the FL of developing bats. Despite the crucial role of *Sox9* in the formation of digits it appears that the Sox9 transcription factor is not responsible for the unique, elongated digit morphology in the bat FL compared to the HL. This is supported by a study that states the wnt/ β-catenin, Sox9 and the BMP network are involved in the periodic patterning of digits, where Sox9 corresponds to digit zones and Wnt/ β-catenin to interdigit zones (Raspopovic et al. 2014). If this is the true then an increase in *Sox9* would lead to a greater number of digits and not elongated digits. There is no difference in the number of digits between the bat FL and HL autopods .The observation that there is no significant difference in levels of Sox9 transcripts between FL and HL autopods, is thus consistent with the proposal that Sox9 determines the number of digit fields, rather than the size of the individual digit fields.

With Sox9 no longer a candidate for digit elongation it is thus necessary to turn to other genes that are involved in the digit formation process. Of the genes analysed*, Sox6* has the highest expression of the *Sox* trio and is the only one of the *Sox* transcription factors that is differentially expressed between the FL and HL. *Sox6* upregulation in the FL was evident at CS15 and is in accordance with high ratio of acetylation to methylation at this locus in the FL

at this stage. The digit condensations first form at CS15 (Hockman et al. 2009). Thus, if there are differences in condensation size, it is expected that the expression patterns of the *Sox* genes would reflect these differences at this stage. *Sox9* plays a role in activating *Sox6* expression (Lefebvre et al. 2001, Akiyama et al. 2002), however it has also been reported that the BMP pathway is involved in the activation of *Sox6* and *L-sox5* expression (Nordin and LaBonne 2014, Kozhemyakina et al. 2015). It is thus possible that the effects of the upregulated BMP pathway is bypassing *Sox9* and directly effecting *Sox6* expression. It is interesting that this is not the case for the redundant *Sox6* paralogue, *L-Sox5* as this gene is not differentially expressed between the FL and HL. The *Sox* trio bind to the *Col2a1* enhancer, with Sox9 being the main driver of expression while Sox6 and L-Sox5 enhance the expression levels (Lefebvre et al. 2001, Akiyama et al. 2002, Lefebvre and Bhattaram 2016). Another trend picked up by these chondrocyte markers is that the *Sox* trio and *Col2a1* all have very similar chromatin patterns across the three stages. At CS15 all, but *Sox6*, show greater acetylation to methylation in the HL compared to the FL. At CS16 the HL is drastically hyper-acetylated in all four genes while the FL is not and at CS17 the FL acetylation matches that of the HL.

While *Col2a1* was not upregulated, Eckalbar et al. (2016) reported an upregulation of *Acan* in the FL at CS15 and CS16. This gene codes for Aggrecan, a proteoglycan that forms an important component of the extracellular matrix of the cartilage digits (Velleman 2000) (Kiani et al. 2002). Aggrecan plays a role in mediating chondrocyte-chondrocyte interactions, as well as chondrocyte-matrix interactions and is also responsible for the elasticity of cartilage (Velleman 2000, Kiani et al. 2002). A homozygous mutation of *Acan* is responsible for a chicken cartilage mutation, nanomelia, which causes shortening of limbs and a parrot-like beak (Argraves et al. 1981). According to Pennypacker and Goetinck (1976), in the absence of Aggrecan, the extracellular matrix space around chondrocytes is greatly reduced. *Acan1* has a highly conserved enhancer located 10 Kb upstream of the gene, which is bound by the Sox trio (Han and Lefebvre 2008). Specifically, Sox6 and L-sox5 binding to the enhancer increases the efficiency with which Sox9 binds and activates the enhancer (Han and Lefebvre 2008). It can thus be hypothesised that an overexpression of Aggrecan in the bat FL digits, possibly mediated by Sox6 enhancing Sox9 activity at the Acan enhancer, may cause an elongation of the cartilage templates, with greater spaces between chondrocytes. To test this, either an electrophoretic mobility shift assay could be performed with Sox6 transcription factor on the *Acan1* promotor

or it would be useful to upregulate the *Sox6* gene in the FL of mice using a Cre-lox system and then compare *Acan1* expression level in mutant to wildtype mice. It would also be useful to use histological techniques to visualise the digit development of these mutant mice in comparison to wildtype condensation size.

This *in silico* work has revealed that the expression of the chondrogenic master transcription factor, *Sox9*, does not play a role in the accelerated elongation of bat FL digits. However, the downstream Sox9 targets, such as *Sox6* and *Acan*, do show differential expression in the developing limbs and thus form the foundation for new hypotheses with respect to the genetic control of bat digit elongation.

Chapter 3:

Comparative mesenchymal development in bats and mice

3.1 Introduction

Eckalbar et al. (2016) found the IPA analysis of RNA-seq data from the CS15 and CS16 bat transcriptomes, predicted that the Wnt/β-catenin pathway is down-regulated in developing bat FL autopods compared to HL autopods. Wnt/β-catenin signalling is known to suppress chondrogenesis and expression of the Sox9 transcription factor (Solursh 1984, Chimal-Monroy et al. 2003, Raspopovic et al. 2014). Despite chapter 2's findings that Sox9 is not differentially expressed between FL and HL, it would still be interesting to investigate whether the prediction of down-regulation of the Wnt/β-catenin signalling pathway is consistent with larger fields of condensing mesenchymal cells in the CS15 and CS16 FL autopods.

The very first sign of digit formation is the condensation of mesenchymal cells where the digits will develop. As discussed in Chapter 1 and 2, the condensation of these cells causes expression of differentiation markers and in turn mesenchymal cells at the centre of the condensed zone begin to differentiate into chondrocytes which then proliferate. There are multiple steps in the differentiation of chondrocytes (see Figure 1.4) before they apoptose, leaving gaps which will be filled by bone tissue (Hall and Miyake 1992, Hall and Miyake 2000, Akiyama et al. 2002). While these condensed cells differentiate, mesenchymal cells continue to be recruited to the proximal and distal ends of the digits (Goldring et al. 2006, Kozhemyakina et al. 2015). As condensed mesenchymal cells are the first template for the digit metacarpals, it would be interesting to see if there are any differences seen between the bat FL and HL as these fields emerge and the digits continue to recruit cells around them.

Much of our understanding of how digit bones form comes from research done on skeletal development. The vertebrate skeleton is initiated during development as cell condensations, collectively known as the membranous skeleton (Grüneberg 1963). Grüneberg (1963) demonstrated that a number of mutations that affect skeletal development, primarily act on the mesenchymal condensations. If the condensation zone is reduced below a critical threshold, either chondrogenesis will be delayed resulting in a smaller cartilage elements or

chondrification will be absent all together (Gruneberg, 1963). For example it has been demonstrated that initial cell density required for normal chondrogenesis in mice is 5000 cells/mm^2 (Umansky 1966). Many studies on mutations affecting chondrogenesis have shown evidence how these early stages of skeletal development can shape the adult skeleton. An example is Brachypod mice in which digits are reduced due to the increased cell-to-cell adhesion properties of condensing mesenchymal cells. A result of this change in adhesiveness is delayed formation of cartilage and a reduction in the number of cartilaginous elements that finally form (Milaire 1965, Grüneberg and Lee 1973). Extensive work in this field led to the understanding that these mesenchymal condensations play an essential role in skeletal development and in constructing the limb morphology during development which is altered across various vertebrate species (Atchley and Hall 1991).

A number of studies have already looked at potential factors in early limb development that contribute to morphology in the adult limbs. An example is looking at heterochrony, or differences in developmental timing between FL and HL (or between species) that has translated to morphological differences in the adult FL and HL (Bininda-Emonds et al. 2007, Richardson et al. 2009, Hugi et al. 2012). The early *Sox9* expression in the FL of the Talpid mole compared to the HL, discussed in Chapter 2, is an example of where heterochrony is likely underlying the morphological disparity between the size of the FL and HL in the adult (Bickelmann et al. 2012). However it has been noted by Richardson et al. (2009) and Bickelmann et al. (2012) that it is important to take a quantitative approach when looking at heterochrony in developing limbs, as often temporal differences appear obvious at first sight however these differences are not significant. An example is a study performed on the bat species *Rousettus amplexicaudatus*, in which the greatly enlarge adult FL appears to be reflected during early stages of development, however this was not supported by statistical analysis (Bininda-Emonds et al. 2007, Richardson et al. 2009).

Another study on bats has tried to establish when during development the differences between bat FL and mouse FL begin to diverge and when the uniquely elongated digits of the bat wing begin to elongate (Sears et al. 2006). This study used Alcian blue to show that digit condensations and segmentation patterns in bat FL autopods are similar in size and position to those of mice at CS16 and E12.5 respectively. The study however did not present data on the HL cartilage templates at this stage. In addition Haematoxylin and eosin (H&E) staining of CS18

to CS22 bat embryos compared to E13.5 to E15.5 mouse embryos showed that bat FL digits do not begin rapid elongation relative to those of mouse until CS20. At CS20, the hypertrophic chondrocyte zone greatly increases in size, a process that depends on the high proliferation and differentiation of chondrocytes. They found that bat FL digits show relatively high rates of chondrocyte proliferation and differentiation but only starting at CS20.

However, in contrast Hockman et al. (2008) and(2009) reported that mouse and bat FL digit development is seen to differ as early as CS16 in the bat and mouse equivalent, E13. At CS16 Alcian blue cartilage staining reveals asymmetry in the bat hand plate with digits II to V being considerably longer than the thumb (Hockman 2008). In contrast the mouse FL is relatively more symmetrical with digits I and V shorter than II and IV, which in turn are shorter than digit three (Wanek et al. 1989, Hockman et al. 2009). Both these papers looked at cartilage staining which requires the differentiation of mesenchymal cells into chondrocytes. One of the limitations of Alcian blue staining is that it does not mark the earliest stages of digit condensations. The Alcian blue stain recognizes proteoglycan components of the extracellular matrix (both sulfated and carboxylated acid mucopolysaccharides and sulfated and carboxylated sialomucins (glycoproteins)) produced by differentiated chondrocytes.

This study aims to use peanut agglutinin (PNA) staining at these earlier stages (CS15, CS16 and CS17) of bat development, as PNA staining will detect digit chondrogenesis before Alcian blue staining is detectable. PNA staining specifically binds galactose/N-acetylgalactosamine on the cell surface of condensing mesenchymal cells (Zimmermann and Thies, 1984; Milaire, 1991). This allows me to capture digit formation prior to mesenchymal differentiation into chondrocytes. In addition the limb sections were stained with Hoechst, a nuclei dye, to determine cell density and observe limb shape. To establish a better morphology of the developing limbs and digits, serial sections of FLs and HLs of each stage were stained with H&E. This process is carried out in mice of equivalent stages to ascertain if any differences seen between the bat limbs can be attributed to typical FL and HL differences.

Characterisation of mesenchymal condensation behaviour has not been described using PNA in whole mouse limbs during four consecutive stages of development. Thus I will use this opportunity to observe this aspect of digit formation in mice, with aid of the bats limbs as well.

3.2 Methods and Material

3.2.1 *Animal collection and storage*

Mouse (*Mus musculus*; strain C57BL6) embryos were dissected from sacrificed females. Timed-matings were carried out by the Animal Unit at the University of Cape Town Medical School (Faculty of Health Sciences Animal Ethics Committee (FHS AEC), University of Cape Town application number: FHS AEC 014/07 and FHS AEC:15/032; Science Faculty Biological Safety Committee application: BSC009_2015). Females were sacrificed at either 11.5, 12.5, 13 or 13.5 days after cervical plug identification. Embryos were transported in the uterus in cold PBS and dissected out of the decidual tissue within 2 hours for further processing. Whole embryos were fixed in 4% Paraformaldehyde (PFA) for 2 hours at room temperature (RT). The embryos underwent three 5 minute washes in PBS and were stored overnight in 30% sucrose in PBS at 4°C.

M. natalensis embryos were collected from wild-caught females at the guano cave in De Hoop Nature Reserve, South Africa (34°26'S; 20°25'E) on 2 October 2015 and 24 September 2016 (permit Western Cape Nature Conservation Board permit number: AAA007-00170-0056; Science Faculty Animal Ethics Committee (SFAEC), University of Cape Town application number: 2014/V14/NI; Science Faculty Biological Safety Committee application: BSC009_2015). Bats were caught using a harp trap and screened as described previously (Mason et al. 2010) to ensure that only 54 pregnant females (excluding first-time pregnancies) were taken for embryo extraction. Females were euthanised in a chamber containing halothane soaked cotton-wool for a minimum of 5 minutes. Additionally, cervical dislocation and severing of the diaphragm was performed to ensure death. The uterus was surgically removed and placed in cold PBS to enable removal of the embryo from the decidual tissue. Each embryo was staged as described previously (Hockman et al. 2009).

Bat embryos of stages CS14, CS15, CS16 and CS17 were used for histological studies. These embryos were fixed in 4% PFA for 3 hours at 16°C (measured room temperature) after which they underwent three five-minute washes in PBS and were then stored in 30% sucrose in PBS at 4°C for 5-6 days.

3.2.2 *Embedding and sectioning*

The FLs and HLs of sucrose-stored embryos (*M. musculus* and *M. natalensis*) were removed in 30% sucrose in PBS as close to the body as possible. Each limb was placed in a tinfoil mould, filled with Tissue freezing medium (Leica Biosystems), and positioned dorsal side up before being frozen in liquid nitrogen and stored at -80°C. The limbs were sectioned at 8µm using a Leica CM1850 cryotome at -20°C and collected on superfrost® plus slides (Thermo Scientific 1014356190) as described in Figure 3.1. Slides were stored at -20°C until required for staining procedures.

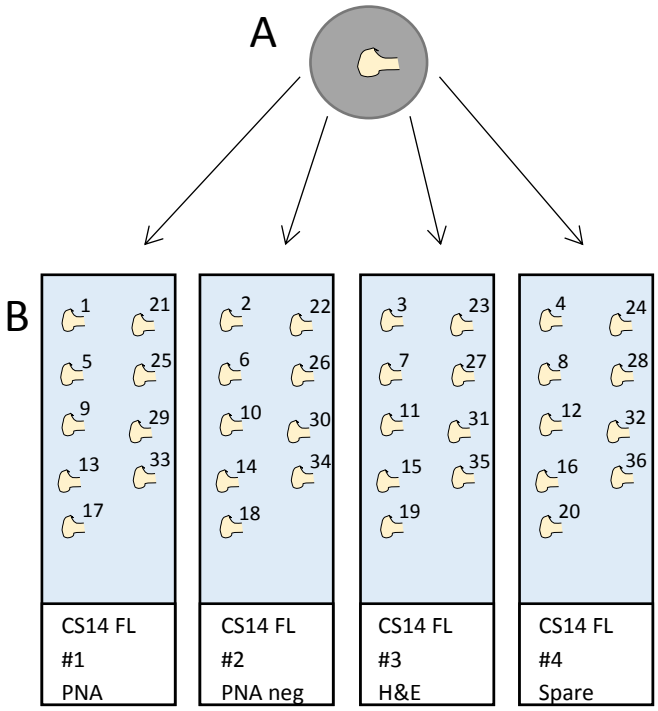

Figure 3.1: Serial section collection on slides. *For each limb embedded in Tissue Freezing Medium (A), four slides were used to collect multiple sections (B). Sections were carefully collected to ensure ventral side was touching the slide in order to keep track of limb orientation. Sections were picked up one at a time alternating between the four slides. Numbers next to each section represent the section number as it comes off the frozen tissue block (A). Thus section 1 will be the most dorsal section while section 36 will be the most ventral. This allows for four comparable slides with a series of continuous sections. The slides are labelled according to the limb, the slide number per limb and the stain that each slide will receive.*

3.2.3 *Staining and visualisation*

3.2.3.1 Haematoxylin and Eosin staining

Sections from the FL and HL of one mouse per embryonic stage (embryonic day (E) 11.5, E12.5, E13 and E13.5) and one *M. natalensis* embryo for each embryonic stage (CS14, CS15, CS16 and CS17) were used for H&E staining to visualise the morphology of the limbs of both species across sequential stages.

Optimisation of the protocol was done on extra mouse limb sections by altering the duration of the H&E exposure and by introducing a differentiation step (acid alcohol) that extracts unwanted haematoxylin from the cytoplasm (Gill & Ascp n.d.). Figure 3.2 presents the optimised protocol used for the sections that were analysed. This protocol produced the greatest contrast between the Haematoxylin in the nuclei and eosin-stained cell structures. Coverslips were mounted with DPX mountant for histology (Sigma 44581) and dried at room temperature (RT) overnight before storage at RT.

The slides were imaged using a Nikon Ti-E inverted microscope under bright field. Images were captured at 4X and 20X.

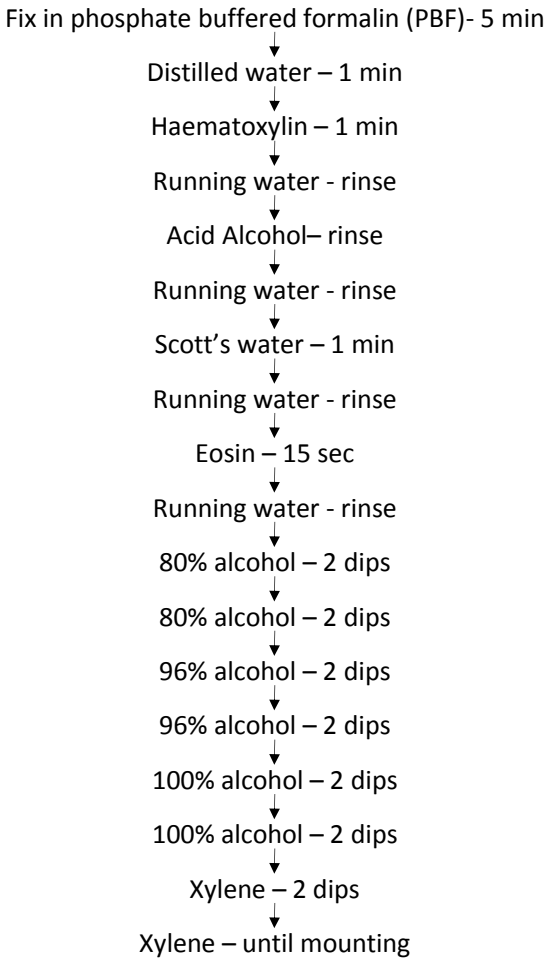

Figure 3.2: Protocol used for H&E staining. M. musculus *and* M. natalensis *autopod sections for final analysis were stained using this protocol where 'min' is minutes and 'sec' is seconds.*

3.2.3.2 Peanut agglutinin (PNA)-FITC conjugate

FL and HL sections were used from three biological repeats of mouse stages E11.5, E12.5, E13 and E13.5 as well as three biological repeats of *M. natalensis* stages CS14, CS15, CS16 and CS17. Slides were fixed for 10 min in acetone and washed in PBS three times for five minutes each time. A one hour block in 3% bovine serum albumin (BSA) (sigma A7906) in PBS for was kept at RT. Sections were incubated with 100 µg/ml peanut fluorescein isothiocyanate (FITC)-lectin (Sigma L7381) in 3% BSA/PBS at 4°C overnight in a dark and humid chamber. Biological FL and HL were always stained in the same experiment along with a PNA control which was incubated with 3% BSA/PBS to normalise for background fluorescence. All slides were washed in PBS and stained for 10 minutes in 1 µg/ml Hoechst nuclei stain, before another three PBS

washes and coverslip mounting with ProLong Gold antifade reagent (Life Technologies, P36934). Slides were allowed to dry at RT in the dark over a period of 2-4 days, thereafter stored at 4°C (protocol adapted from Kroll et al. (2005)).

Slides were visualised and each section was photographed on a Nikon Ti-E inverted microscope using an excitation filter of 460-500 nm and emission of 505-560 nm for FITC detection. Excitation filter of 320-380 nm and emission filter of 435-485 nm for Hoechst detection. All camera settings were kept constant unless stated otherwise. FITC was captured at one exposure time for bat sections (30 ms) and two different exposures in the mouse sections, 30 ms and 100 ms.

3.2.4 *PNA intensity quantification*

Intensity quantification of PNA staining was calculated across all images for all three biological repeats for stages CS14/E11.5, CS15/E12.5 and CS16/E13. Photographs of the PNA and Hoechst sections taken at 30 ms for FITC were processed using NIS elements AR analysis 4.20. For each photograph the section was selected as the region of interest in which the number of pixels at a given intensity (0-255 units) was recorded for both FITC and Hoechst fluorescence (Figure 3.3). Hoechst is presumed to be equally intense in each cell, thus the total FITC intensity was normalised as follows:

```
Sum of (FITC intensity X number of pixels) / Sum of (Hoechst intensity X number of pixels)
```

This value was calculated for each section within a limb (Supp. Fig. 3.1). The top two normalised values for each limb were averaged and then the average across the biological replicates was calculated for each species and stage. These averages were plotted as a bar graphs comparing bat FL and HL as well as mouse FL and HL with standard deviation of the biological variance. In order to perform a student t-test the average for each biological replicate was $\log_2$ transformed to create a normalised distribution of the data. To compare FL and HL within each species a two-tailed, paired student t-test was performed, while to compare bat limbs to that of mice, a two-tailed heteroscedastic student t-test was used. Differences were considered significant when the p-value was less than 0.05.

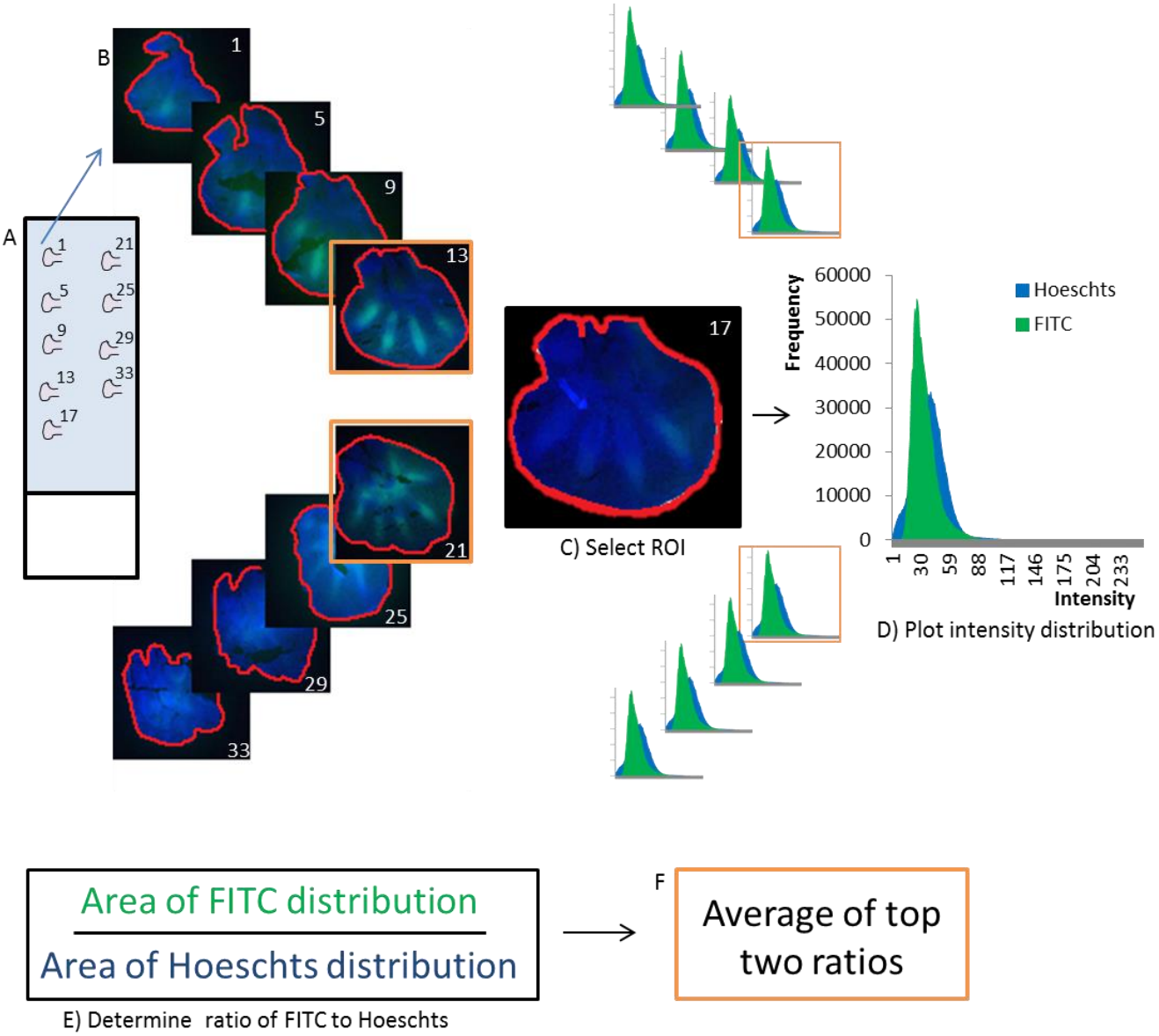

Figure 3.3: PNA intensity quantification*: For each biological repeat, both limbs of the mouse and bat across the stages CS14/E11.5, CS15/E12.5 and CS16/E13, the following process was carried out* ***A****: Slides collected sections that been stained with PNA and Hoechst.* ***B****: Each section per slide was imaged to pick up FITC and Hoechst fluorescence.* ***C****: In each image a region of interest (ROI; red outline) was selected to include the whole section using NIs elements.* ***D****: For each ROI the number of pixels (frequency) was plotted for each discrete level of intensity.* ***E****: The ratio of FITC to Hoechst was calculated for each frequency plot.* ***F****: The average of the two highest ratios (orange boxes) was calculated and used in downstream calculations.*

3.2.5 *Quantifying digit length of PNA digit condensations*

A single photograph of a section containing the greatest number of visible digits at their maximum length was selected per biological replicate of CS16 bat FL and HL autopods. For each selected image the digit length was measured and recorded for digits I through V (where possible) using the length measuring tool in NIS elements AR analysis 4.20 for the FL and HL of

the three biological replicates (Supp. Table 3.2). The average FL-HL difference in digit length for digit I-V was plotted with calculated standard deviation. To determine if the difference between FL and HL was statistically significant a two-tailed, paired student t-test was performed for each digit. In addition the difference between the FL and HL in digit I was statistically compared to the difference seen between FL and HL in digits II-V which was also performed using a two-tailed, paired student t-test.

In order to take the same measurements in mice, the PNA sections taken at 100 ms were used from both E13 (CS16 equivalent) and E13.5 as described above (Supp. Table 3.2). In the mouse autopods there were no sections in which all five digits were present, often with only three present in a given section. Replicates were chosen only if at least one of the same digits was present in both FL and HL so that each FL digit measurement could be compared to its biological HL equivalent. As a result the digits are composed of the following biological repeats - digit 2: 2 x E13 and 2 x E13.5; digit 3: 3 x E13 and 2 x E13.5; digit 4: 3 x E13 and 1 x E13.5; digit 5: 2 x E13.5. The same data presentation and statistical analyses were performed as described with the CS16 bat sections.

3.3 Results

Both H&E and PNA stains worked successfully in staining the cryosections of mouse autopods. While the intensity of the H&E stain was similar in mouse compared to bat sections, the PNA was noticeably more intense in the bats than the mice (Figure 3.4 and Figure 3.5, and see section 3.3.3.1 for quantitative analysis). Due to this discrepancy the mouse sections were photographed at the same exposure time as the bats (30 ms, images labelled “i” in Figure 3.4) for intensity quantification, and at a longer exposure time (100 ms, images lablled “ii” in Figure 3.4) for length measurements and visual comparisons of the mesenchymal condensation histology.

3.3.1 *Characterisation of mesenchymal condensation mouse autopods*

The H&E stain provides contrast to see detail of the development of the cartilage templates before ossification in mouse autopods (Figure 3.4 A, C, E, G, I, K, M, O, Q & R). PNA staining has captured mesenchymal cells that are condensed or recruited for condensation (Figure 3.4 B, D, F, H, J, L, N, O, & P).

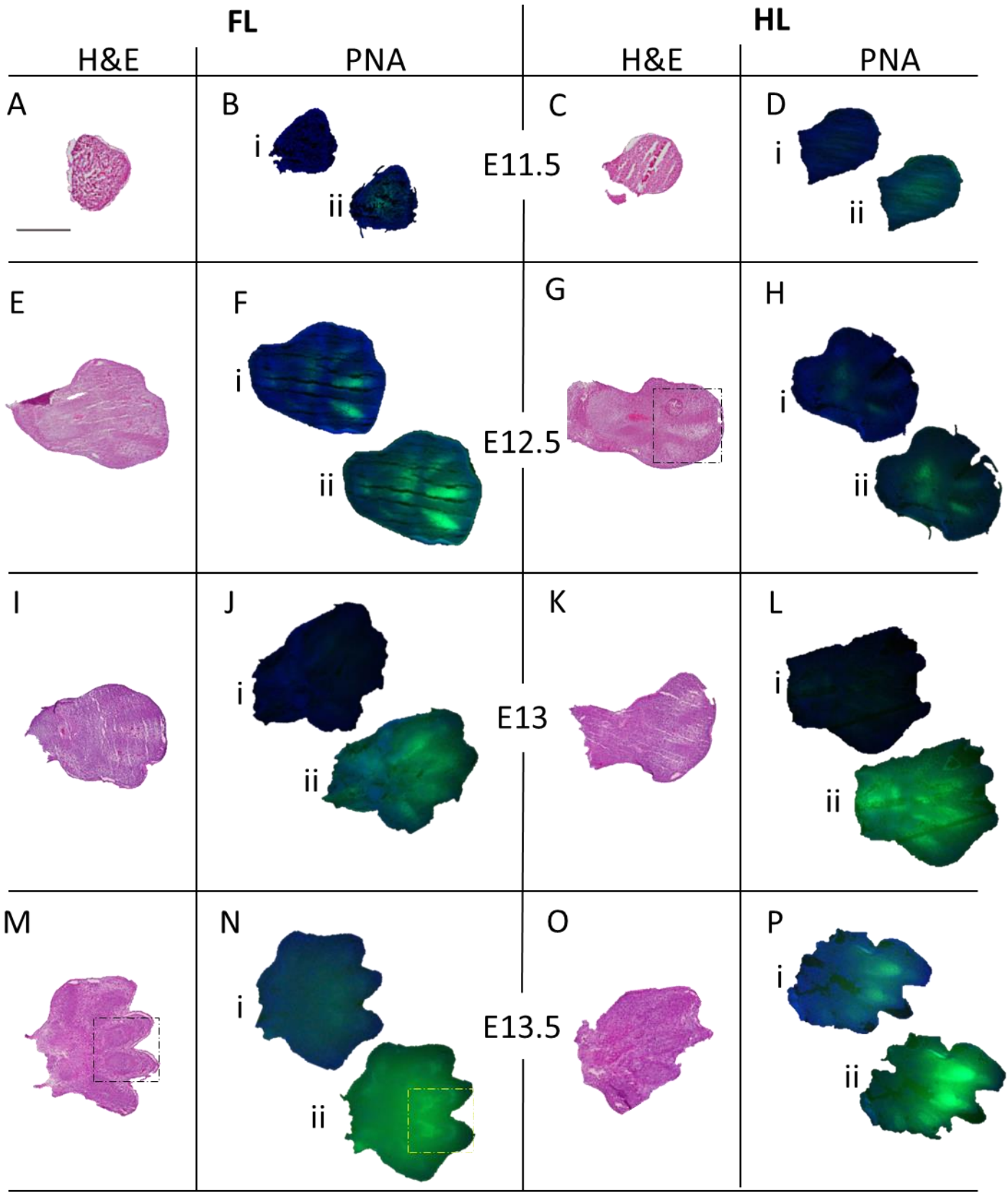
FL
HL
H&E
PNA
H&E
PNA
A
B
i
ii
C
D
i
ii
E11.5
E
F
i
ii
G
H
i
ii
E12.5
I
J
i
ii
K
L
i
ii
E13
M
N
i
ii
O
P
i
ii
E13.5

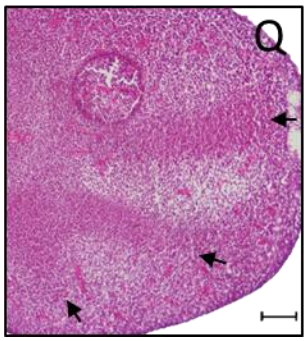
Q

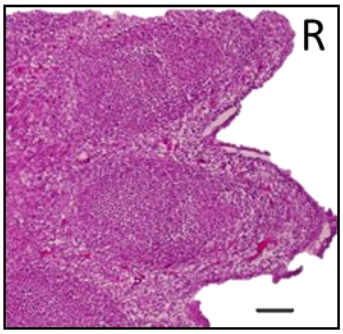
R

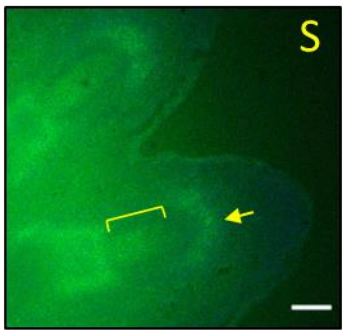
S

Figure 3.4: H&E and PNA autopod sections of developing mouse FL and HL. *Representative sections of the mouse FL and HL. The PNA and H&E stains at each stage were on done on serial sections with exception of the E12.5 and E13 H&E (G, I, K) which are from a different individual to the PNA stain. The PNA FL and HL sections in each stage are from the same individual. PNA sections marked "i" are images taken at the same exposure as the bat PNA images (30 ms) while images marked "ii" are taken at 100 ms to observe mesenchymal structures. Images A-P are all taken at 4X and are to scale with the scale bar in A representing 500 µm. The scale bars in Q-S all represent 100 µm. The boxes in G, M and N demarcate the regions illustrated in Q, R and S respectively. Arrows in Q represent emerging digits, while in S it points to the condensation arc. The bracket in S indicates the shaft region of the digit at E13.5. Brightness and contrast were altered differently in each image to better visualise digit formation.*

At the earliest stages examined, E11.5 H&E staining shows an even spread of mesenchymal cells across the developed FL and HL autopods (Figure 3.4 A & C). The PNA staining is also diffusely stained across the FL and HL autopods at this stage, with the greatest intensity at the centre on the autopod (Fig 3.4 B & D).

At E12.5, the PNA stains for FL and HL, as well as the H&E FL are from the same individual; however the H&E HL is from another E12.5 mouse embryo. The mouse FL H&E stain only appears to have digit condensations for digits III and IV (Figure 3.4 E), while the corresponding PNA stain reveals these two digit templates with strong staining and what appears to be digit II with faint staining (Figure 3.4 F). The mesenchymal condensation for this digit is not visible in the H&E stain. In the E12.5 HL H&E stain we can see three digit condensations, assumed to be digit II, III and IV (Figure 3.4 G & Q) as indicated by the arrows. However only digits III and IV are seen in the E12.5 HL PNA section (Figure 3.4 H). At this stage condensations are evident by the presence of a higher density of cells in the H&E stains (Figure 3.4 E, G & Q) and intense PNA staining in the digit region (Figure 3.4 F & H); however it is not possible to ascertain whether or not the cells have differentiated.

At E13, the H&E sections shown both for HL and FL are not from the same individual as the PNA stains. The H&E staining resembles what is seen at E12.5, with four digits now visible in the FL and three in the HL (Figure 3.4 I & K). The PNA staining at E13 reveals digits II-V in both the mouse FL and HL (Figure 3.4 I, J, K & L). In digits III and IV in both limbs we see the pattern of brighter PNA staining surrounding the digit shaft while there is fainter PNA at the centre of the shaft, likely due to the differentiation of mesenchymal cells into specialised chondrocytes (Figure 3.4 J & L).

At the last documented stage all five digits are present and have taken on a more complex morphology (Figure 3.4 M, N, O, P, R, & S). The digits zones appear to now comprise of multiple cell types as seen in the H&E stains (Figure 3.4 M, N & R). The PNA stains reveal a shaft region which is long and tubular (Bracket in Figure 3.4 S), on either side of which is a larger concentration of condensing mesenchymal cells compared to the shafts (Figure 3.4 N, P & S). Another interesting feature revealed by the PNA staining is the small condensation arcs seen at the distal tip on the mouse FL digits (Figure 3.4 N & S), a feature which cannot be seen in the corresponding H&E stain (Figure 3.4 M & R).

3.3.2 *Characterisation of mesenchymal condensation bat autopods*

At the earliest stages examined, CS14, H&E staining shows an even spread of mesenchymal cells across the developed FL and HL autopods (Figure 3.5 A & C). The PNA section for CS14 HL autopod showed a similar pattern of diffuse PNA staining throughout the autopod (Figure 3.5 D). The section displayed for the corresponding PNA CS14 FL (Figure 3.5 B) shows localised PNA expression and a close inspection of the corresponding H&E stain shows that mesenchymal cells are indeed denser over the area corresponding to the PNA staining (Figure 3.3 A & Q). It is important to note that the distribution of the PNA staining across the CS14 FL varied according to the plane of section. The section in Figure 3.5 B was selected to show PNA staining localised specifically to a forming digit. Figure 3.6 shows the PNA staining in the CS14 FL also displayed widespread staining across the autopod in the dorsal- and ventral- most sections and thus was similar to the CS14 HL staining (Figure 3.5 D) in this respect. Localised PNA staining was not seen in any of the CS14 HL sections.

At CS15 the FL begins to show condensation of three digits, digits II, III and IV (Figure 3.5 E, F, S & T, arrows), while in the HL only two digit condensations are present, possibly digit III and IV (Figure 3.5 G & H). These condensations are seen by the presence of a higher density of cells in the H&E stains (Figure 3.5 E, G & S); however it is not possible to ascertain whether or not the cells have differentiated. The PNA sections reveal forming digits with varying intensities of green but only where mesenchymal condensations are present. In the bat FL digit fields we see an absence of green at the centre of the digit shaft (Figure 3.5 F & T), indicating that these cell are no longer condensing mesenchymal cells and have likely differentiated into chondrocytes.

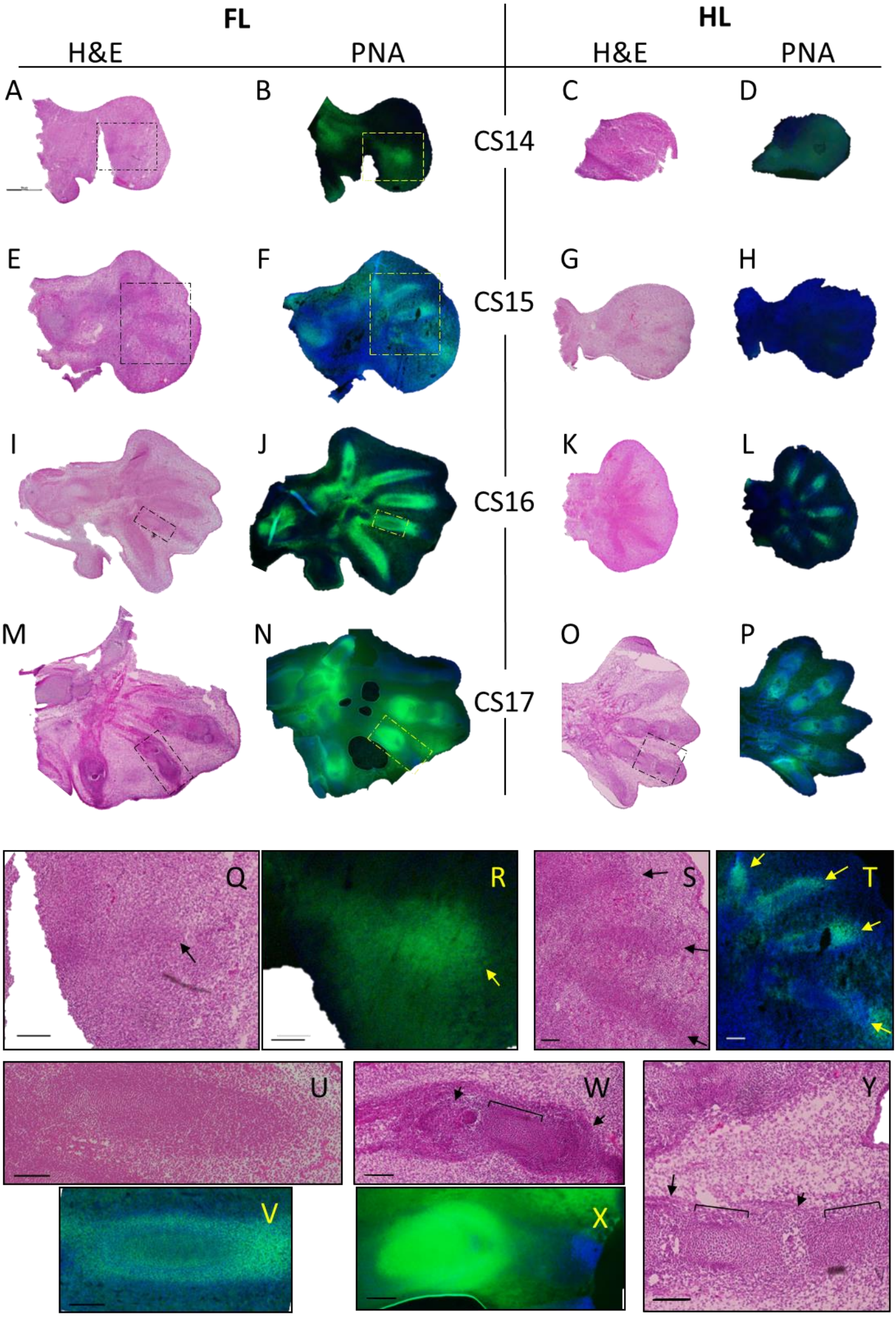
FL
HL
H&E
PNA
H&E
PNA
A
B
C
D
CS14
E
F
G
H
CS15
I
J
K
L
CS16
M
N
O
P
CS17
Q
R
S
T
U
W
Y
V
X

Figure 3.5: H&E and PNA autopod sections of developing bat FL and HL. *A representative section of the FL and HL from each of the consecutive embryonic stages CS14, CS15, CS16 and CS17 studied in the bat species* M. natalensis. *The PNA and H&E stains at each stage were on done on serial sections, and the FL and HL in each stage is from the same individual. The boxes in A, B, E, F, I, J, M, N and O demarcate the regions illustrated in Q, R, S, T, U, V, W, X and Y respectively. Images A-P were all taken at 4X and are to scale with the scale bar in A representing 500 µm. The scale bars in Q-Y all represent 100 µm. Arrows in Q, R, S and T all point to emerging digits, while in W and Y they indicate pre-articulate regions. Single square brackets in W and Y indicate digit shaft regions. Brightness and contrast were adapted differently in images to improve visualisation of the forming digits.*

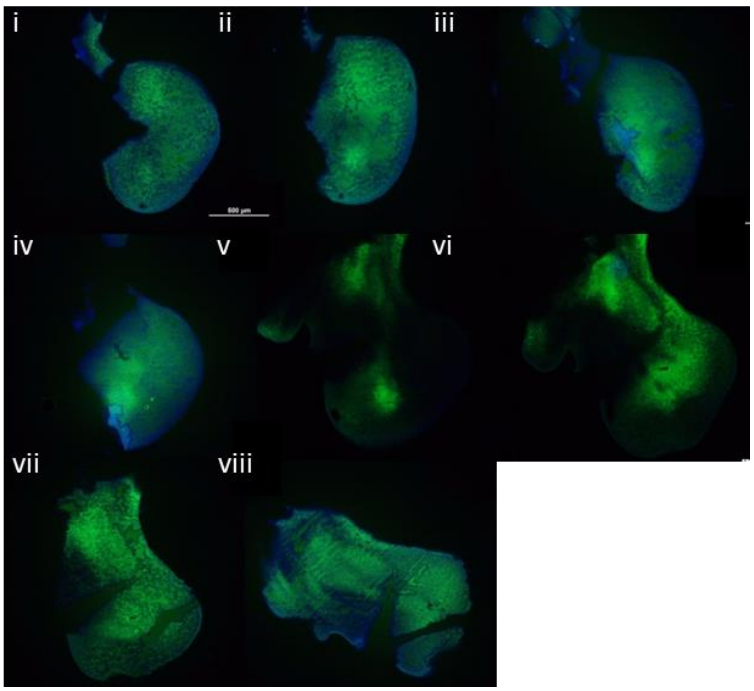

Figure 3.6: PNA staining of CS14 FL moving dorsoventrally through the limb. *The full series of sections collected for bat CS14 FL shows that the dorsal- and ventral – most sections (i-iv and vii-viii) display diffuse PNA staining. The central sections (v and vi) show localised PNA staining where a single digit is forming. All images are to scale, scale bar in i represents 500 µm.*

By CS16 all five digits are evident in the FL and HL (Figure 3.5 I, J, K, L & U). In both bat autopods at this stage, but more evidently in the FL, the cells near the centre of the condensations have differentiated into specialised chondrocytes. This is seen in the PNA sections, where in digits I-IV in the FL and digit II in the HL there is an absence of PNA staining surrounded by the stained mesenchymal cells (Figure 3.5 J, L, V).

At the last documented stage, CS17, the digits have taken on a more complex morphology with a great variation of cell types (Figure 3.5 M, N, O, P, W, Y & X). The digit zones appear to now comprise of two shaft regions which are long and tubular (Figure 3.5 W & Y, brackets). At the centre of the shafts the cells are less dense, likely the hypertrophic chondrocytes. As you move toward the proximal and distal ends of the shaft the cells appear ordered and stacked, characteristic of columnar chondrocytes. In between and on either side of these shafts are joints which in the H&E stains have the appearance of bulbous regions of large cells (Figure 3.5

M, O, W & Y, arrow). The PNA staining reveals these bulbous joints to have a high concentration of condensing mesenchymal cells compared to the shafts (Figure 3.5: N, P & X).

3.3.3 *Qualitative and quantitative comparison of PNA stains of FL and HL of mouse and bat*

The PNA intensity comparisons in this section are only made between images taken at 30 ms for the FITC emission and higher exposures are not considered. However length measurements were done on bat sections at 30 ms and mouse at 100 ms. Importantly, the qualitative data discussed refers only to the images displayed, while quantitative analysis takes into account all the images from the biological replicates (See 3.2.4 and 3.2.5).

3.3.3.1 PNA staining intensity

In looking at the PNA images displayed in Figure 3.4 and Figure 3.5 it is apparent when comparing the PNA sections at the same exposure (30 ms) that there is a higher PNA staining intensity in the bats compared to the mice, especially at earlier stages. Quantitative analysis of the PNA intensity was measured for the three earlier stages, CS14/E11.5, CS15/E12.5 and CS16/E13 when mesenchymal cells aggregate to form the digits. These data agree with the qualitative data showing that the bat FL of CS14, CS15 and CS16 has significantly greater intensity than the mouse FL at equivalent stages ($p=0.01$, 0.002, 0.03 and 0.03 respectively, $n=3$) (Figure 3.7 A, B & C). This same trend is seen in the HL, however only significantly so at CS14/E11.5 and CS16 /E13 ($p=0.04$ and 0.01, respectively, $n=3$)

While there does not seem a difference in PNA intensity between mouse FL and HL, there does appear to be a greater intensity in the bat FL compared to the bat HL at all comparable stages. The quantitative data shows no statistically significant difference between FL and HL in the mouse or bat (Figure 3.7). In the mouse, the pattern of higher intensity alternates between the FL and the HL and P values range from 0.051 to 0.77. However, in the bat we see a consistent pattern of higher normalised PNA fluorescence in the FL compared to the HL for stages CS14, CS15 and CS16 (Figure 3.7 A, B & C) with p-values of 0.07, 0.63 and 0.12 respectively ($n=3$).

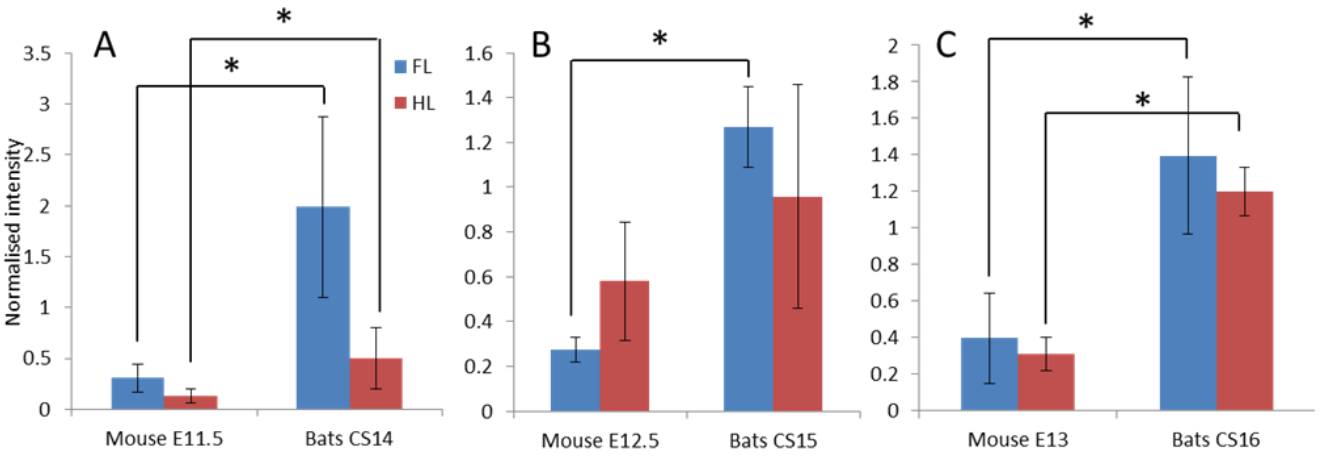

***Figure 3.7: The normalised intensity of PNA staining of mesenchymal cells in the autopods of mouse and bat**. Normalised intensity was calculated as described in 3.2.4 using all PNA sections captured at 30 ms exposure for FITC from all biological repeats for each stage: CS14/ E11.5 (A), CS15/E12.5 (B), and CS16/ E13 (C). The FL and HL of both mouse and bat were compared, with the asterisk (*) indicating a statistically significant difference between two limbs ($p<0.05$, $n=3$). Error bars represent standard deviation between biological replicates.*

3.3.3.2 FL and HL length differences in mouse and bat

The mouse digit length data was only collected for digits II-V for E13 and E13.5 (Figure 3.8 A). Neither the FL nor the HL consistently has longer digits and there is no significant difference between FL and HL for any of the digits measured ($p>0.05$, n varies between digits, see 3.2.5)

The length of all five digits was successfully measured in the bat FL and HL of each of the three biological replicates (Figure 3.8 B). Data analyses revealed that in the FL each digit was longer than their comparative digit in the HL, with digit II and V being significantly longer ($p=0.002$ and 0.007 respectively, $n=3$). It is also noticeable that the difference between the FL and HL digit I is less than the difference between FL and HL in digits II-V, although this is only significant in comparison to digits II and V ($p=0.003$ and 0.01 respectively, $n=3$)

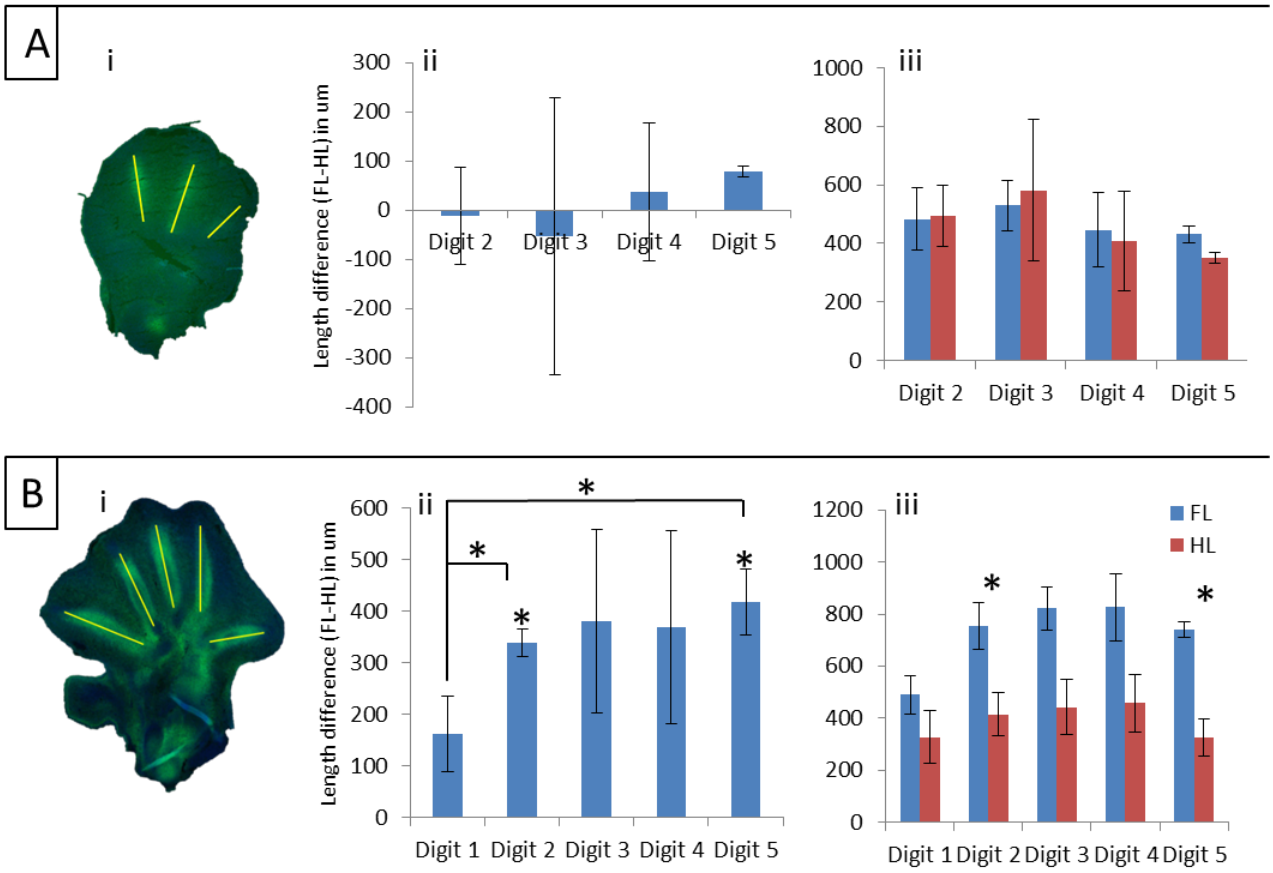

Figure 3.8: The length difference between FL and HL digits in mice and bats. *Digit length comparison between FL and HL of E13 and E13.5 mouse embryos* ***(A)*** *and CS16 bat embryos* ***(B)****. i) An example limb and the length measured is indicated in yellow. ii) The average difference in length between the FL and HL (HL subtracted from FL) of corresponding digits in three biological repeats in bat and multiple biological repeats in mice (see 3.2.5). iii) The average length of each FL digit compared to corresponding HL digit for the same stages as described in ii. Asterisk (*) above a single column (ii) or column pair (ii) indicates the difference between FL and HL is statistically significant ($p<0.05$) while asterisks between two columns indicates the size difference in the difference between FL and HL in the two digits is statistically significant (ii, $p<0.05$). Error bars represent standard deviation between biological repeats.*

3.3.4 *PNA staining dorsoventrally through the limb*

A feature noticed when analysing sections was that the PNA staining intensity would change as the depth of the section changed in what became a predictable pattern. This pattern was only easy to discern when an entire autopod was collected from the most ventral section to the most dorsal. Typically the PNA intensity would start out low and increase as the sections moved dorsally through the limb. The peak in intensity was bimodal with a dip in intensity at the centre of the 3D autopod. After the second peak in PNA intensity the staining would

steadily decrease again. This is illustrated in the sections collected from a bat CS16 HL (Figure 3.9 A). Alongside these are the intensity curves created from all the sections of four autopods obtained from the data collected for 3.3.2.1 (Figure 3.9 B).

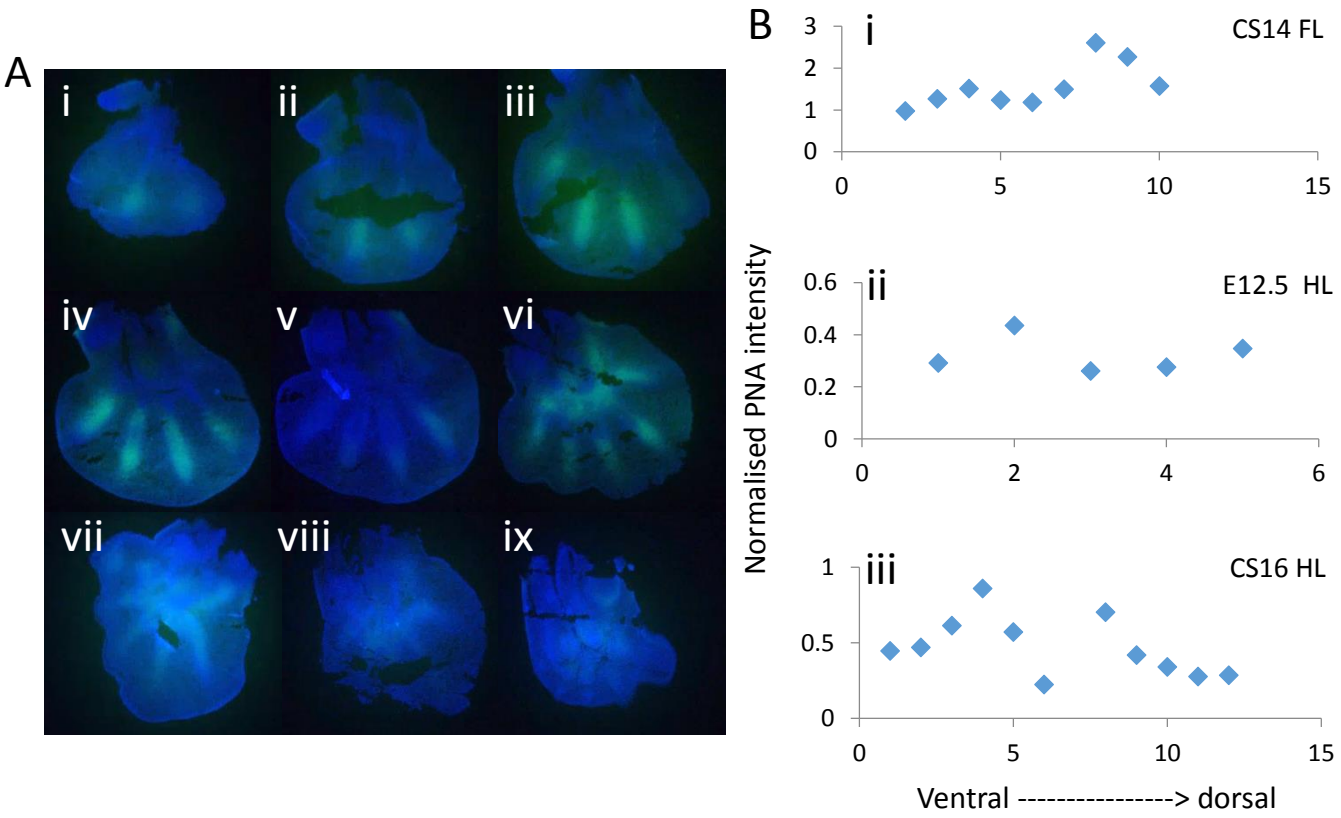

Figure 3.9: PNA intensity moving dorso-ventrally through the limb. A: CS16 bat HL sections starting with the most ventral and moving sequentially through the limb to the most dorsal section. This demonstrates how the PNA staining intensity changes and shows two peaks in intensity likely on either side of the central section (Av). B: Three quantitative distributions, one per stage, of the normalised PNA intensity as section moves from ventral to dorsal sides of the limb. Bi) CS14 FL (bat), Bii) E12.5 HL (mouse), Biii) CS16 HL (bat)

3.4 Discussion

The PNA staining of mouse and bat digit development successfully revealed the patterns of initial mesenchymal condensation during digit formation. Both qualitative and quantitative data has allowed valuable comparisons between the FL and HL digit development of bats in light of the same comparisons in mice. The H&E results produced a set of morphological data

which have been used to validate and enhance the interpretation of the qualitative and quantitative results for the PNA staining in this project. In addition, some of the data can be used to support and enhance the comparative descriptions between *M. natalensis* and mice made by Hockman et al. (2009).

3.4.1 *Using PNA staining of mesenchymal cells to describe digit formation*

Digit formation is a complicated process. In the past the morphological process has been described using various techniques such as staining thin autopod sections with a wide variety of stains such as Alcian blue (cartilage marker) (Hall and Miyake 1992), H&E (Goldring et al. 2006) and immunohistochemistry using Sox9, Noggin or Col2a1 as an early digit markers (Lefebvre et al. 2001, Zhu et al. 2008). Studies have also been done using tissue culture (Umansky 1966, Ahrens et al. 1977, Guntakatta et al. 1984, Diederichs et al. 2016) and in more recent studies 3D tissue culture (Fennema et al. 2013) as well as recombinant limb grafts have been used to further understand limb development (Cooper et al. 2011). PNA, along with other lectins, has also been used before to look at mesenchymal condensations in digit formation (Milaire 1965, Zimmermann and Thies 1984). However this is the first comprehensive study to characterise the behaviour of condensing mesenchymal cells during four consecutive stages of digit formation in the whole mouse and bat autopod using PNA.

It is important to note that mesenchymal condensations are only one part of a bigger picture in the formation of digits. However they hold much importance in being the primary resource from which the skeleton is built (Hall and Miyake 2000). Although PNA only stains the mesenchymal cells, we are able to ascertain a lot of detail regarding the digit shape, length, stage of development and even where further differentiation of mesenchymal cells has occurred as seen in the images presented in this study. While shape and length are easily determined using Alcian blue and many of the immunohistochemistry stains, many of these stains have caveats. For example, Alcian blue will stain the chondrocytes allowing visualisation of digit formation but only after mesenchymal cells have differentiated, thus missing the earliest stages. Labelling of *Sox9* or *Noggin* will allow visualisation of both mesenchymal cells and chondrocytes; however it will not be possible to differentiate between the two cell types (Lefebvre et al. 2001, Zhu et al. 2008). In addition to gaining insight into the digit morphology,

this study also aided in describing some interesting features or behaviours of these mesenchymal condensations.

3.4.1.1 Dispersed PNA staining prior to and during early digit formation

Firstly, it was interesting to see that as the digits condense, and even just before digit condensation has occurred, the cell surface molecules on which PNA lectin adheres are already present in the dispersed mesenchymal cells, as evident by the green fluorescence which coloured most of the section of the autopod in both bat and mouse at CS14/E11.5. It suggests the programming of a mesenchymal cell to condense is not initially dependent on positional information within the autopod. Raspopovic et al. (2014) suggested that the periodic digit and interdigit fate of cells is set up by the interaction of diffusible molecules, as discussed in Chapter 1. Thus it is suggested that the diffusion molecules have not begun interacting at this early stage and that all cells have the potential to become digits cells.

In the CS14 bat FL the H&E revealed a single, narrow zone of mesenchymal condensation that appeared in the region digit IV would be expected to form. It has been reported in mice that digit IV is the first digit to form during development (Zhu et al. 2008), and thus seems to also be the case in bats. This feature was confirmed by the corresponding PNA section where the intensity of FITC signal gets stronger in the same region but over a much larger area. The fact that PNA fluorescence is over a larger area is likely due to the fact that all mesenchymal cells initially are able to bind the lectin but later this ability is lost in peripheral and interdigital cells.

However the more dorsal and ventral sections of the same limb showed that despite a digit beginning to form, the PNA still stained generally in the limb, suggesting these more dorsal and ventral cells have not yet had their digit/interdigit fate determined, as seen in the corresponding bat HL and both limbs of the mouse at the equivalent stage. It does not appear that the interactions between the Turing-like diffusible molecules occur throughout the limb simultaneously. Perhaps the interaction begins in the region of the first forming digit and then expands to create the alternating digit/interdigit rays described in Raspopovic et al. (2014) and seen in the E12.5 and E13 H&E mouse sections in this study.

3.4.1.2 Order of digit appearance

The presence of two to three digits in autopods is observed at CS15 in the bats and E12.5 in the mice. In mice, it has been reported that after digit IV the order of digit appearance is digit II, then digit V, followed by digit III and finally digit I (Zhu et al. 2008). However a more recent paper suggested that digit IV is followed by digit III, then II then V and lastly digit I (Raspopovic et al. 2014). While the initial order is not clear in either the bat or the mouse digit formation in this study, the first three digits that appeared in the mouse were digits II, III and IV which agrees with the more recent findings by Raspopovic et al. (2014). The E13 mouse limbs then reveal digit V, again supporting the findings of Raspopovic et al. (2014). The PNA stain of the CS15 bat FL section suggests that the next digit to appear after digits II, III and IV is digit I, which is contrary to the two studies mentioned previously as well as the mouse data. However it is likely that the embedded limb was at a slight angle during sectioning and digit V is thus not seen. At CS16 we see all five digits and digit V appears longer than the others, again supporting the idea that it was present at CS15, just not intersected in the displayed section.

3.4.1.3 PNA staining allows us to determine differentiated chondrocytes and joints

A study by Aulthouse and Solursh (1987) showed that PNA was only able to bind to pre-chondrogenic cells using cell cultures and as soon as cells differentiated the binding ability of the lectin was abolished. Similarly both Zimmerman and Thies (1984) and Milaire (1965) reported weak PNA binding to chondrocytes compared to mesenchymal cells and the perichondrium in developing mouse limb skeletal elements. In this study we see a near-absence of FITC at the centre of the digit zone in the CS15 bat FL which is likely due to mesenchymal cells differentiating into chondrocytes. However the size and shape of these differentiated cells is not discernible from the mesenchymal cells at the observed magnification of the corresponding H&E section and thus this differentiation event is missed if only looking at cell morphology.

At CS16/E13 the now elongated condensations all have a central zone with weaker PNA binding and little information regarding cell identity in this central region. In the next developmental stage these previously continuous condensations segment to form two pre-articular zones separating the digit shafts. The PNA FITC stain reveals the high number of mesenchymal cells aggregating at the joints compared to in the digit shaft in line with what was reported in Milaire

(1991). Within the shaft, the H&E stain allows us to see the predicted stages of differentiation as you approach the centre of the shaft, with columnar chondrocytes on either end and hypertrophic chondrocytes at the centre (Akiyama et al. 2002, Kozhemyakina et al. 2015). In the mouse limbs the arcs of PNA staining could be one of two features; one possibility is that the mouse paw sectioned was curved, resulting in the second pre-articulation mostly lying in a more ventral plane. This arced feature may then be the start of this second joint. Alternatively the arc could be what has been described as the organising centre of the digits under the apical ectodermal ridge that consists of a continual accumulation of new pre-chondrogenic cells required for the growth of the cartilage element (Hiscock et al. 2017). This region is termed the digital crescent or pharynx forming region (Montero et al. 2008, Suzuki et al. 2008).

3.4.1.4 H&E and PNA staining comparison

Overall the H&E stain allowed visualisation of some specific features of digit formation, such as the more intense condensations and the latter stages of cell differentiation into the columnar chondrocytes and hypertrophic chondrocytes. The PNA on the other hand was able to detect mesenchymal condensations at lower densities and better define the digit boundaries at the earlier stages of digit formation. It also allowed us to visualise the recruitment of more mesenchymal cells, such as at the joints in CS17, which was not possible from the H&E stains alone. The PNA lectin allowed us to distinguish between mesenchymal cells and cells that had differentiated into chondrocytes (no longer stained), unlike the H&E. Together, the two stains used worked well in supplying detailed information of the process of digit formation.

3.4.2 *A comparison between bat and mouse digit formation*

The bat species in this study, *M. natalensis*, has been comprehensively compared to mouse development by Hockman et al. (2009). However this study seeks to focus on the development of the digits in sections of the autopods, using the H&E and PNA stains.

In visualising the PNA staining comparisons between the FL and HL in mouse and bats, it was immediately obvious that the bat sections showed greater PNA intensity than the mice. This was then confirmed by the quantitative analysis in which the bat autopods at each stage showed an average intensity far greater than the corresponding mouse autopod, and of the six

comparisons, five were significantly greater. The higher intensity of PNA staining would suggest there are a larger number of condensing mesenchymal cells in the formation of bat FL and HL digits compared to that in mice. It is also possible that the bat mesenchymal cells contain more cell surface molecules that bind the PNA than the mouse cells do. While the bat limbs were all dissected and processed for embedding at the same time, the various mouse limbs were processed at multiple time points over two years. Thus it is unlikely that this contrast in PNA intensity is due to preparation differences alone as there not more variation amongst the mouse sections than the bats.

In order to then visualise the mouse digit formations, the exposure time of the PNA sections was increased which revealed similar patterns of digit formation as seen in the bat limbs. The timing of digit formation was similar in the mouse and bat stages, supporting the classification by Hockman et al. (2009) of comparable mouse and bat developmental stages. The two species both enter the first process of chondrogenesis between equivalent embryonic stages, CS14 - CS15 in bats and E11.5 - E12.5 in mice as supported by the literature (Raspopovic et al. 2014, Kozhemyakina et al. 2015). The HL of the bat and mouse at these equivalent stages are incredibly similar in appearance. The mouse FL was closer in size to the two HLs compared to the bat FL which was larger than all other limbs compared at these stages. Additionally, there was a single digit, digit IV, present in the FL of the CS14 bat embryo displayed in Figure 3.5 A and B; however this was not seen in the other two biological repeats of the bat FL. Although the bats and mice were comparably staged, the differences in the early stages can be a matter of hours to days (Cretekos et al. 2005) and the this particular bat embryo was classified as CS14 'late' while the other two biological repeats were CS14 'very early'.

At CS16 in bats, the limbs begin to differ morphologically from the mouse, acquiring their bat-like appearance. This data is supported by the staging analysis of this species by Hockman et al. (2008) and (2009). Interestingly all five digits in the bat FL and HL are visible in each biological replicate, while in the mouse autopods no more than four digits are present at one time in the sections. This may suggest dorsal-ventral curvature of the mouse paw at E13 on the proximal and distal sides. At E13.5 we now see all five digits however the H&E sections do not nearly show the same detail as the CS17 bat autopods which clearly display the formation of the joints and digit shafts. We are, however, able to see these features in the mouse through the PNA staining.

Overall the bat sections provided more insight into the behaviour of both mesenchymal cells as well as the general process of digit formation which is likely due to the bat limb being larger in size in the later stages of development.

3.4.3 *A comparison between bat FL and HL*

The hypothesis that a higher activity of the Wnt/β-catenin pathway in the bat HL, reported in Eckalbar et al. (2016), would result in smaller fields of chondrocytes was tested in a number of ways which yielded varying results. Firstly the PNA intensity was compared in the bat FL and the HL with no statistical difference found. However the pattern showed that the average intensity in the FL was higher compared to the HL in the earlier stages, CS14, CS15 and CS16, corresponding with when the Wnt/β-catenin pathway is significantly downregulated at CS15 and CS16 (Eckalbar et al. 2016). The difference at CS14 was close to significance with a p value of 0.07 and perhaps with an increased sample size the difference in intensity may become significant. This difference however was also seen at the equivalent stage in mice (p=0.051) suggesting that the intensity difference maybe be a result of a developmental lag between the FL and the HL as suggested by Hockman et al. (2009) and Cretekos et al. (2005). Another report that looked at the synchrony of FL and HL development in 14 different vertebrate species reported that there was no developmental lag seen in the bat species *Rousettus amplexicaudatus* (Bininda-Emonds et al. 2007).

In this study the evidence for the developmental lag of the HL in *M. natalensis* is the first seen at CS14 when a single digit primordium appears at the centre of the autopod. There is no evidence of any condensations occurring in the same individuals HL. In the next stage, at CS15, the bat FL clearly contains three digit condensations while only two have appeared in the bat HL. Only one other biological replicate was collected at CS15 and the FL of this individual shows two digits while none are seen in the HL. By CS16 it becomes more difficult to discern whether there is a developmental lag as all digits are present and any difference may be attributed to FL/ HL morphological differences as opposed to heterochrony.

Although there was no difference seen between the bat FL and HL PNA staining intensity, there was a significant difference in the PNA intensity between the bat FL and mouse FL across all four stages, while at only two stages did we see the same pattern in the HLs. In addition there was less of a developmental lag noticed in the mouse HL. Bickelmann et al. (2012) suggests

that differences in timing during development can have an influence of adult morphology such as in the example of the Talpid mole discussed in Chapter 2.1.

Another aspect compared between the FL and HL of the bats was the length of the condensations at CS16. The down-regulation of the Wnt/β-catenin in the FL autopods was seen at CS15 and CS16, thus these are the two optimal stages to compare condensation size. However, at CS15 not all digits were present and only two biological replicates were sectioned in the bats. The measurements were thus taken from the CS16 embryos which contained all five digits in both FLs and HLs. As expected there was no significant difference between the FL and HL of digit I of the bat as this digit does not elongate as digits II-V do in the adult. Of the digits seen to be greatly elongated in the adult FL, all were already seen to be longer in the CS16 FL compared to HLs, with two of the digits significantly so. To add to this, the mouse digit length data did not resemble that of the bats at all. There was little difference between FL and HL and no differences were significant. This contradicts the report by Sears et al. (2006) that suggests differences between the bat digits and that of mice can only be seen at CS20. While these results add to the reports by Hockman et al. (2009) that suggest differences between bat FL and HL are first seen at CS16.

The hypothesis that a higher activity of the Wnt/β-catenin pathway in the bat HL would result in smaller fields of chondrocytes was thus supported in that smaller zones of pre-chondrogenic cells are measured in the HL compared to the FL. This difference is seen in the last stage, CS16, in which Wnt/β-catenin is upregulated. However this data is only correlative and causation would need to be assessed via the means of genetic manipulation.

3.4.4 *The challenges of sectioning*

3.4.4.1 Varying intensities of PNA when moving dorso-ventrally through the limb

As demonstrated in the results, the limb sections do not have a consistent intensity of PNA as you move dorsoventrally through the limb. From the pattern seen in a limb in which many consecutive sections were collected and stained, the PNA intensity decreases in the centre-most section. It is hypothesised that in the later stages of digit condensation, once central mesenchymal cells have begun to differentiate, the mesenchymal condensations exist at the periphery of the 3-dimentional digit oval as illustrated in Figure 3.10 A. As a result, sectioning

this shape will mean the lowest cross-sectional area of mesenchymal cells will exist in the centre most section (Figure 3.10 B). The reason the PNA starts out low is possibly because the digits are placed centrally and thus the dorsal- and ventral-most section will not yet have intersected with the digit fields. In favour of this theory is that there are some sections within a limb that do not show the differentiation of cells at the centre of the digit shaft, but instead digits appear as a large oval region of purely condensed mesenchymal cells as explained in Figure 3.10.

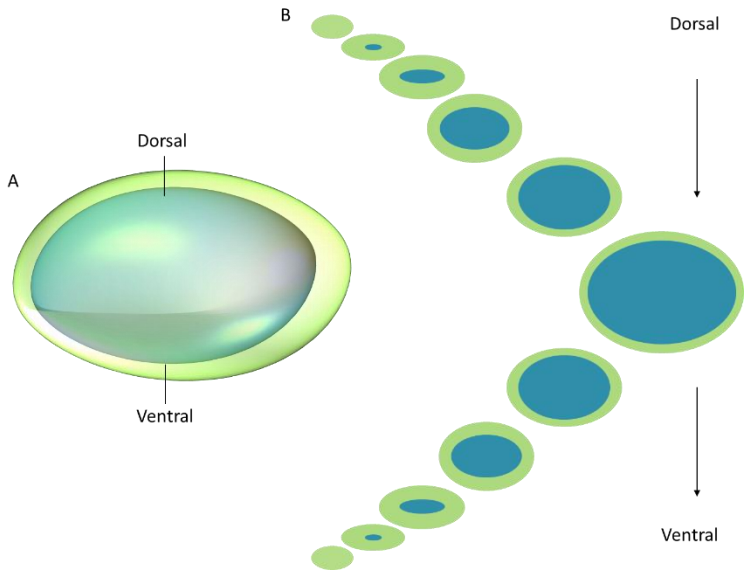

Figure 3.10: Schematic of PNA-stained digit sections and hypothetical model of PNA staining of 3D digits. *A: a hypothetical representation of a 3-dimensional developing digit field stained with Hoeschts (blue) surrounded by a layer of condensing mesenchymal cells stained with PNA-FITC (green). B: Sections of 8 um were taken from embryonic limbs with developing digits from the ventral side of the digit, down to the dorsal most section. This creates a pattern of FITC florescence (green) around each digit as illustrated, initially seeing small digit fields condensations. As we move though the digit, the digit gets larger and mesenchymal region is seen mainly on the peripheries of each digit. The halfway mark will contain the least FITC fluorescent as just a thin layer of mesenchymal cells is present on the peripheries. From here, the pattern will reverse and digit fields will get smaller with a greater region of condensing mesenchymal cells present until the digit section is, again, only made of condensing mesenchymal cells.*

The variation in the PNA staining intensity is not an issue when most of the sections are successfully collected. However, this is not the case for all limbs and often sections were torn or folded, resulting in the number of sections obtained for a given limb ranging from 1-14. Having as few as 1-3 sections means there is not enough context to discern where those sections lie in the dorso-ventral plane which in turn makes comparisons between two limbs difficult. When displaying images, often compromising the perfection of a section for better representing the staining potential is required as well. In addition there are situations when the three biological replicates are displaying a very different trend which again makes it difficult

to draw conclusions. It thus important to do quantitative analysis using as many of the sections as possible in order to minimise any bias introduced in describing the qualitative data.

3.4.4.1 Quantifying images

It is easy to qualitatively assess the images however quantifying images is inherently difficult. For example, visually, the bat FL sections seem to show much greater PNA intensity compared to the bat HLs. However when attempting to quantify this, the results came out as not significant. The method used to quantify PNA intensity was one of many that could have been selected, each with caveats. Due to the varying quality, number and size of the sections across stages, species and replicates it was decided to normalise the PNA fluorescence to the Hoechst stain which should stain each cell equally. Effectively the amount of PNA intensity per cell was calculated. The problem with this method is that in the older bat embryos the number on non-stained cells (i.e. interdigital cells) will be high in the FL, as the bats retained their FL interdigital webbing, compared to their HL, where interdigital tissue regresses. These means the ratio values will be lower in the FL due to more interdigital cells rather than because there are less mesenchymal cells. An alternative method to quantify the PNA may be to find the average intensity in the 10% of pixels emitting the highest FITC intensity. This would then eliminate the area of the interdigital region confounding my results and may lead to significant differences seen between the PNA intensity in the FL and HL of bats.

3.4.5 *Conclusion*

This work has successfully added additional information to the behaviour of mesenchymal cells during digit formation and supported much of the work on limb development in both mice and bats. In addition we have gained quantitative evidence that the bat wing digits are already longer than that of the HLs at the early stages of digit formation during mesenchymal condensation. This suggests molecular instruction to pattern the layout of the wing digits is in action from these early stages and gives support to the RNA-seq studies by Eckalbar et al. (2016) and in Wang et al. (2014) analysing these key stages of bat development.

Chapter 4:

Steps towards developing an experimental system for functional genetic studies in bat limb cells.

4.1 Introduction

In the recent RNA-seq study conducted on developing *M. natalensis* limbs, nearly 3000 genes were found to be differentially expressed between the FL and HL, providing a suite of candidate genes that likely play a role in the development of the bat wing (Eckalbar et al. 2016). One such gene was *Hoxd11* which was found to be significantly upregulated in the bat FL compared to the HL across stages CS15, CS16 and CS17, a pattern which is not seen in similar staged mice (Mason 2016). In addition the spatial and temporal patterns of *Hoxd11* have been characterized by *in situ* hybridisation, however further experimental systems are needed to dissect the gene regulatory elements that are driving the differences in gene expression.

Functional genetics can be used to dissect the role and regulation of genes during development. *In vivo* studies are the ideal method for looking at pathway interactions and the processes that govern limb development. Genes or pathways of interest can be analysed within the context of all other influential factors. *In vivo* studies of transgenic lines are however only possible when working with model organisms where the accessibility to embryos is not limiting and where protocols have been developed for manipulating gene function, including generation of embryonic stem cells, harvesting of blastocyts and implantation into surrogate mothers.

Transgenic *in vivo* studies are currently not possible to conduct in wild, non-model organisms, where sample size is limited and the methods for manipulating embryos and adult females to create transgenic offspring do not exist. In addition it is not ethical to manipulate wild animals. The bats used in the RNA-seq study as well as my work, *Miniopterus natalensis*, are particularly constraining for a number of reasons. Unlike mice, each pregnant female only carries one embryo per year, meaning a female is removed from the population for each embryo required (Kunz and Kurta 1987, Mason et al. 2010). While *in vivo* techniques such as *in situ* hybridisation and histological stains are possible, it is not sustainable or ethically justifiable to be killing up

to three bats and embryos, one gene at a time, for evolutionary development work. Therefore, other methods need to be developed to study how gene regulation in bats has changed.

Another system for pathway and gene expression studies is to develop primary cell cultures *in vitro*. Primary cell cultures can be made from an entire limb or autopod, which is homogenised into a cell suspension and plated as a single layer of cells on a culture dish. In this case all cell types will be present, potentially influencing the expression profiles of surrounding cells. For example in Cooper et al. (2011) a cell culture system was developed from chicken HH18 proximal mesenchymal cells which were reported to have differentiated soon after plating, coinciding with *Sox9* expression increasing as soon as 10 hours after plating. To maintain cells in a non-differentiated state, the researchers added Wnt3a, Fgf8 and Retinoic acid factors to the media, which resulted in the suppression of *Sox9* expression.

Primary cell cultures have the added advantage that they can also be cryopreserved by freezing and then thawed so experiments can be carried out at a later time, a benefit unfeasible in an *in vivo* setting. Experiments on primary cultures include manipulation of gene expression and cell behaviour via the supplementation of known signalling molecules, the results of which can be quantified, facilitating a better understanding of pathways and gene interactions (Cooper et al. 2011). For example, a study on osteoarthritis, looking at human articular chondrocytes, successfully knocked out an inflammatory receptor, IL1R1, using CRISPR/Cas9 to determine the receptors effects on chondrogenic re-differentiation potential of the cells. This was assessed by looking at the relative levels of *Acan* and *Col2a1* mRNA and protein levels of cells grown in re-differentiation medium with and without recombinant IL1R1 (rIL1R1). The results showed that cells had no re-differentiation ability in the presence of rIL1R1 as *Acan* and *Col2a1* expression was inhibited. In the absence of rIL1R1 a significant upregulation of *Acan* and *Col2a1* was seen (Karlsen et al. 2016). This shows the potential functional studies that can be carried out *in vitro* through manipulations of genes and external factors such as media supplementations. However, a major limitation of primary cell cultures, is that they eventually die as they have a finite number of cell divisions (Hayflick 1965). Thus use of primary cell culture does not negate the need to collect fresh embryos and sacrifice mothers, thus it remains ethically questionable.

Immortalising cells in primary cultures removes the life span limitation of primary cell cultures, and the need for continued harvesting of bat embryos. However, unlike primary cell cultures, immortalized cell lines are derived from a single cell and are thus homogeneous. This can be advantageous for certain assays such as dissecting gene regulatory elements driving differential gene expression in FL vs HL cells, and for looking at differences in chromosome confirmation architecture. There are thus three potential systems for looking at candidate genes post the RNA-seq and ChIP-seq which have advantages and disadvantages depending on the assay, which have been summarised in Table 4.1 below.

Table 4.1: Advantages and disadvantages of functional genetics experimental systems. *Three systems that can be used to functionally test candidate genes after RNA-seq and ChIP-seq assay from* M. natalensis

	Experiment types	Advantages	Disadvantages
In vivo system	- *In situ* hybridisation - Histological stains	- Spatial and temporal expression of differentially expressed genes - Most biologically relevant	- Information gained per embryo is low - Requires many embryos
Primary cultures	- Reporter gene assays - Chromatin confirmation - Enhancer element analysis	- maintains partial biological relevance - Multiple experiments per embryo	- Cells have a life span - Requires continual embryo collection - Variation in results due to multiple cell types cell types
Immortalised cell lines	- Chromatin confirmation - Enhancer element analysis	- Few embryos required once off - Perpetual supply of cells - Homogeneity of cell type allows for clearer results and more information	- Limited in which experiments are biologically relevant

To create an immortalised cell line, primary cells are mutated either naturally (Syverton and Scherer 1952) or intentionally via an array of techniques used to stop cell cycle arrest and senescence, thus allowing the cell to continue dividing indefinitely. Typically, when producing a new immortalised cell line, a single cell type is isolated to form a monoclonal culture (Boolay 1999, Illing et al. 2002). Immortalised cell cultures are advantageous over primary cultures in that it only requires one initial tissue collection, reducing the ethical implications of a study. In addition, due to the homogeneity and perpetuation of the cells, experiments are more comparable across time points and study groups.

In terms of limb studies however, the complexity of the limb system will be reduced in a monoclonal culture. Although cell lines cannot be used to study interactions between different

cell types, they are useful for analysing the regulation of specific genes, for example *Hoxd11*. Although the use of an oncogene to immortalise cells can affect the cell properties, the cell lines are still a useful resource if expression of genes of interest remains unchanged. In addition, methods have been developed to reverse the rapid cell division and immortalisation effects in a conditional manner, thus restoring some of the natural gene expression and cell behaviour (May et al. 2005).

Since transgenic studies in wild bats is not possible, and material for primary cell cultures is limited, an immortalised bat FL and HL autopod cell line would enable genetic manipulation and observation within the context of the bat system. The advantages of an immortalised cell line which can be used for functional studies far outweigh the disadvantages. Induced differentiation or expression of specific genes can be quantified after the supplementation specific ligands as seen in Rodrigues et al. (2017) where Shh and Fgf8 were added at varying concentrations to observe the quantitative effects on *Hoxd13* expression. It would also provide a homogenous group of cells on which gene editing techniques such as CRISPR/Cas9 could be used to create enhancer manipulations and gene knockouts.

Before bat limb cell lines can be established, a protocol to produce a viable primary cultures from tissue collected in the field needs to be developed. Once the methodology for preparing primary cultures has been established, the primary cultures can be infected with the temperature sensitive (ts) A58 SV40 large T antigen oncogene (Illing et al. 2002). The large T antigen (Tag) is important for immortalization of cells via the inhibition of p53 and Rb-family of tumour suppressors (Ahuja et al. 2005). The SV40 Tag is isolated from the SV40 viral genome; however this process intentionally removes the genes required to package and encapsulates the viral DNA (Brown et al. 1986). In order for the isolated SV40 Tag construct to be transfected and integrated into the genome of target cells, a retrovirus shuttle system has to be created (Mann et al. 1983). The viral genes *gag, pol* and *env*, coding for the viral packaging, reverse transcriptase and envelope proteins respectively, needed to be added to the construct to house the ts SV40 Tag for transportation and also to facilitate entry into the target cell. However, if the new combined construct would be transferred to the target cells, those cells too, would become infectious which could pose a health risk for the researcher as well as an undesired function within the target cells. To reduce this risk, these additional viral genes have been integrated into the packaging cell lines to which the immortalisation viral construct can

be added (Figure 4.1). The packaging cell lines will then produce the viral construct as well as the genes required to house the construct for efficient transformation into the host (Mann et al. 1983).

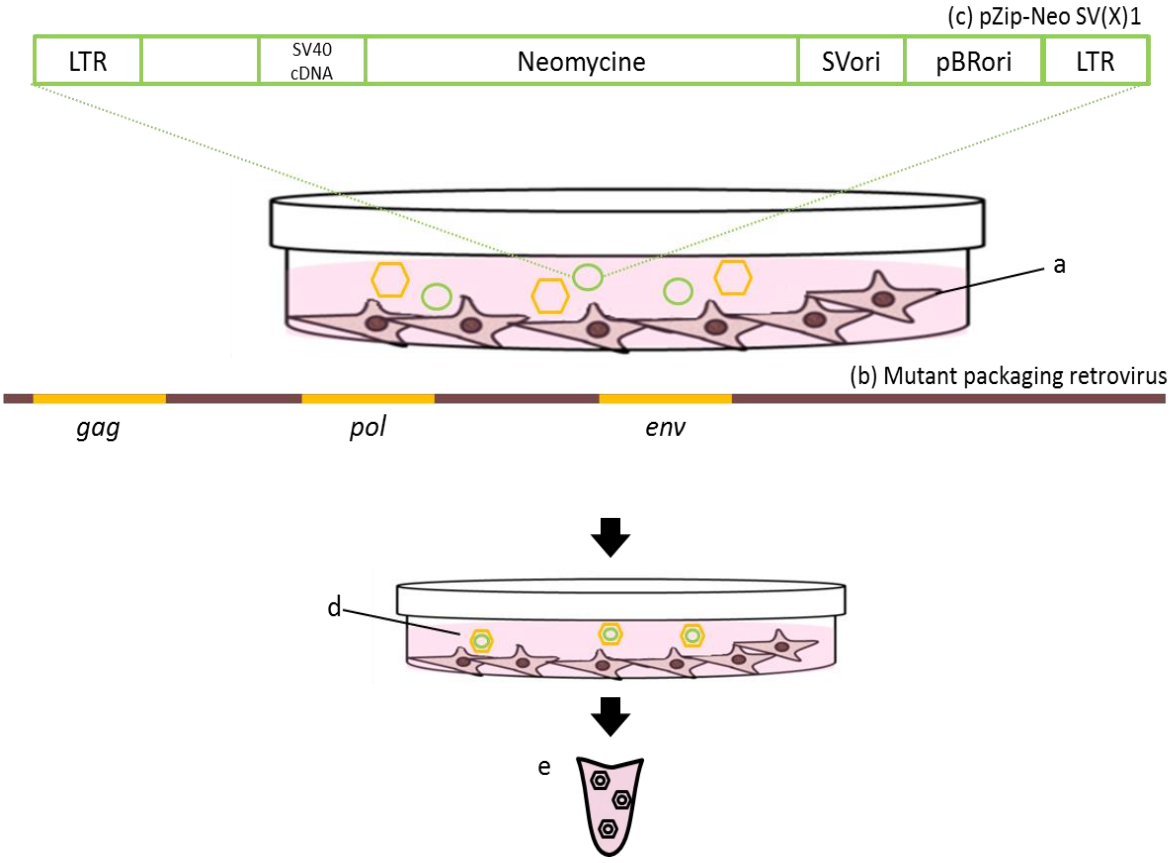

Figure 4.1: Packaging cell line and SV40 immortalisation system. *A cell line (a) is transformed with a retrovirus packaging mutant that expresses three viral packaging genes: gag, pol and env (b). The pZip-Neo SV(X)1 shuttle vector(c), containing a temperate sensitive SV40 Tag cDNA, is transduced into the same cell line (a). When the packaging cell line (a) divides it replicates the pZip-Neo SV(X)1 shuttle vectors (green circles). This vector will be housed in the packaging material (yellow hexagons) (d) necessary for successful infiltration into the target cell. The packaging cell lysate is collected which now contains the immortalisation agent ready to transfect the target cells (e).*

The ts SV40 Tag has been used in a number of successful cell immortalisations including rat brain, endothelium and epithelium cells (Greenwood et al. 1996), mouse cerebellum cells (Redies et al. 1991) and olfactory placode cells (Illing et al. 2002). Most applicably, cells from

20 different tissue types of the Black Flying Fox (*Pteropus alecto*), including foetal cells, have been successfully immortalised by viral introduction of an SV40 Tag (Crameri et al. 2009).

In this study, it was investigated as to whether primary cultures could be maintained that were derived from bat and mouse FL and HL autopods, and whether retrovirus carrying the ts SV40 Tag could be used to immortalize these primary cultures to produce bat and mouse FL and HL cell lines.

4.2 Methods and materials

4.2.1 *General cell culture*

The methods used in general cell culture and in immortalising a cell line were based on the methods described in (Illing et al. 2002). All work with cells was carried out in a P2 facility and, where applicable, inside a sterile biosafety cabinet. Unless otherwise stated all media and solutions that came into contact with the cells were sterile and pre-warmed in a 37°C water-bath prior to use

4.2.1.1 Thawing, maintenance and freezing cells

If cells were cultured from a frozen aliquot, a 1.8 ml vial of cells was removed from -80°C and thawed in a 37°C water-bath for 3 minutes until the majority of the vial was defrosted. The cells were suspended in 10 ml of DM-10[3] before centrifugation at 500 g for 10 minutes. The media was removed and the cell pellet was re-suspended in 5 ml DM-10. This was then plated into a Greiner T25 culture flask (Sigma, C6481) and maintained in a humid 33°C incubator with 5% CO_2 until 80% confluency (surface density), thereafter expanded to a Greiner T75 culture flask (Sigma, C7231).

Cell cultures were maintained in a volume of DM-10 approximately $1/5^{th}$ of the culture dish surface area (cm^2). Media was changed twice a week until cells reached 80% confluency. At this point the cell culture was split by aspirating the old media (DM-10) and washing the cells with PBS. After PBS was removed, roughly 1 ml of 0.25% trypsin /0.1% EDTA (Sigma T4049; here forth referred to as trypsin) was added to the cells which were then incubated at 33°C for 3 minutes to dislodge the adherent cells. After ensuring all cells were dislodged, 8 ml DM-10

[3] Dulbecco's modified Eagle medium (DMEM) (Sigma D0819) supplemented with 10% FCS (Sigma F2442) and 1% penicillin-streptomycin (Sigma P4333)

was added to the flask to inhibit the trypsin reaction. The cell suspension was transferred to a sterile tube and centrifuged at 250 g for 3 minutes. The media was removed and the cell pellet was re-suspended in 5 ml DM-10. When required, cells were counted as described in 4.2.2.2 and plated into a tissue culture flask or dish. Waste solutions removed from the cells were treated with 1% virkon (Kemclean) and in cases where viral particles or primary cell debris were likely present the waste was autoclaved before disposal. Cells were checked daily under the microscope (10X) to ensure cultures were free of bacterial or fungal contamination and to monitor the confluency of the culture.

In order to maintain stocks of cells for later use, cells were frozen down and stored at -80^{o}C. To prepare cells for freezing, media was changed when cells were 70% confluent. The next day cells were washed in PBS, treated with trypsin and dispersed in DM-10 as with the procedure to spilt flasks. However, before centrifugation, cells were counted to determine total number of cells to be frozen. A normal centrifugation at 250 g for 3 minutes was done and then cells are re-suspended in ice-cold DM-10 supplemented with 10% DMSO (Sigma-aldrich, Z374431) to give a final concentration of 3x10^{6} cell/ml. Tubes with cells were placed on ice for 10 minutes then aliquoted into cryotubes. These were transferred to -20^{o}C for 1 hour and then into a -80^{o}C freezer for long term storage.

4.2.1.2 Counting cells for plating or freezing

To count cells a 5 µl aliquot of cells in suspension was mixed with 5 µl trypan blue - a vital dye. This mixture was placed on a haemocytometer under a cover slip. Cells were counted manually under the microscope, ensuring to only include cells that are alive - those that had not taken up the blue dye. The number of cells counted across the 4 quadrants on the haemocytometer was multiplied by 2x10^{4} to account for the dilution in trypan blue and to work out the number of cells per ml. The number of cells plated into the various tissue culture dishes and vessels is summarised in Table 4.2 below.

Table 4.2: Cell culture vessels and plating density.

Cell culture vessel	Surface area (cm^2)	No. of cells to plate
6-well plate	9	$0.3X10^6$
35 mm dish	9	$0.3X10^6$
T25 flask	25	0.7×10^6
T75 flask	75	2.0×10^6

4.2.2 *Animals*

Mouse embryos were collected and processed as described in Chapter 3.2.1. Females were sacrificed at 13.5 days after cervical plug identification. Embryos were transported in the uterus in cold PBS[4] and dissected out of the decidual tissue within 2 hours for further processing. *M. natalensis* embryos were collected and processed as described in Chapter 3.2.1.

Both mouse and bat embryos intended for cell culture purposes were immediately placed in a fresh solution of PBS to rinse off any internal fluids. These embryos were then transferred to a petri dish containing cold calcium- and magnesium-free Hanks Balance salt solution (hereafter referred to as HBSS; Thermofisher Scientific, 14170088). The FL and HL autopods of the embryos were carefully dissected and further processed depending on the downstream protocol.

4.2.3 *Preparation of primary cultures*

4.2.3.1 Testing the viability of primary cells after 16hrs storage prior to plating

To test whether a viable primary cell line could be made several protocols were performed on the autopods of two E12.5 mouse embryos to determine the number of cells that survived each treatment. For these experiments each embryo's FL and HL were pooled together and placed in one of the two dissociation media and further processed as described in Figure 4.2. Based off the studies by Bobick and Cobb (2012), Marędziak et al. (2014) and Stott and Chuong (2000), three variables were assessed: the solution in which the limbs were stored (Figure 4.2

[4] Phosphate buffered saline (1XPBS) made from tissue culture grade sodium chloride, potassium chloride, disodium phosphate and potassium phosphate monobasic anhydrous at pH 7.3. Autoclaved for sterilisation

i), the effect of straining the cells before plating (ii) and the density at which to plate the cells (iii).

The cells were checked daily for signs of contamination and to analyse the behaviour of the plated cells. After five days, the cells were harvested and counted. The cell counts were analysed in Microsoft Excel (2010), and paired student t-tests were used to determine whether any of the three variables significantly affected the survival of the cells.

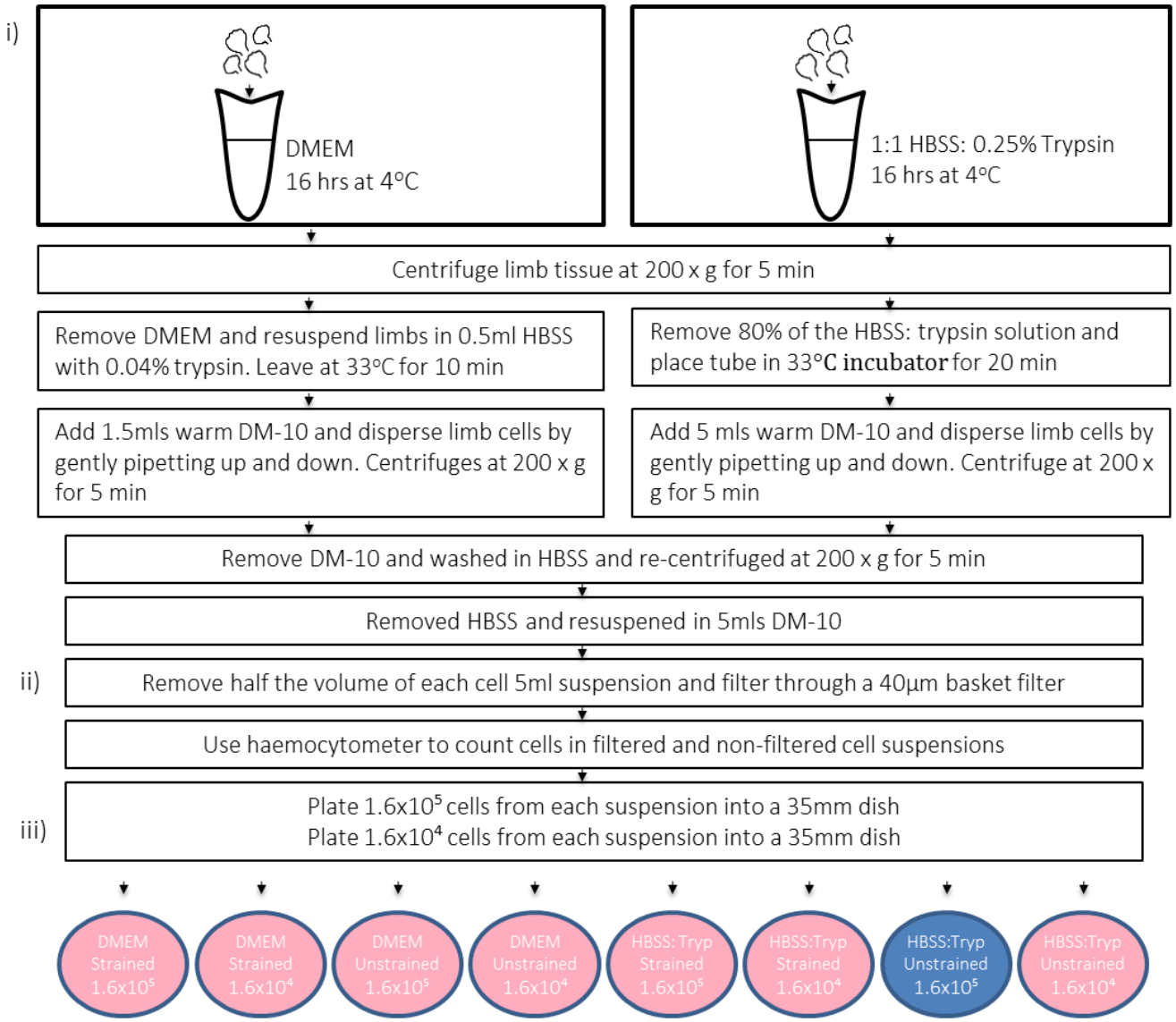

Figure 4.2: Protocols tested for optimum cell survival following 16-hour storage of limb tissue. *The first parameter (i) is the solution in which the limbs are suspended for 16 hours (hrs) where DMEM is Dubucco's modified Eagle medium and HBSS: Tryp is a 1:1 calcium- and magnesium- free Hank's balanced salt solution with 0.25% trypsin. The second parameter tested (ii) is a comparison between cell suspensions that are strained to remove debris, allowing through only single cells and unstrained cell suspensions. The third variable (iii) is the density at which the cells were plated. DM-10 refers to DMEM supplemented with 10% FCS and 1% penicillian- streptomycin. The protocols were derived from Bobick & Cobb (2012), Marędziak et al. (2014) and Stott (2000). The pink and blue circles represent the 8 final experimental dishes of primary cells. The blue circle represents the protocol used, with exception to plating density, for further cell line experiments.*

4.2.3.2 Tissue storage, dissociation and plating of limb tissue

In all cases, other than when establishing a viable protocol (section 4.2.3.1), dissected FLs and HLs of bat and mouse were pooled into separate tubes of HBSS: trypsin solution[5] (Figure 4.3). In order to match the time period that dissected bat limbs would have to be kept on ice while being transported from the field; mouse limbs were stored in HBSS: trypsin for 21 hours at 4°C. In the case with the bats obtained in the field, the limbs in HBSS: trypsin were kept on ice during transportation and moved to 4°C once at the university. Bats limbs were also kept cold for 21 hours before processing.

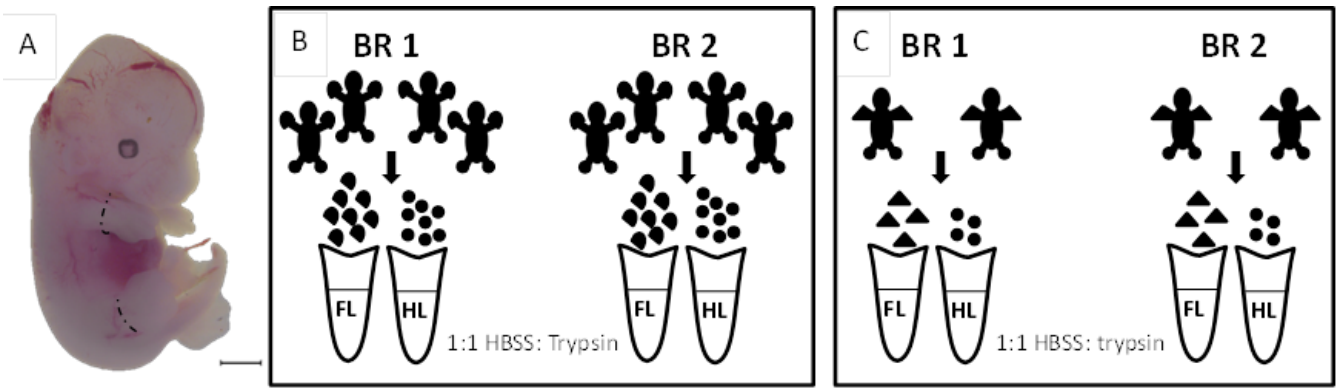

Figure 4.3: Tissue pooling for limb cell cultures*. A: Dashed lines indicate where limbs were dissected from an E13.5* M. musculus *embryo for cell culture with a similar line of dissection on bat embryos. Scale bar represents 0.5 mm. B: The forelimbs (FL, half-moons) and hindlimbs (HL, circles) of eight E13.5* M. musculus *embryos were dissected and pooled to form two biological replicates (BR). C: The forelimbs (FL, triangles) and hindlimbs (HL, circles) of four CS17* M. natalensis *embryos were dissected and pooled to form two biological replicates (BR).*

4.2.3.3 Dissociation and plating of limb tissue

After 21 hours in cold storage, limbs in the HBSS: trypsin solution were taken into a P2 facility and spun at 250 g for 3 minutes. Inside the sterile biosafety cabinet 80% of the HBSS: trypsin solution was removed and the cells were placed in a 37°C incubator for approximately 30 minutes. To inhibit the trypsin action, 5 ml DM-10 was added to each tube and the tissue was dissociated through gentle pipetting. Cells were centrifuged at 250 g for 5 minutes, washed by resuspension in HBSS, pelleted again at 250 g for 5 minutes and re-suspended in 10 ml DM-10.

[5] A 1:1 ratio of HBSS and 0.25% Trypsin/ 0.1 EDTA

Mouse cells were counted and plated into a 6-well plate at a density of $1X10^4$ cells/cm^2 and placed in a humid 33°C incubator with 5% CO_2. At the same density, bat primary cells were plated into 35 mm petri dishes which were housed inside a 10 cm petri dish to minimize contamination. In order to encourage adhesion of the cells, the 35 mm petri dishes were coated with 0.75 ml 15 µg/ml poly-L-ornithine (filter-sterilized; Sigma, p3655) and incubated for 40 minutes at 33°C. The excess poly-L-ornithine was removed and the plates were washed three times in PBS before storing the plates at 33°C, covered with 2 ml PBS, until they were used.

4.2.4 *Immortalisation of primary cells*

4.2.4.1 Preparation of retrovirus used for immortalisation

The packaging cell line, Ψ^2, contains the pZIPNeoSV40U-19tsA58TAg retrovirus that carries the SV40 TAg with two temperature sensitive mutations, as well as G418 resistance (Almazan and McKay 1992) (a gift from R. D. G. McKay, National Institute of Neurological Disorders, Bethasda). The virus is transcribed, packaged and released into the media of the Ψ^2 cell line, ready to transform other cells. The Ψ^2 cells were maintained in T75 flasks at 33°C in DM-10 until they reached 70% confluency at which point the media was replaced with 20 ml fresh DM-10 per flask. The next day the media, containing the packaged retrovirus (viral lysate), was collected and centrifuged at 1000 g for 4 minutes. The viral-containing supernatant was filtered through a 0.45 µm filter and stored in 10 ml aliquots either at -70°C for later use or used immediately.

4.2.4.2 Immortalisation and isolation of a limb cell line

Primary cells were maintained in the 33°C incubator before proceeding with immortalisation of cells in the experiment or 'Treatment A'. Media from FL and HL plates was removed and replaced with 33°C viral lysate adjusted to contain 8 µg/ml polybrene (Sigma, P3655). The cells were incubated at 33°C in the viral lysate for 2 hours and then the viral lysate was replaced by DM-10. Selective media, DM-10 supplemented with 200 µg/ml G418 (Gibco, 10131035), was added 3 days later to the cells from Treatment A, as well as to a control plate of primary limb cell cultures that had not received viral lysate (Treatment B). Selective media was replaced every 4 days and photographs were taken in triplicate for each plate before selection was

started and there after every 7-8 days. Plates containing primary cells receiving neither viral lysate nor selective media were analysed (Treatment C) alongside the experiment and control plate. The experimental set up of treatments is illustrated in Supp. Fig. 4.1.

G418 resistant, immortalized cell colonies were identified after 3-4 weeks, and were isolated and expanded in 48-well plates. To isolate a colony the dish containing colonies was aspirated and washed with PBS. Having removed the PBS, a trypsin soaked 3.2 mm cloning disc (Sigma, Z374431) was squeezed out to remove any excess trypsin and placed over the colony (visible to the naked eye). After 3 minutes at room temperature (RT) the disc was lifted with sterile forceps and scraped gently to maximise the number of cells transferred. The disc was placed in a well of a 48-well plate (Costar, 3548) containing DM-10. Cells were expanded once confluent, first cells were expanded into a 12-well plate (Greiner bio-one, 655180), then into a T25 flasks and subsequently further expanded into T75 flasks.

4.2.5 *In vitro gene expression analysis*

4.2.5.1 RNA extraction from primary and immortalized cell limb cells

A tissue culture dish or flask containing at least $5x10^6$ cells was aspirated, washed and trypsinised as per normal cell splitting. After addition of DM-10, to inhibit the trypsin, the cells were counted and 5 $x10^6$cells were aliquoted into a sterile tube to be pelleted at 500 g for 3 minutes. The liquid was removed from the pellet and the cells were re-suspended in ice cold PBS. The tube was spun at 1000 g for 5 minutes, aspirated and transferred from the P2 facility to the lab where cells were suspended in 500 µl of TRIzol™ and transferred into a NoStick Hydrophobic microtube. After an addition of 100 µl chloroform, the RNAeasy® mini kit (Qiagen) was used following manufacturer's guidelines, omitting all optional steps. Once the RNA was eluted into RNase-free water, 2x volume 100% ethanol and 0.1 x original volume sodium acetate was added to encourage precipitation and improve RNA quality, before storing the RNA at -80°C.

After no longer than 1 week at -80°C the RNA was pelleted by centrifugation at 12000 g for 15 minutes at 4°C. The liquid was removed and pellets were washed in 700 µl 70% ethanol before centrifugation at 12000 g for 6 minutes at 4°C. Ethanol was removed and pellets were air dried, then re-suspended in 10 µl RNase-free water. RNA concentration and quality was determined

using a Nanodrop 3000 by measuring the absorbance at 260 nm and 280 nm. The integrity of the RNA was determined by gel electrophoresis on a 1% formaldehyde denaturing gel[6].

The RNA sample was prepared for gel electrophoresis using 1 µg of RNA in 2x volume RNA loading buffer[7] heated at 65˚C for five minutes. All RNA was stored in RNase-free water at -80^{o}C.

4.2.5.2 RNA extraction from embryonic tissue

E13.5 mouse embryos that were used for tissue RNA extractions were freshly removed from deicidal tissue and placed in RNA*later*™ (Thermo fisher Scientific, AM7020) for storage at -20^{o}C for no longer than 18 months. The limbs from these embryos in RNA*later*™ were dissected under a stereomicroscope, pooling FLs and HLs but separating species and limb type into NoStick Hydrophobic microtubes. Initially 100 µl of TRIzol™ was added to each tube and a disposable plastic pestle was used to homogenise the tissue manually. An additional 900 µl TRIzol™ was added and the tube incubated at RT for 3 minutes, before 200 µl chloroform was added. The RNA was extracted and assessed according to the same protocol as performed on the cells (Section 4.2.5.1). However, once eluted in RNA-free water, no precipitation or quality enhancement step was performed and the RNA quantity and quality analysis was performed immediately.

4.2.5.3 DNase I treatment and cDNA synthesis

All RNA was treated with RQ1 RNase-Free DNase (Promega, M6101) using 1 µg of RNA and instructions provided by the manufacturer. The total volume of DNase treated RNA was converted to 20 µl of cDNA using SuperScript® IV First-Strand cDNA synthesis following the manufacturer's protocol using 50 µM oligo(dT)$_{20}$ primers. cDNA was stored at -20^{o} C for no longer than a week before use.

4.2.5.4 Primer design

Primers were designed for 7 genes to be amplified either through PCR or RT-PCR to determine whether the primary and immortalized cells maintained their limb-specific gene expression profiles. Of these genes amplified, 6 are known to be expressed in developing limbs of bats

[6] Agarose, DEPC water, 1X MOPS, Formaldehyde
[7] deionized formamide, 37% formaldehyde, 5x MOPS and 1% ethidium bromide

and mice and one is a house-keeping gene, TATA box binding protein-like 1 (*Tbpl1*) – already validated as a reference gene on bat and mouse embryos of the same age (Mason, 2016) (Table 4.3). Newly designed primers were designed in PerlPrimer (Marshall 2004), ensuring amplicon size was no larger than 200 base pairs (bp). All primers were assessed in Oligo Analyser 3.1 (PrimerQuest® program) for primer dimers. BLASTn (Altschul et al. 1990) against the *M. musculus* transcriptome was used to check for off target alignments.

The primers for *Hoxd13* and *Tbpl1* were previously designed to the bat *M. natalensis*. However alignment of these 2 primer sets to the relevant mouse genes in Mega5.2 (Tamura et al. 2011) showed fewer than 2 mismatches so the same primers were used to amplify up mouse cDNA as well as bat.

Table 4.3: Summary of PCR primers used for expression analysis of mouse and bat limb patterning genes.
The primer names, sequences, melting temperatures, amplicon sizes and purpose in this study are shown. Melting temperatures were calculated using OligoAnalyzer 3.1 (IDT).

Primer name	Primer sequence (5'-3')	Tm (°C)	Amplicon size (bp)	Use in this study	Reference
Tbx4_UTR_Mouse_Fwd Tbx4_UTR_mouse_Rvs	TAG CGG CCC TTT CTT TCT ACA C TCC TGA AAG AAT AAA GGT CTC CAC	56.9 54.4	171	HL marker for immortalised mouse cell lines	This study
Tbx4_bat_Fwd Tbx4_bat_Rvs	CAA GGT AAA AGT CAC GGG CA TTC CCT GCC ACC ATC CAT TT	59. 56 63.22	117	HL marker for primary bat cells	This study
Tbx5_UTR_mouse_Fwd Tbx5_UTR_mouse_Rvs	TGA AGC TCA AAG ACA TTC CCT TAC AAC TCG GTG GCT GAC TC	54.1 56.6	155	FL marker for immortalised mouse cell lines	This study
Tbx5_bat_Fwd Tbx5_bat_Rvs	GTG GTT GTT GGT GAG CTT GA GCA GAT AAC AAA TGG TCG GTG A	58.61 59.59	144	FL marker for primary bat cells	This study
Hoxd11_bat_Fwd Hoxd11_bat_Rvs	ATG AAC GAC TTT GAC GAG TGC GG ATT GCT GGC GAA GTC CGA CG	59.7 60.5	93	Bat specific FL marker for primary bat cells	Mason (2016)
Hoxd13_bat_Fwd Hoxd13_bat_Rvs	AGC TAC CAC TTC GGC AAC GG ACA CGT CCA TGT ACT TCT CCA CCG	60.1 60.5	130	limb marker for primary bat cell lines and immortalised mouse cell lines	Mason (2016)
Msx2_Mouse_Fwd Msx2_Mouse_Rvs	GAG CAC CGT GGA TAC AGG AG TCC AAG GCT AGA AGC TGG GA	62.5 62.99	139	Interdigital call marker for immortalised mouse cell lines	This study
Sox9_mouse_Fwd Sox9_mouse_Rvs	GGA GCT CAG CAA GAC TCT GG CCG TTC TTC ACC GAC TTC CT	62.73 62.3	156	Digital cell marker for immortalised mouse cell lines	This study
Tbpl1_bat_Fwd Tbpl1_bat_Rvs	GGC AGA CAG TGA TGT TGC ATT GGA C GGT TCC TGA GGA CCA AAT TGC AGC TG	60.5 62	190	House-keeping gene for primary bat cells and immortalised mouse cell lines	Mason (2016)

4.2.5.5 Quantitative PCR (qPCR) of genes in bat primary cells

4.2.5.5.1 Standard dilutions

Standard dilutions were created from a pool of the two different cDNA sources: bat FL primary cells and bat HL primary cells to determine the efficiency of each primer set in the qPCR reaction (Figure 4.4). Standard dilutions were made in large volumes to be run in duplicate for each primer set.

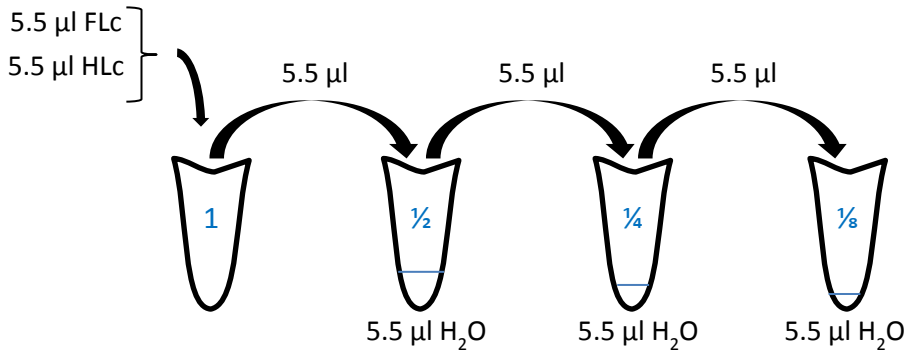

Figure 4.4: Standard dilutions prepared for relative gene expression analysis by qPCR. *The cDNA extracted from forelimb tissue (FLt), hindlimb tissue (HLt), forelimb primary cells (FLc) and hindlimb primary cells (HLc) was pooled in the 1X cDNA standard tube (Blue no. 1). This was mixed and a portion of this pooled cDNA was transferred to an equal volume of ultrapure PCR water (H_2O) to create a 0.5 X cDNA standard (blue no ½). This serial dilution was continued to create four standards of concentration 1 X, 0.5 X, 0.25 X and 0.125 X cDNA.*

4.2.5.5.2 qPCR protocol

The qPCR reactions for Tbx4_bat, Tbx5_bat, Hoxd11_bat, Hoxd13_bat and Tbpl1_bat primer sets were set up together. The reactions with *Tbx* primer sets were run independently from the *Hox* gene primer sets due to limited space in the Rotor-Gene 6000 (Corbett Research Pty Ltd). The house keeping gene *Tbpl1* was included in each run. The reactions were set up in a sterile laminar flow hood on a pre-cooled block (Figure 4.5).

Reaction tubes were placed in a ring of 100 tubes, and sealed with Rotor-Disc® heat sealer prior to qPCR in the Rotor-Gene 6000. Using the Rotor-Gene software 6.1.93, a two-step qPCR with the following profile was set up for both *Hox* and *Tbx* primers: 95°C for 10 minutes, 40 cycles of 95°C for 15 seconds, 60°C for 15 seconds and 72°C for 20 seconds. A melt from 72°C to 95°C of 1 second on the first step and 5 seconds on the following steps thereafter was included for melt curve analysis.

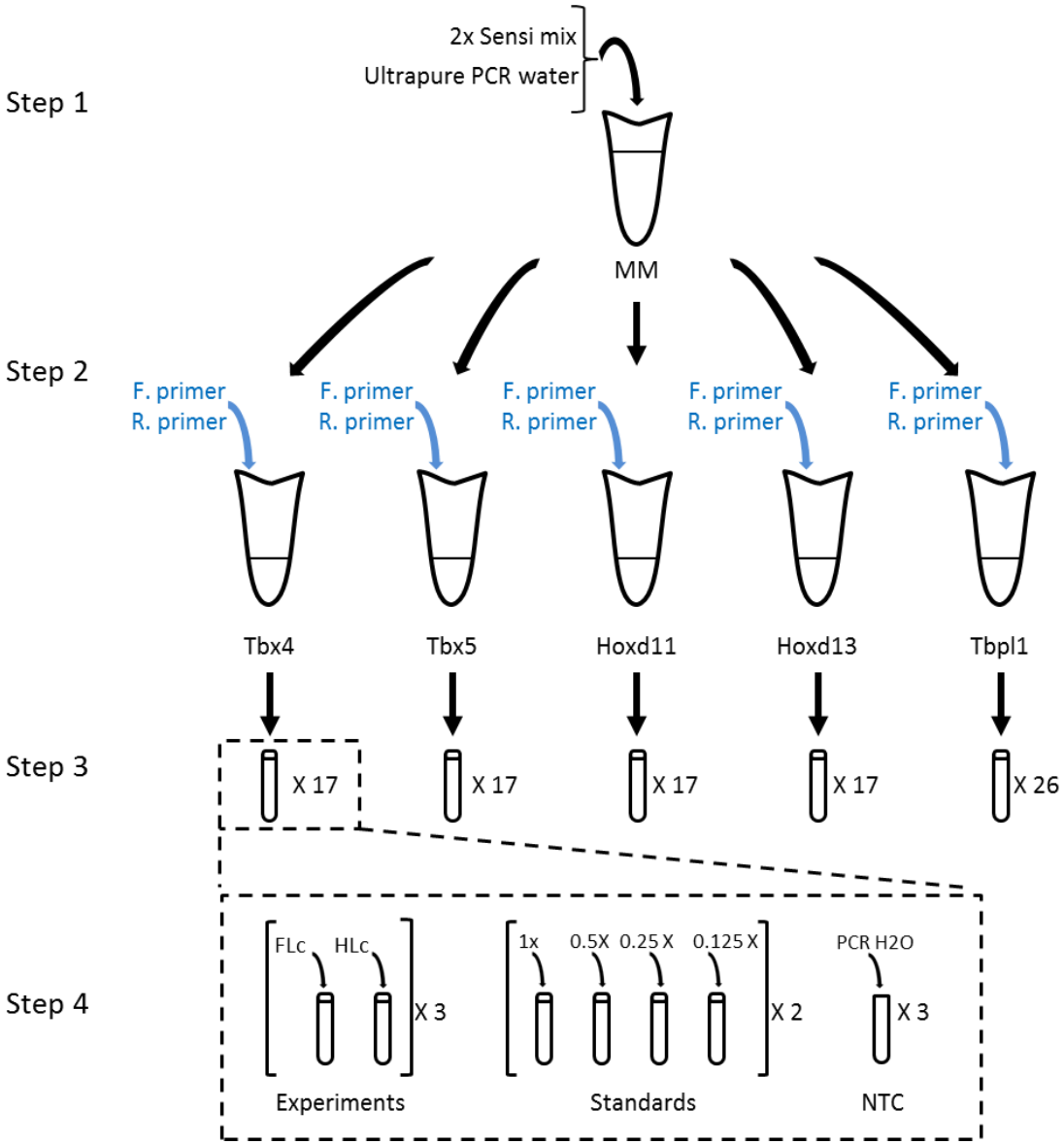

Figure 4.5: The experimental set up for relative gene expression analysis in bat limb primary culture cells. *Step 1: To set up 12.5 µl final reaction volumes, an initial master mix (MM) was set up with the addition of 6.25 µl of 2x SensiMix™ SYBR No ROX (Bioline) and a calculated volume ultrapure PCR water per reaction tube. Step 2: the master mix was aliquoted into 1.5 ml tubes for each primer set. Forward (F.) and reverse (R.) primers of the corresponding genes were added to ensure a final concentration of 250 nM. Step 3: 11.5 µl of the each primer-specific solution was further aliquoted into 17 qPCR tubes. An additional nine tubes were prepared for the Tbpl1 primer set. Step 4: 1 µl of a cDNA was added to each tube as indicated for each primer set. An example of the setup is shown for the Tbx4 primer set. All primer sets follow the same set up except Tbpl1 where the setup is repeated, omitting the standards on the second repeat. cDNA synthesised from forelimb primary cells (FLc), hindlimb primary cells (HLc) and the standards are a pool of these cDNA samples at the following concentrations 1 x cDNA (1x), 0.5 X cDNA, 0.25 X cDNA (0.25x) and 0.125 X cDNA (0.125x). The no template controls (NTC) received one µl of ultrapure PCR water (PCR H_2O) each.*

4.2.5.5.3 Data analysis

Quantification, run efficiency and melt curve were analysed using the Rotor-Gene software 6.1.93. The threshold was kept constant for all primer sets at 0.1 and the first 15 cycles were eliminated from the analysis. All Ct values and standard concentrations were exported into Microsoft Excel (2010) for further analysis. Outliers in the standard curves were removed using Dixon's Q test (Rorabacher 1991) after log transforming the data and subtracting the observed concentrations from the expected concentrations. Calculations for differential expression and were performed according to the equation:

$$R = \frac{E_{GOI}^{(control\ ave\ Ct - Sample\ TR\ 1\ Ct)}}{Eref^{(control\ ave\ Ct - Sample\ ave\ Ct)}}$$

Where:

R - normalised sample
E_{GOI} - gene of interest efficiency + 1
E_{REF} - reference gene efficiency + 1 (in this case the reference gene was *Tbpl1*)
Control ave Ct - average of control cDNA Ct values to which all sample Ct values are normalised (the FL cell cDNA Ct values were the control in this case)
Each technical repeat (TR) was subtracted individually from the control ave Ct and standard deviation of the technical repeats was calculated.

The average normalised sample values and standard deviation for each gene and cell type was plotted. The statistical significance was calculated for differential expression using a one-tailed, two-sampled student t-test. P-values less than 0.05 were considered significantly differentially expressed. In addition fold difference between FL and HL was calculated for each gene by dividing the larger value by the smaller of the two numbers.

Differential expression from the RNA-seq data (Eckalbar et al. 2016) was calculated as described in 2.2.3. The read count values for the three biological repeats of stage CS17 were extracted for *Tbx4*, *Tbx5*, *Hoxd11* and *Hoxd13*. Average read count and standard deviation between biological repeats was plotted as described above. The same statistical analysis was also performed for significance and fold difference.

4.2.5.6 PCR of genes in immortalised mouse cell line

The PCR was performed on mouse cDNA from immortalised cells as well as whole tissue using real time 2x SensiMix™ SYBR No ROX (Bioline) and run on the Rotor-Gene 6000 (Qiagen) using conditions that had been optimised previously (Mason, 2016). The experimental set up (Figure 4.6) was prepared on a pre-cooled freezer block to keep samples at 4°C. *Tbx5* primers were used only on FL tissue cDNA and *Tbx4* primers were used only on HL tissue cDNA.

Reaction tubes were placed in a ring of 100 tubes, and sealed with Rotor-Disc® heat sealer prior to running the PCR in the Rotor-Gene 6000. Using the Rotor-Gene software 6.1.93 (ScreenClust HRM software) a two-step PCR with the following profile was set up for *Hoxd13*, *Tbpl1*, *Sox9* and *Msx2* primer sets: 95°C for 10 minutes, 40 cycles of 95°C for 15 seconds, 62°C for 15 seconds and 72°C for 20 seconds. While the two *Tbx* primer sets were run with the same profile except the annealing temperature which was adjusted from 62°C to 57°C.

All PCR products were mixed with 2 µl loading dye and 6 µl was run on a 2.5% agarose gel along with a 100 bp ladder (New England Bio Labs, N04675). The presence of a band in the

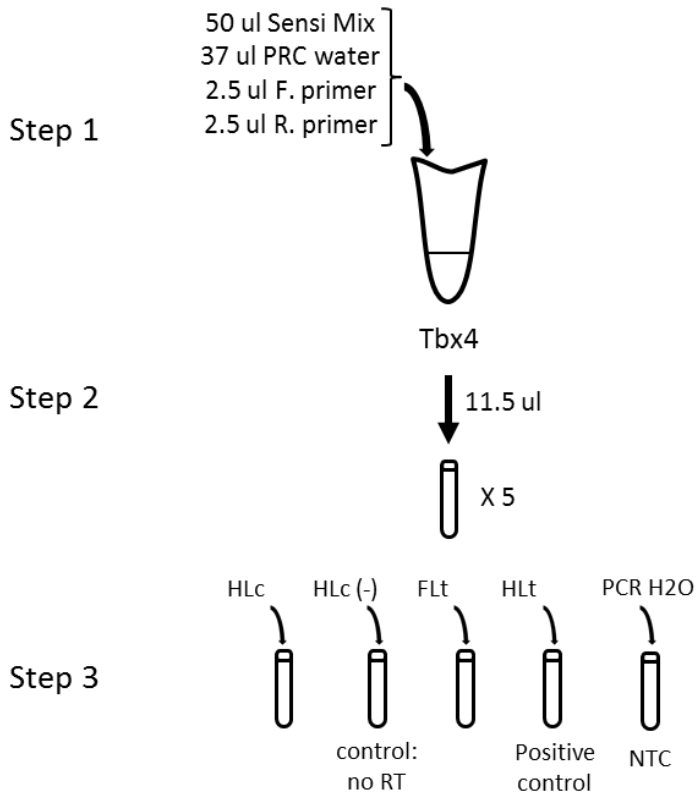

Figure 4.6: Reaction tubes set up for expression characterisation of immortalised mouse limbs cells. *In step 1 an initial master mix (MM) is set up for each set of primers (here illustrated is the* Tbx4 *primer set) using qPCR Taq polymerase, 2x SensiMix™ SYBR No ROX (Bioline). In the second step the primer-specific solutions were further aliquoted into five qPCR tubes per primer set. In the fourth step one ul of a specific cDNA is added to each tube for each primer set. All primer sets follow the same set up. The specific cDNA's were extracted and synthesised from immortalised hindlimb cells (HLc), immortalised hindlimb cells (HLc) in which reverse transcriptase (RT) was omitted from the cDNA synthesis reaction, forelimb tissue (FLt), hindlimb tissue (HLt) – a positive control. The no template control (NTC) received 1 ul of ultrapure PCR water (PCR H_2O).*

immortalise HL cell cDNA run was understood to indicate expression of the gene of interest, provided controls behaved as expected.

4.3 Results

4.3.1 *Establishing conditions for primary limb cultures from field to the lab*

Before any experiments could be performed on bat tissue, a system for tissue collection and processing had to be set up taking into account the 16 hour period between tissue harvesting and processing. Various storage and plating experiments on E12.5 mouse limbs found cells could be successfully processed and plated with no contamination over a five-day period. The surviving cells after 5 days were counted using trypan blue and the experiment showed that limb tissue was able to survive for 16 hours before being further processed and plated. On average 7.46% of the plated cells were alive after five days and proportionately there was no significant difference ($p=0.5$, $n=3$) in the survival of cells plated at different densities. The unstrained sample consistently had a 0.63±0.06 times lower yield in surviving cells than the strained samples, however this was not significant ($p=0.06$, $n=3$). Suspending limbs in HBSS with 0.125% trypsin resulted in 0.24±0.28 more living cells, but was not significantly different ($p=0.24$, $n=3$) to using DMEM.

A final protocol was drawn up to use for processing bat tissue in the field and plating primary cells (Supp. Fig. 4.2)

4.3.2 *Bat limb cells in primary culture maintain identity after 2 months*

4.3.2.1 Bat limb cells in primary culture can remain dividing for 2 months

Embryonic bat FLs and HLs were dissected from CS17 in the field laboratory at de Hoop Nature reserve, before being transported back to the University of Cape Town, where they were successful dissociated and plated as single cell suspensions at a density of 1×10^4 cells/cm^2 on a 9 cm^2 surface area. After 24 hours, cells had settled and adhered at 20% confluency (Figure 4.7 A & B). It took 9 days for the CS17 FL cells and 15 days for the CS17 HL cells to reach 90% confluency (Figure 4.7 C & D). The primary cultures were expanded to 25 ml flask a surface area of 25 cm^2 and both FL and HL primary cells divided rapidly covering the new surface area within four and eight days respectively. Once expanded into a surface area of 75 cm^2 the HL primary cells ceased their rapid division and reached a maximum confluency of 55%. The FL

cells on the other hand continued their expansion and underwent two more passages before cell division slowed down 46 days after initial plating. This suggest the FL cells were more proliferative compared to the HL cells and had a greater life span.

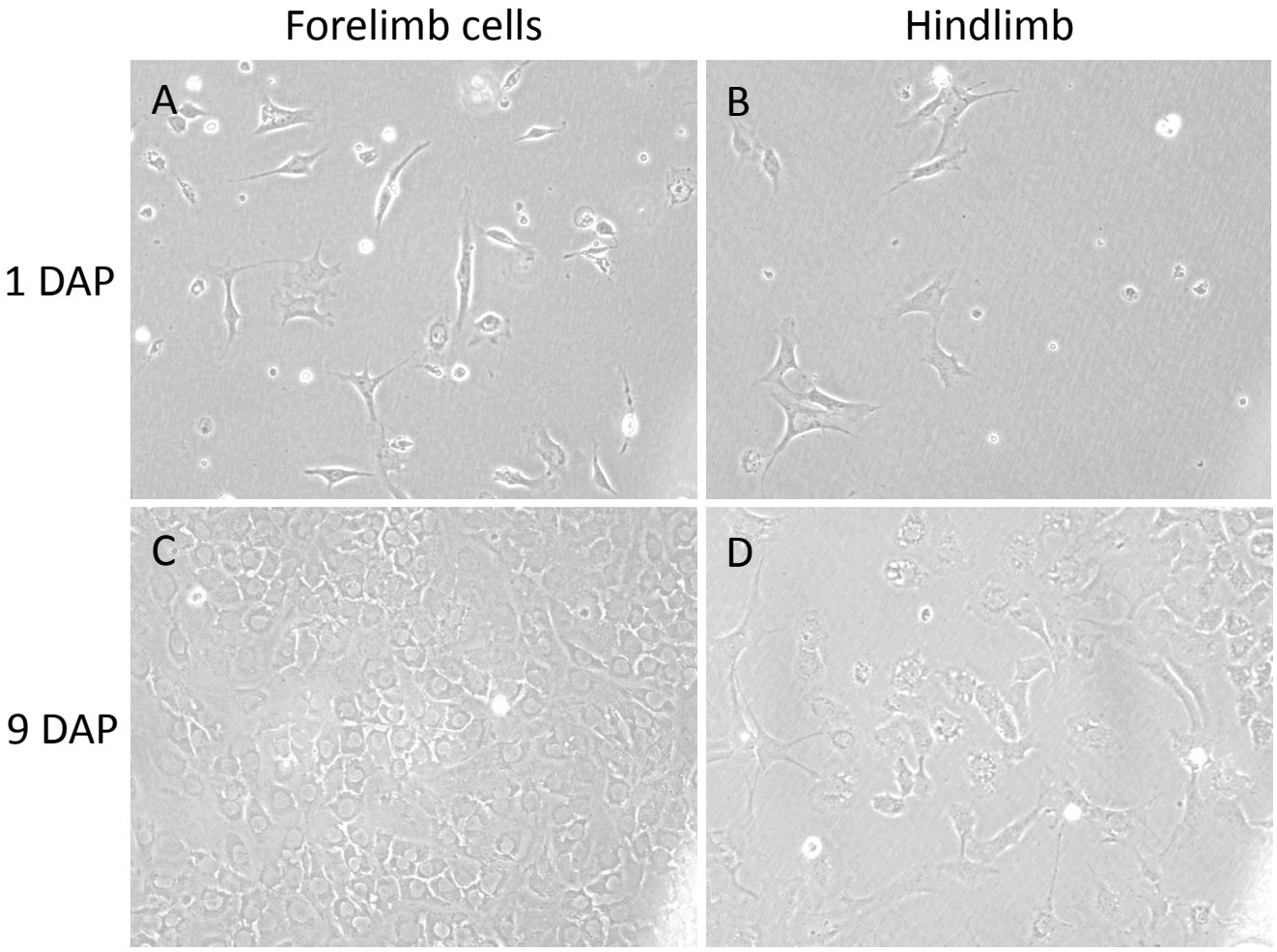

Figure 4.7: Bat limb primary cells in culture. *FL cells (A) and HL cells (B) were plated at an initial density of 1 x10^4 cells/ cm^2 on a 9 cm^2 surface area and photographed 1 day after plating (DAP). Both FL (C) and HL (D) cells were photographed at 9 DAP when FL cells were confluent and ready for expansion. HL cells reached this point 6 days later.*

4.3.2.2 qPCR analysis of primary cell cultures confirms FL and HL identity as well as expression of key limb development genes

To determine whether the bat primary cultures retained their CS17 FL and HL identity after being in culture for 2 months, transcript abundance of 4 limb specific genes (*Tbx5*, *Tbx4*, *Hoxd11* and *Hoxd13*) and one house keeping gene (*Tbpl1*) was measured. Previous RNA-seq analyses showed that *Hoxd10* and *Hoxd11* genes were differentially expressed between FL and HL in the bat at CS17 (Eckalbar et al. 2016). Thus, to assess if the primary cells maintained the

expression profiles of CS17 bat limbs, the expression of *Hoxd11* was characterised as it was found to have significantly higher expression in the bat FL compared to the HL, a trait that is not apparent in mice (Eckalbar et al. 2016, Mason 2016). Expression of *Hoxd13*, which is not differentially expressed between bat FL and HL, was also analysed. Relative expression was looked at between the FL and HL bat cells and compared to the read counts of the same genes, generated from an RNA-seq performed by Eckalbar et al. (2016).

Expression analysis revealed that in CS17 bat FL primary culture cells, *Tbx5* expression was significantly higher HL primary culture cells (p=0.017, n=3), while *Tbx4* was expressed at a significantly lower level than in primary culture HL cells (p= 9.5 E^{-06}, n=3) (Figure 4.8 A). These results mirror the *Tbx5* and *Tbx4* read count results from the CS17 FL and HL RNA-seq datasets (Figure 4.8 C). In the primary culture cells, *Tbx5* expression was 166-fold higher in the FL compared to HL primary cells, while a 1360-fold increase in HL to FL expression was observed in whole-tissue RNA-seq data. For *Tbx4*, a 28-fold increase in the HL to FL primary cells was seen compared to a 27-fold increase in the RNA-seq results. This suggests that the FL identity of *Tbx5* expression has been maintained and the HL expression of *Tbx4* has not only been maintained but the fold difference of *Tbx4* between FL and HL is almost identical to what is seen in fresh tissue RNA-seq read counts.

Similar results were seen for the limb development genes, *Hoxd11* and *Hoxd13* (Figure 4.8 B & D). In the RNA-seq data, *Hoxd11* has significantly higher expression in the developing FL compared to the HL, while *Hoxd13* does not show differential expression but is still expressed in both limbs (Figure 4.8 D). The same pattern is seen in the relative expression results in the primary cell cultures (Figure 4.8 B). The FL primary culture cells show a significant 11-fold increase in *Hoxd11* expression compared to HL (p=6.99E-07, n=3), similar to the 12-fold difference seen in the RNA-seq data. No significant difference in *Hoxd13* expression is seen between the FL and HL primary cell cultures, which mirrors the corresponding RNA-seq data.

The quality of the qPCR did not fulfil MIQE standards as the efficiencies of the primer sets ranged between 0.74 – 0.79 (Supp. table 4.1; Supp. Figure 4.3), outside the optimum range of 0.9 – 1.1 (Taylor et al. 2010). However, importantly the efficiencies of all the primer sets were close to each other including the reference gene, making comparisons between primer sets more valid than if the range of efficiency values was large. The melt curves showed that there was no contamination and each primer set amplified only one product (Supp. Fig 4.3).

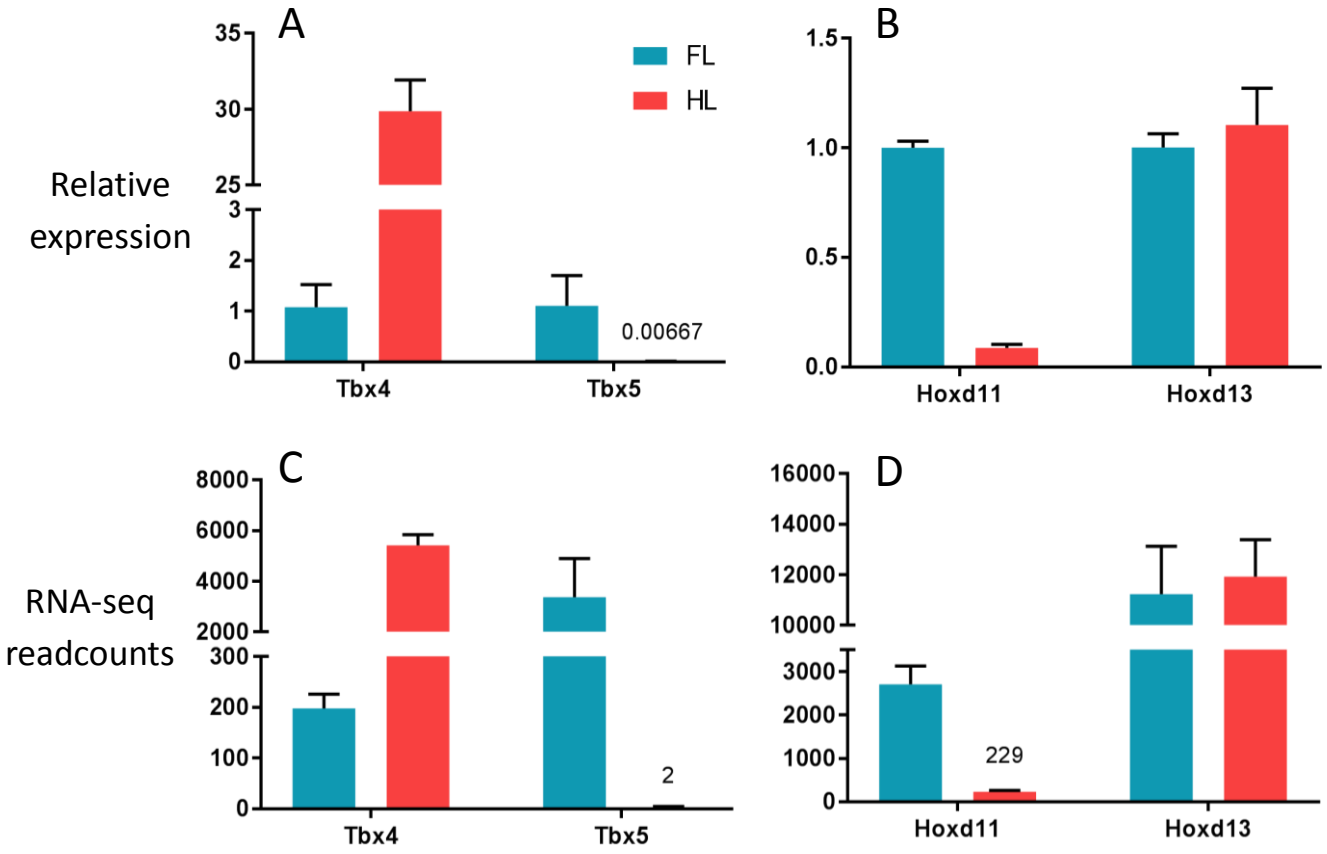

Figure 4.8: Forelimb and hindlimb expression of bat limb development genes in CS17 preserved and cultured tissue. A) The relative FL and HL expression levels of Tbx4 and Tbx5 genes, important for HL and FL identity respectively, in CS17 bat embryo primary cells. B) The relative FL and HL expression levels of Hoxd11 and Hoxd13 genes, important markers for limb development, in CS17 bat embryo primary cells. Cells were in culture for 56 days before RNA was extracted and converted to cDNA. Expression levels were measure by qPCR and normalised to Tbpl1. Error bars represent the standard deviation of three technical repeats. C and D) The FL and HL expression (measured in read counts) of the same four genes from tissue that was placed in RNAlater immediately after embryo retrieval from uterus and then later processed for an RNA-seq study performed by Eckalbar et al (2016). The read counts were produced from the raw sequencing data obtained by Eckalbar et al. (2016). Error bars represent standard deviation of three biological repeats.

4.3.3 *Immortalised embryonic mouse limb cells maintain limb identity but lose key development signals.*

4.3.1.1 Mouse cells immortalise after transformation of SV40 Tag retrovirus

Since primary cultures were demonstrated to be stable, it was tested to see whether mouse cell lines could be generated from mouse primary cultures. Density of the primary cultures prepared from E13.5 mouse FL and HL was low, and cells were maintained in culture for 3 weeks before reaching 30% confluency. (Figure 4.9 A) At this point experimental plates were

infected with the viral lysate. After just over one week of G418 selection, one immortalized colony from the FL primary cultures, and five immortalized colony form the HL primary culture were visible (Figure 4.9 B, C & D). At this point the control plate was void of any live cells (Figure 4.9 E)

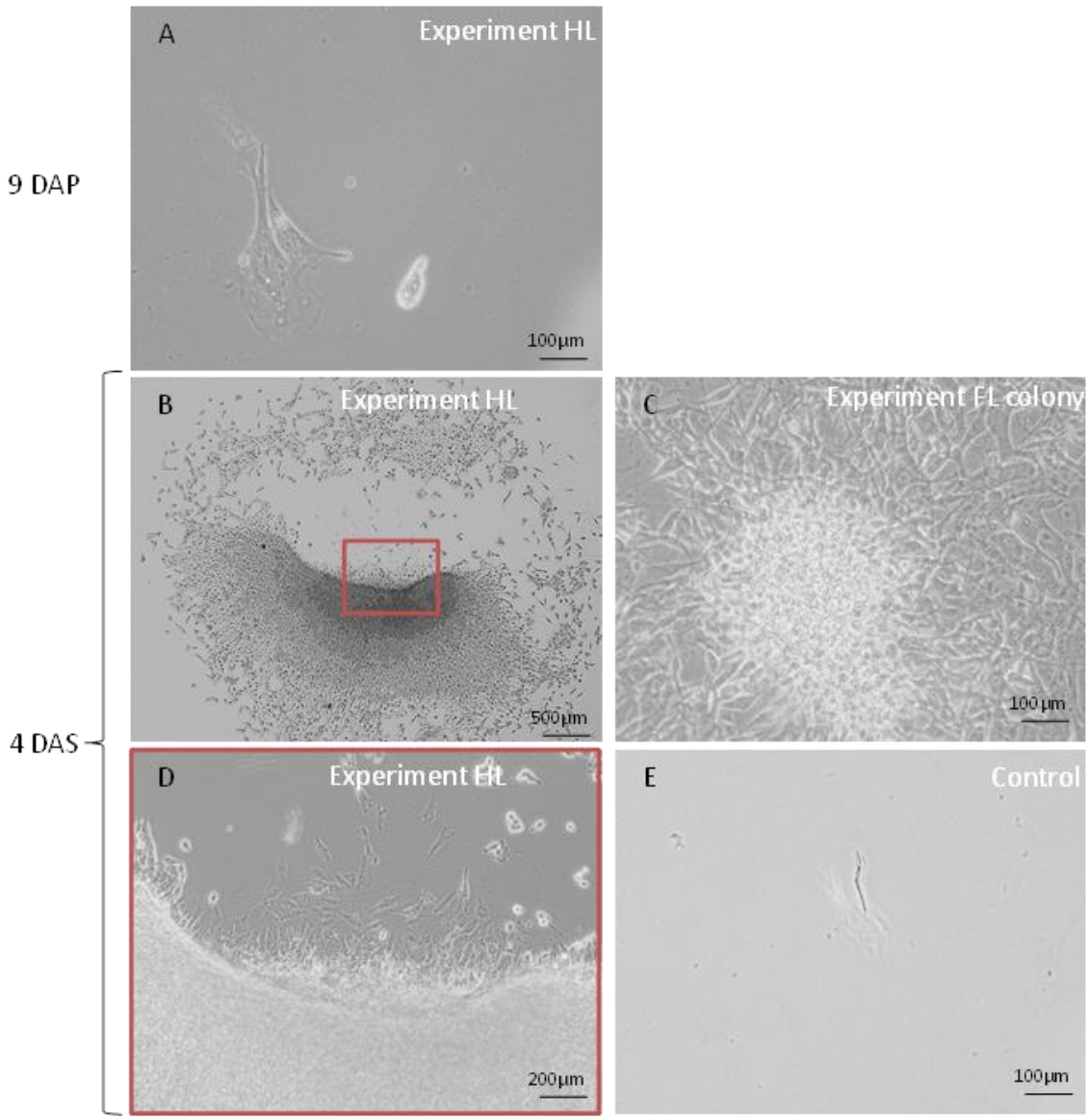

Figure 4.9: Mouse HL cells before and after immortalisation. (A) Cells were plated at an initial density of 1 x10^4 cells/cm^2 on a 9 cm^2 surface area and photographed 9 days after plating (DAP). At 24 DAP, one FL and one HL well of cells were infected by SV40 Tag retrovirus. Shortly after these cells, along with a control plate without infection, were subjected to selective media contain G418. (B) Low magnification view of a HL colony at 4 days after selection (DAS). (C) High magnification view of the region indicated in B. (D) High magnification view of a FL colony. (E) The control well resulted in the absence of cells at 4 DAS.

The transfer of the immortalised cells from the colonies to a 48-well plate was difficult, and five of the six colonies were infected with bacteria during subcloning. Cells from one HL colony

were successfully subcloned and expanded into 10 flasks which were frozen down into 15 vials of stocks, each containing 3 million cells. A sample of these stocks were later thawed and plated, showing viability of the cells after undergoing a freeze-thaw cycle. RNA was extracted from one of the stocks that were revived.

4.3.3.2 Immortalised mouse cells maintain HL digit identity, but lose *Hoxd13* expression

To determine whether the immortalised cells maintained their identity as mouse embryo HL cells, six genes were successfully amplified from the RNA extracted from these cells as well as the FL and HL tissue of a whole E13.5 embryo limbs (see Supp. Table 4.2 and Supp. Fig 4.4 for quality information). First, it was important to show that the limb cells were HL and not FL thus the HL marker *Tbx4* and FL marker *Tbx5* were amplified (Gibson-Brown et al. 1996). *Hoxd13* was amplified to determine whether the cells showed key autopod development characteristics (Davis and Capecchi 1996). Two genes, *Sox9* and *Msx2*, were amplified to determine whether the cells originated from the digit (*Sox9* (Wright et al. 1995)) or interdigital tissue (*Msx2* (Fernández-Terán et al. 2006)) in the limb. And lastly the gene *Tbpl1*, involved in the initiation of transcription, was amplified as a positive control which should be expressed in all cells (Ohbayashi et al. 1999).

The results show that immortalised cells maintain their HL specific identity in expressing the HL marker, *Tbx4*, and did not express the FL marker, *Tbx5* (Figure 4.10). The expression of *Sox9* and not *Msx2* indicates that the immortalised cells are clones from a digit cell and not an interdigital cell. The intact FL and HL expressed both *Sox9* and *Msx2*. This is expected as this tissue is made up of all the cell types in the limb during that developmental stage. *Hoxd13* however, was not expressed by the immortalised HL cells while clear expression was seen in the HL tissue (Figure 4.10). These PCR results were considered reliable as the negative control reaction (no reverse transcriptase and no template control) did not show any amplified products, and while positive controls behaved as expected. In addition the house keeping gene *Tbpl1* was expressed by FL and HL tissue, as well as the immortalised HL cells, as expected.

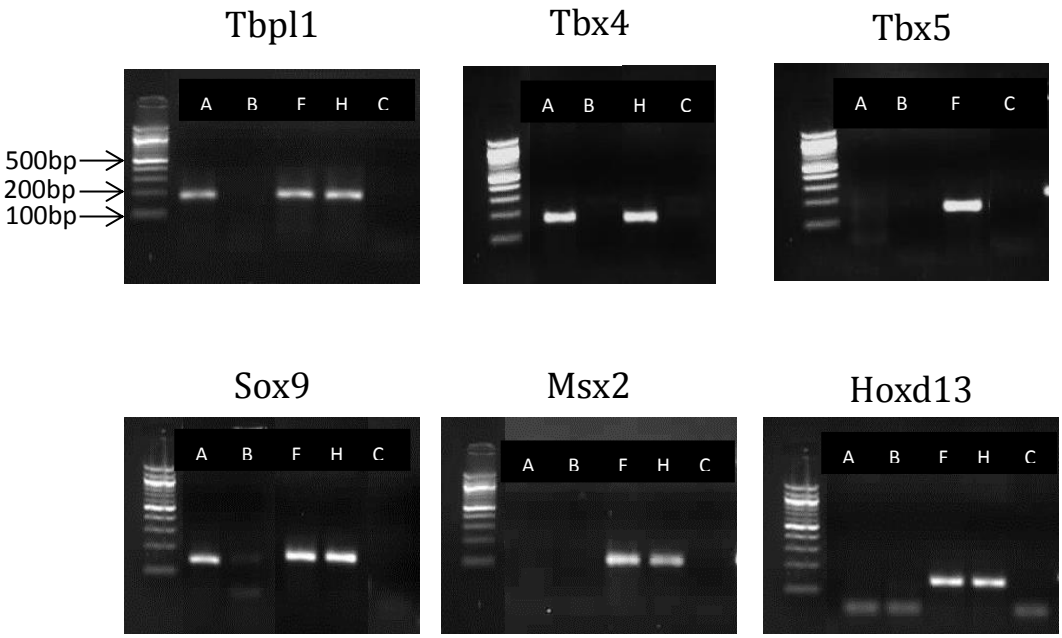

Figure 4.10: Expression of limb development genes in immortalised mouse HL cells compared to fresh tissue. Gel electrophoresis results of PCR products amplified using primers against six different genes. A 100bp ladder was run with each sample. A: immortalised HL cells; B: No reverse transcriptase control; F: pooled E13.5 forelimb tissue stored in RNAlater; H: pooled E13.5 hindlimb tissue stored in RNAlater; C: No template control.

4.3.4 *Bat primary cultures failed to immortalise*

The bat primary cell culture experiment described in section 4.3.2 shows that bat limb cells can be viably plated and maintained as primary cultures which retain their correct limb identity. The next step is to repeat the immortalisation procedure that was performed on the E13.5 mouse limb cells on equivalently staged *M. natalensis* embryo limbs.

The CS17 bat FLs and HLs were dispersed and plated to receive one of 3 treatments once cells were settled and adhered to the dish surface: Treatment A received viral lysate and selection, Treatment B received no lysate but selection and Treatment C received no lysate or selection. Photographs taken of all bat primary cells 3 days after treatment A was infected with retrovirus carrying the SV40 large T antigen showed that treatment plates all started out with a similar confluency prior to selection (Figure 4.11 A, B & C). At 9 days after selection (DAS) both the cells that were infected with the SV40 Tag (Treatment A) and cells that were not infected (Treatment B) had decreased in confluency (Figure 4.11 D & E). Treatment C, having not received viral lysate or selective media, increased in confluency (Figure 4.11 F). At 17 DAS, almost all cells had died in treatments A and B (Figure 4.11 G & H) while treatment C increased in confluency and had to be expanded to a larger surface area by 15 DAS.

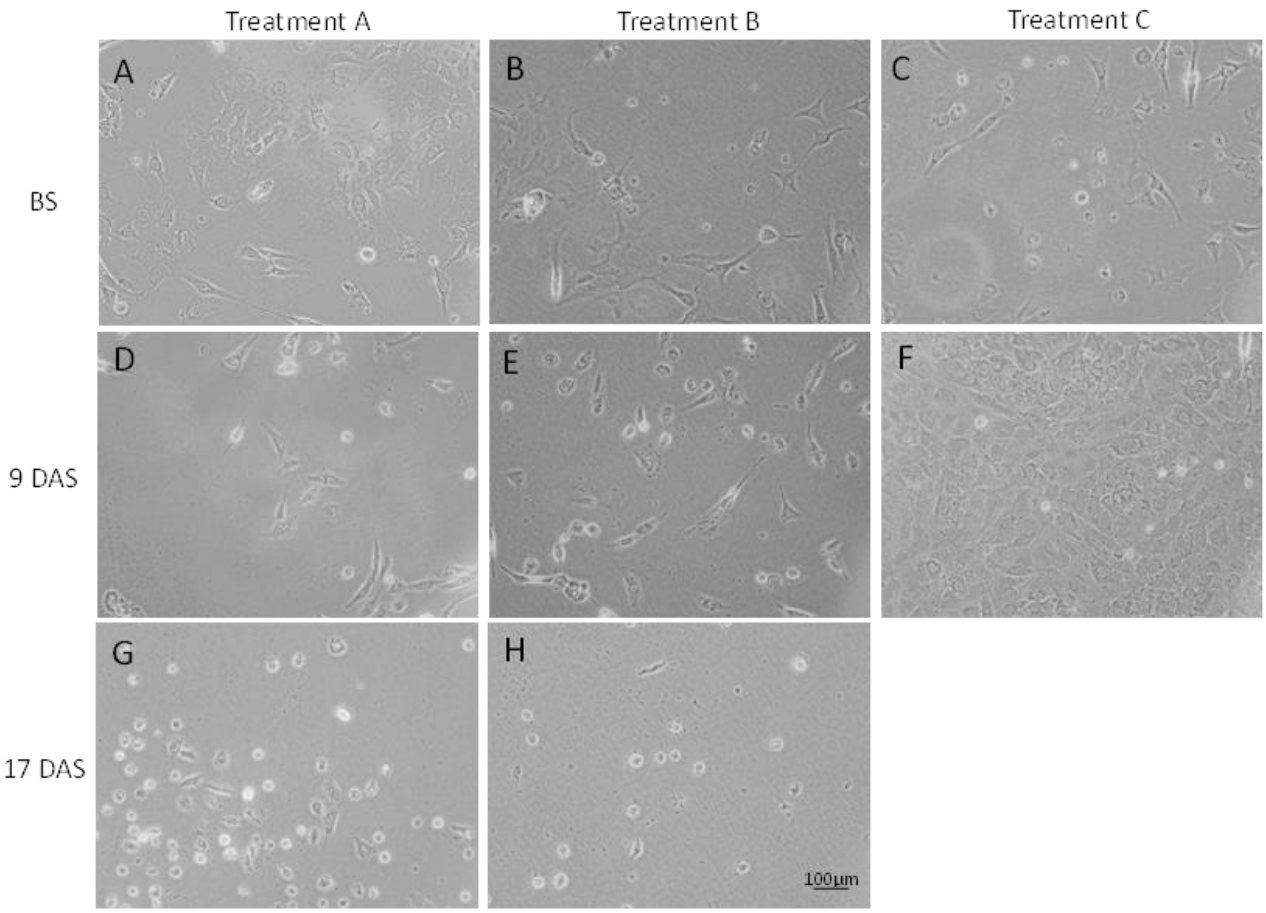

Figure 4.11: Bat HL cells under selection of G418 after attempted immortalisation. *Treatment A, B and C were plated at the same density before selection (BS) started (A, B and C). Treatment A, infected with SV40 Tag and grown in media supplemented with G418 to terminate all untransformed cells, showed a decrease in confluency 9 days after selection (DAS) began (D). At 17 DAS very few adherent cells remained and there were many dead cells in the media (G). Treatment B, not infected with retroviral lysate but received the same selective media as Treatment A, showed a decrease in confluency after 9 DAS (E) and even further decrease 17 DAS (H). Treatment C received neither retroviral lysate, nor selective media and increased in confluency after 9 DAS. The treatment C cells had to be plated onto a larger surface area before 17 DAS. All photographs were taken at 20X microscope magnification and are all to scale.*

This same protocol was repeated twice more on the CS17 FL and HL primary cell cultures (which remained viable), again infecting the cells with fresh viral lysate and monitoring for colony formation in Treatment A. In both cases, Treatment A cells died at the same rate as Treatment B, suggesting that the SV40 Tag was not successfully transformed and thus cells were not immortalised.

4.4 Discussion

An immortalised cell line is an excellent tool for functional genetic studies, especially when working with wild, non-model organisms. Producing an immortalised cell line is an onerous task as the protocol needs to be optimised to the species of interest and desired cell type. The bat embryos used in this study were collected from wild-caught females and were dissected in the field, increasing the need to control for contamination. Added to the careful prevention of contamination was the need to maintain the tissue for 20 hours before further processing could occur in a P2 facility back at the University of Cape Town. The protocols needed for a successful immortalisation were first established on mice due to ease of access. From these optimisation experiments a successful work flow from tissue collection to plating of primary cells was set up for bats caught in the field (Supp. Fig. 4.2).

4.4.1 *Bat primary cultures maintain limb identity*

A successful protocol has been established for the preparation of healthy bat limb primary cultures that divide and retain their FL and HL identities up to 2 months in culture. The FL specific marker, *Tbx5,* shows greater expression levels in the FL cells relative to HL. And conversely higher levels of *Tbx4*, the HL marker, are seen in the HL cells compared to the FL cells. It is particularly interesting that the fold difference of *Tbx4* expression in FL and HL primary cell cultures was very similar to that seen in an RNA-seq study that compared gene expression levels between dissected CS17 bat FL and HL tissue (Eckalbar et al. 2016). It is sufficient to do comparative studies between FL and HL primary cells as they both maintain their identities as FL and HL cells.

In addition to differences between *Tbx5* and *Tbx4* expression, the primary cultures also showed differences in the expression of *Hoxd11*. Both Eckalbar et al. (2016) and Mason (2016) showed that *Hoxd11* had higher FL expression than HL during development, a trait that is not seen in mice. In this study*, Hoxd11* was similarly found to be expressed at higher levels in bat FL than HL primary cells cultures. This further indicates that the identity of the limbs and development process is not lost in cultured primary cells. Again the fold difference in expression of *Hoxd11* between bat primary FL and HL cells was very similar to the that seen in the read count results from the RNA-seq study (Eckalbar et al. 2016). The crucial autopod development gene, *Hoxd13*, was found to be expressed equally in FL and HL in the RNA-seq data (Eckalbar et al. 2016) as

well as in microarray and qPCR results on *M. natalensis* fresh tissue (Mason, 2016). Previous studies have reported a reduction or even the total loss of *Hoxd11* and *Hoxd13* expression in cultured limb cells (Cooper et al. 2011; Rodrigues et al. 2017), thus making the retention of these crucial development gene expressions more interesting.

It was noted during the expansion of the bat primary cell cultures that the FL cells tended to proliferate at a faster rate than the HL cells. Although the initial HL tissue samples were smaller than the FL samples, thus resulting in a larger total number of dissociated FL cells compared HL, the same number of live cells was plated for each limb type. Eliminating starting cell number as the possible reason, another theory is that the HL lags slightly behind the FL in development (Hockman et al. 2009) and thus the FL tissue may have been at a more proliferative stage of development than the HL at the time of dissection and perhaps accelerated proliferation rate is cell autonomous. During the initial stages of digit formation the focus of limb development is on the condensation of mesenchymal cells and subsequently their differentiation into chondrocytes. Once the limb pattern has been laid out then chondrocytes further differentiate into proliferative chondrocytes which will divide, promoting limb elongation at the growth plates (Kronenberg 2003). It is thus possible that in the bat FL cultures there were more proliferating chondrocytes while in the HL cells, the chondrocytes had not yet differentiated into proliferating chondrocytes. In the potential absence of external cues, the HL chondrocytes may have not ever further differentiated, thus the replication time of the cells was slower and ceased sooner.

It is remarkable how a group of cells still growing, but now in disarray, can maintain the expression of four important development genes despite the lack of external temporal cues and special orientation.

4.4.2 *Immortalised mouse cells lose* Hoxd13 *expression but maintain limb cell identity*

The mouse immortalisation took less than two weeks, once selection of G418 was started, to see the immortalised colonies with the naked eye. This is relatively fast as a group immortalising rabbit articular chondrocytes, using a non-ts SV40 Tag construct reported selection continued between 2 to 4 weeks before colonies were isolated (Steimberg et al. 1999). The behaviour of the mouse cells in the colonies was also notably different to the

expansion of the primary cell cultures. The cells tended to grow on top of one another rather than spread out over a larger surface area, thus making the tower of cells easily detectable.

One immortalized HL cell line was successfully subcloned, and characterized by RT-qPCR analysis of marker genes. This cell line is likely to have chondrogenic origins as it expresses the key digit marker, *Sox9* (Wright et al. 1995). The interdigital marker, *Msx2* (Fernández-Terán et al. 2006), was not expressed in the immortalised cell line at all, which provides evidence towards successful isolation of a monoclonal culture. In light of discovering that these are chondrocytes, it is possible that the stacking of cells seen in the initial colonies is due to the behaviour of mesenchymal cells during condensation to form initial digits or recruit more mesenchymal cells at the growth plates. *Sox9* is transcriptionally active in digits of this mouse stage and has been shown to be essential for this condensing behaviour (Akiyama et al. 2002). It has been reported that such nodular condensations are seen in intermediate mesenchymal progenitor cells that have been formed via differentiation of induced pluripotent stem cells (Cheng et al. 2014, Yamashita et al. 2015, Diederichs et al. 2016).

PCR also confirmed that the immortalised mouse HL cells maintained their HL identity as they expressed the HL marker *Tbx4* and did not express *Tbx5*, a marker of FL identity (Rodriguez-Esteban et al. 1999). Unlike the bat primary cells, *Hoxd13* expression was different to that seen in limb tissue samples. In immortalised mouse HL cells, *Hoxd13* expression was either lost or expressed at levels too low for detection via PCR. This may be a result of a number of factors discussed below.

The cells were only infected with retrovirus after 24 days in culture as primary cells, and it is possible that in this time the cell that was immortalized had lost the expression of *Hoxd13*. Mesenchymal cells have been shown to differentiate into chondrocytes and lose expression of *Hoxd11* and *Hoxd13*, when primary cultures of chicken mesenchymal cells were grown in culture at high densities (Ahrens et al. (1977)). However, supplementing the media with Wnt3a and Fgf8 ligands prevented cells from differentiating which saw an up-regulation of *Hoxd13* and *Hoxd11* in the HH18 chicken cells. Alternatively the cell that was immortalised was not a cell that produced *Hoxd13* to begin with.

Additionally, it was reported in Rodrigues et al. (2017) that *Hoxd13* expression in the autopod is dependent on the simultaneous expression of *Shh* and *Fgf8*. Both these ligands are locally

expressed in whole autopod tissue with Shh-expressing cells found in the Zone of polarising activity and Fgf8-expressing cells found in the ectoderm (Riddle et al. 1993, Ohuchi et al. 1997). Since our HL cell line is likely a monoclonal culture of a single digit cell, it is unlikely that either of these two ligands is expressed in the culture and thus *Hoxd13* is not activated in the cells. This highlights some of the advantages of a heterogeneous primary culture over cell lines.

The SV40 construct used in this study was designed to be temperature sensitive (Boolay 1999). At 33^{o}C the SV40 Tag maintains the cells in an undifferentiated state, rapidly dividing. However, if cells are moved to the non-permissible temperature, 39^{o}C, the SV40 Tag genes will not be expressed and as a result cell division will slow down, returning the cells to their original phenotype. In future experiments, *Hoxd13* expression could be analysed at this non-permissive temperature to see if the original expression levels are restored when media is supplemented with Wnt3a, Fgf8 and Shh.

Additional experiments should be performed on the cell line to infer further evidence that the cell line is both immortalised and monoclonal. This can be accomplished by performing a Western blot to check expression of the SV40 Tag (Rodrigues et al. 2017). The clonality of the cell line can be confirmed by using a Southern blot analysis of a chromosomal restriction enzyme digest to determine if the SV40 Tag construct is inserted into the same locus in the genome for all cells. A single band would be expected should all the cells be from a single individual and thus contain the SV40 construct in the same site (Boolay 1999).

The frozen down stocks of the immortalised E13.5 mouse HL cell line has supplied the lab with a source of homogenous embryonic mouse HL digit cells on which enhancer manipulations and novel experiments can be carried out and optimised before the immortalised bat cell line is produced.

4.4.3 *Inability to transform bat cells with SV40 Tag*

Although it was possible to immortalize cell lines from primary cultures of mouse FL and HL limb buds, the experiments on bat primary cultures were not successful. There are a number of factors that can be taken to into consideration to explain this result, including whether the SV40 large T antigen is effective in immortalizing bat cells, or whether the murine retroviral packaging is able to infect bat cells.

It is clear that the SV40 large T antigen is effective in immortalizing bat cells. Crameri et al. (2009) attempted to immortalise 20 different tissue types from Australia's Black Flying Fox (*P. alecto*). Of the 20 tissue types that were established into primary cell cultures 15 were successfully immortalised, of which 5 had monoclonal colonies isolated. In these cases the primary cells were immortalised through the same stable integration of SV40 Tag genes, cloned into pQCXIH (Clontech), in into the bat chromosomal DNA, as used on the embryonic mouse limb cells in this study. We thus know from Crameri et al. (2009) that many bat tissues, including foetal tissue, are able to be immortalised via the SV40 Tag construct.

However an important distinction between the immortalisation constructs used in Crameri et al. (2009) and this study is the pseudotyping of the SV40 construct within the packaging cell line. One plausible reason for the failure to transform the SV40 Tag genes into the bat genome is that viral packaging produced by the ψ2 cells failed to infect bat cells. For the SV40 Tag genes to be successfully integrated into the target cell genome, the packaging cell line produces packaging and envelope proteins in unison with the viral transcript carrying SV40 Tag genes (Greenwood et al. 1996, Kim et al. 2016). The envelope proteins mediate the entry of this viral construct into the target cell by binding to receptors on the target cell surface (Stripecke and Kasahara 2007).

Crameri et al. (2009) psuedotyped the SV40 construct with vesicular stomatitis virus G glycoprotein (VSV-G). The vesicular stomatitis virus belongs to the same family as the well-known rabies virus (Finkelshtein et al. 2013). This is a commonly used envelope used for viral coating due to its broad tropism to many mammalian cell types (Burns et al. 1993).

The Ψ^2 packaging cell line used in my project contains *gag* and *env* genes for packaging derived from the Moloney murine leukemia virus (MLV; (Hoffmann et al. 1982)). This virus is so named due to its ability to cause cancer in mice, however it has been noted that they can affect other vertebrates (Apte and Sanders 2010). A study done on the infectious ability of MLV in the cell lines of 6 mammalian species showed that while NIH3T3 mouse derived cells were able to restrict infection but not block reverse transcription of the viral RNA, some of the mammalian cell lines could block viral DNA integration post reverse transcription of the viral RNA. Bats and primates however were able to block the infection prior to this reverse transcription, but the mechanism of this were not further tested (Besnier et al. 2003). It thus is understandable that the SV40 Tag successfully integrated in the mouse genome to immortalise the mouse cell lines.

However it is plausible that the virus envelope used was not able to penetrate the bat cell membrane, which could potentially explain why the SV40 did not integrate into the genome and immortalise the cells.

To test this hypothesis it is possible to transiently transfect the ψ2 cells with a vector expressing the VSV-G broad spectrum protein, which would be integrated into the viral particles, expanding their host range. If this new envelope system is successful then this study will also provide insight into mammalian differences in infection response to specific viral particles.

The successful isolation of immortalized bat FL and HL cell lines will open up opportunities for functional genetics experiments, and will minimise the need to return to the field to harvest new specimen each year. It will open up new avenues of research such as enhancer and gene manipulations. Biochemical assays can be used to further our understanding of the mechanism of bat-specific gene expression, such as the upregulation of *Hoxd11*. Simple experiments such as manipulation of the media via addition of ligands, such as Shh and Fgf8 will also show novel insights yet to be seen in a bat limb cell line.

Chapter 5:

Conclusions and future work

This project aimed to contribute to the understanding of the molecular mechanisms involved in extensive elongation of the bat wing. Following the publication of an RNA-seq and ChIP-seq experiment on the CS15-CS17 embryos of *M. natalensis*, many candidate genes and pathways have been implicated in the evolutionary development of this mammals extreme FL (Eckalbar et al. 2016). The hypothesis drawn from both the literature and the recent RNA-seq results was that the observed, decreased Wnt/β-catenin signalling and increased BMP signalling in the bat FL may lead to elevated levels of *Sox9* expression, and larger fields of mesenchymal condensations. This project focused on testing this hypothesis, as well as establishing an immortalised cell line from bat limb tissue to be used as a tool for future functional studies.

The expression of *Sox9* was investigated from the RNA-seq results; however it was discovered that *Sox9* had not been annotated in the *M. natalensis* genome and thus no RNA-seq or ChIP-seq reads counts were associated with this gene. Further investigation found that there were large sequencing gaps in the region suspected to contain the *Sox9* locus, likely the reason for a lack of annotation. To determine the expression levels of *Sox9* between the two limbs in early stages of development, first the missing sequence had to be filled in. This was successfully achieved and revealed *Sox9* to have three exons, as seen in the mouse and human orthologues. Some confirmed differences between the bat *Sox9* locus and mouse orthologue is the much smaller 5' UTR in the bat compared to the mouse and also that the second exon was slightly bigger in the bats than that found in mouse and human.

Expression patterns of the now complete *Sox9*, revealed no differential expression between the FL and the HL. Thus, it does not appear the upregulation of the *Sox9* activator – the BMP pathway – or the down regulation of the *Sox9* inhibitor – the Wnt/β-catenin pathway – are influencing the expression of *Sox9*. Instead a downstream target of Sox9, *Sox6*, was found to have significantly higher expression in the bat FL compared to the HL at CS15, when digits are first forming. A study of the literature revealed that the BMP signalling pathway has been shown to effect the expression of *Sox6* as well as *Sox9* (Nordin and LaBonne 2014, Kozhemyakina et al. 2015). In addition a target of the Sox trio (*Sox9*, *Sox6* and *L-Sox5*),

Aggrecan, which plays an important role in digit condensation, was reported to be significantly upregulated in the FL at CS15 and CS16. It is thus now hypothesised that *Sox6* is causing the upregulation of *Aggrecan* during development which may, in part, be responsible for the longer digits found in the adult bat wing.

To functionally determine the effects of the upregulated BMP signalling and suppression of Wnt/β-catenin on the formation of digits in the bat FL, the behaviour of condensing mesenchymal cells using PNA staining of relevant stages was visualised. Using this stain and H&E staining a large set of image data across four consecutive autopod development stages for both bat and mouse was produced. The data included sections moving ventrodorsally through the limb which revealed a number of interesting features. Firstly, the PNA was found to stain mesenchymal cells prior to them condensing to form digits, suggesting that all mesenchymal cells have the potential to be either digit or interdigit cells at this stage. Once condensed, the PNA evidently only stained condensed mesenchymal cells and as soon as these differentiated into chondrocytes at the centre of the digit shaft there was an absence of PNA. At later stages of digit formation, the mesenchymal cells now make up the joint regions on either side of a long shaft containing chondrocytes at various stages of differentiation.

Previous studies have characterised differences in the formation of bat FL and HL digits using other visualisation techniques. Sears et al. (2006) did a direct comparison of mouse and bat FL digits based on Alcian blue and claimed that accelerated growth in the bat FL was due to an increase in the zone of hypertrophic chondrocytes seen at CS20. Unlike Alcian blue staining, PNA does not rely on mesenchymal cells having already differentiated into chondrocytes and thus allows analysis of limb formation at earlier stages. PNA stains revealed that differences in length between the bat FL and HL can already be seen by CS16 while no differences is seen between the mouse FL and HL at the equivalent stage, E13 (Figure 3.8). In addition there was significantly more PNA staining in the bat sections compared to the mouse sections consistently across the comparable stages. While visually there appeared to be more staining in the bat FL compared to the HL, this was not shown to be statistically significant. However, with more biological replicates and interrogation of the data set for an optimal way to quantify the staining intensity, these differences may become significant.

These experiments characterize the predicted consequences of Wnt/β-catenin and BMP signalling in bat and mouse FL and HL autopods. However, a thorough test of the mechanisms of Wnt/β-catenin signalling, BMP signalling and Sox6 activity during bat wing development would require manipulation of the components of these pathways. It is not possible to do these functional experiments in bat embryos; however, a bat limb cell line would be a valuable experimental tool for functional validation and biochemical characterization of developmental pathways.

In order to take steps towards enabling functional analyses of genes during bat limb development, the second aspect of this project focused on the feasibility of establishing conditionally immortalised cell lines from developing mouse FL and HL, as proof of concept for similar work on bat autopods. Immortalised cell lines provide a constantly accessible and renewable tool on which functional experiments can be done to better understand the biochemical pathways and the functions of genes expressed in a specific tissue type. Once cell lines are established, manipulations of the genes and regulatory regions can be done without need for further harm to animals or requirements for further ethical consent. The immortalization process can be achieved in a number of ways (reviewed in Irfan Maqsood et al. (2013)) and often fixes cells at a definite stage of differentiation while they continue to divide (Boolay 1999).

A temperature sensitive version of the SV40 Tag was used to conditionally immortalize cells from dissociated mouse FL and HL autopods. A retrovirus carrying the SV40 Tag can be harvested from the media of Ψ2 packaging cell line, which produces the construct and necessary viron-production components, *in trans*, for successful transformation (Mann et al. 1983). Successfully transformed cells were selected using an antibiotic, G418, which selects against cells that do not contain the SV40 construct. The remaining immortalised autopod cells were isolated and cultured into a homogenous cell line. The identity of the cell line was determined to be a digit cell due to the characteristic expression of *Sox9* (Wright et al. 1995).

While bat FL and HL primary cell cultures were successfully cultured and sustained for two months – retaining their key gene expression profiles – immortalisation was not achieved. It was subsequently discovered within the literature that bat cells have defences against the MLV psuedotyping of the SV40 construct used in ψ^2 packaging cells, thus the SV40 Tag was not

integrating into the bat genome. To circumvent this issue the VSV-G envelope proteins could be cloned into the ψ^2 cells to facilitate entry of the SV40 construct into the bat cells.

References

Ahrens, P. B., et al. (1977). "Stage-related capacity for limb chondrogenesis in cell culture." Developmental biology **60**(1): 69-82.

Ahuja, D., et al. (2005). "SV40 large T antigen targets multiple cellular pathways to elicit cellular transformation." Oncogene **24**(52): 7729.

Akiyama, H., et al. (2002). "The transcription factor Sox9 has essential roles in successive steps of the chondrocyte differentiation pathway and is required for expression of Sox5 and Sox6." Genes & development **16**(21): 2813-2828.

Almazan, G. and R. McKay (1992). "An oligodendrocyte precursor cell line from rat optic nerve." Brain research **579**(2): 234-245.

Altschul, S. F., et al. (1990). "Basic local alignment search tool." Journal of molecular biology **215**(3): 403-410.

Alvarez, J., et al. (2001). "The perichondrium plays an important role in mediating the effects of TGF-β1 on endochondral bone formation." Developmental Dynamics **221**(3): 311-321.

Anders, S., et al. (2015). "HTSeq—a Python framework to work with high-throughput sequencing data." Bioinformatics **31**(2): 166-169.

Apte, S. and D. A. Sanders (2010). "Effects of retroviral envelope-protein cleavage upon trafficking, incorporation, and membrane fusion." Virology **405**(1): 214-224.

Argraves, W., et al. (1981). "Absence of proteoglycan core protein in the cartilage mutant nanomelia." FEBS letters **131**(2): 265-268.

Atchley, W. R. and B. K. Hall (1991). "A model for development and evolution of complex morphological structures." Biol Rev Camb Philos Soc **66**(2): 101-157.

Aulthouse, A. L. and M. Solursh (1987). "The detection of a precartilage, blastema-specific marker." Developmental biology **120**(2): 377-384.

Barna, M. and L. Niswander (2007). "Visualization of cartilage formation: insight into cellular properties of skeletal progenitors and chondrodysplasia syndromes." Developmental cell **12**(6): 931-941.

Barski, A., et al. (2007). "High-resolution profiling of histone methylations in the human genome." Cell **129**(4): 823-837.

Bejder, L. and B. K. Hall (2002). "Limbs in whales and limblessness in other vertebrates: mechanisms of evolutionary and developmental transformation and loss." Evolution & development **4**(6): 445-458.

Besnier, C., et al. (2003). "Characterization of murine leukemia virus restriction in mammals." Journal of virology **77**(24): 13403-13406.

Bi, W., et al. (1999). "Sox9 is required for cartilage formation." Nature genetics **22**(1).

Bickelmann, C., et al. (2012). "Transcriptional heterochrony in talpid mole autopods." EvoDevo **3**(1): 16.

Bininda-Emonds, O. R., et al. (2007). "Forelimb-hindlimb developmental timing changes across tetrapod phylogeny." BMC evolutionary biology **7**(1): 182.

Blackwood, E. M. and J. T. Kadonaga (1998). "Going the distance: a current view of enhancer action." Science **281**(5373): 60-63.

Blanco, M. J., et al. (1998). "Heterochronic differences of Hoxa-11 expression in Xenopus fore-and hind limb development: evidence for lower limb identity of the anuran ankle bones." Development genes and evolution **208**(4): 175-187.

Bobick, B. E. and J. Cobb (2012). "Shox2 regulates progression through chondrogenesis in the mouse proximal limb." J Cell Sci **125**(24): 6071-6083.

Boolay, S. (1999). Immortalisation, characterisation and differentiation of temperature sensitive cell lines from the Olfactory Neuroepithelium, University of Cape Town.

Bowles, J., et al. (2000). "Phylogeny of the SOX family of developmental transcription factors based on sequence and structural indicators." Developmental biology **227**(2): 239-255.

Brown, M., et al. (1986). "A recombinant murine retrovirus for simian virus 40 large T cDNA transforms mouse fibroblasts to anchorage-independent growth." Journal of virology **60**(1): 290-293.

Burns, J. C., et al. (1993). "Vesicular stomatitis virus G glycoprotein pseudotyped retroviral vectors: concentration to very high titer and efficient gene transfer into mammalian and nonmammalian cells." Proceedings of the National Academy of Sciences **90**(17): 8033-8037.

Carroll, S. B. (2008). "Evo-devo and an expanding evolutionary synthesis: a genetic theory of morphological evolution." Cell **134**(1): 25-36.

Cheng, A., et al. (2014). "Cartilage repair using human embryonic stem cell-derived chondroprogenitors." Stem cells translational medicine **3**(11): 1287-1294.

Chimal-Monroy, J., et al. (2003). "Analysis of the molecular cascade responsible for mesodermal limb chondrogenesis: Sox genes and BMP signaling." Developmental biology **257**(2): 292-301.

Clevers, H. (2006). "Wnt/β-catenin signaling in development and disease." Cell **127**(3): 469-480.

Clevers, H. and R. Nusse (2012). "Wnt/β-catenin signaling and disease." Cell **149**(6): 1192-1205.

Cooper, K. L., et al. (2011). "Initiation of proximal-distal patterning in the vertebrate limb by signals and growth." Science **332**(6033): 1083-1086.

Cotney, J., et al. (2012). "Chromatin state signatures associated with tissue-specific gene expression and enhancer activity in the embryonic limb." Genome research **22**(6): 1069-1080.

Crameri, G., et al. (2009). "Establishment, immortalisation and characterisation of pteropid bat cell lines." PLoS One **4**(12): e8266.

Cretekos, C. J., et al. (2001). "Comparative studies on limb morphogenesis in mice and bats: a functional genetic approach towards a molecular understanding of diversity in organ formation." Reproduction, Fertility and Development **13**(8): 691-695.

Cretekos, C. J., et al. (2008). "Regulatory divergence modifies limb length between mammals." Genes & development **22**(2): 141-151.

Cretekos, C. J., et al. (2005). "Embryonic staging system for the short-tailed fruit bat, Carollia perspicillata, a model organism for the mammalian order Chiroptera, based upon timed pregnancies in captive-bred animals." Developmental Dynamics **233**(3): 721-738.

Creyghton, M. P., et al. (2010). "Histone H3K27ac separates active from poised enhancers and predicts developmental state." Proceedings of the National Academy of Sciences **107**(50): 21931-21936.

Davis, A. P. and M. R. Capecchi (1996). "A mutational analysis of the 5′ HoxD genes: dissection of genetic interactions during limb development in the mouse." Development **122**(4): 1175-1185.

De Crombrugghe, B., et al. (2000). "Transcriptional mechanisms of chondrocyte differentiation." Matrix Biology **19**(5): 389-394.

Diederichs, S., et al. (2016). "Differential regulation of SOX9 protein during chondrogenesis of induced pluripotent stem cells versus mesenchymal stromal cells: a shortcoming for cartilage formation." Stem cells and development **25**(8): 598-609.

Duprez, D., et al. (1996). "Overexpression of BMP-2 and BMP-4 alters the size and shape of developing skeletal elements in the chick limb." Mechanisms of development **57**(2): 145-157.

Eckalbar, W. L., et al. (2016). "Transcriptomic and epigenomic characterization of the developing bat wing." Nature genetics **48**(5): 528.

Farnum, C. E., et al. (2008). "Forelimb versus hindlimb skeletal development in the big brown bat, Eptesicus fuscus: functional divergence is reflected in chondrocytic performance in autopodial growth plates." Cells Tissues Organs **187**(1): 35-47.

Fennema, E., et al. (2013). "Spheroid culture as a tool for creating 3D complex tissues." Trends in biotechnology **31**(2): 108-115.

Fernández-Terán, M., et al. (2006). "Birth and death of cells in limb development: a mapping study." Developmental Dynamics **235**(9): 2521-2537.

Finkelshtein, D., et al. (2013). "LDL receptor and its family members serve as the cellular receptors for vesicular stomatitis virus." Proceedings of the National Academy of Sciences **110**(18): 7306-7311.

Gibson-Brown, J. J., et al. (1996). "Evidence of a role for T-□ genes in the evolution of limb morphogenesis and the specification of forelimb/hindlimb identity." Mechanisms of development **56**(1): 93-101.

Gierer, A. and H. Meinhardt (1972). "A theory of biological pattern formation." Biological Cybernetics **12**(1): 30-39.

Gill, Z. (2016). Characterization of transcription factors and LncRNAs involved in the development of the bat wing, University of Cape Town.

Goldring, M. B., et al. (2006). "The control of chondrogenesis." Journal of cellular biochemistry **97**(1): 33-44.

Greenwood, J., et al. (1996). "SV40 large T immortalised cell lines of the rat blood-brain and blood-retinal barriers retain their phenotypic and immunological characteristics." Journal of neuroimmunology **71**(1): 51-63.

Grüneberg, H. (1963). "The pathology of development. A study of inherited skeletal disorders in animals." The pathology of development. A study of inherited skeletal disorders in animals.

Grüneberg, H. and A. Lee (1973). "The anatomy and development of brachypodism in the mouse." Development **30**(1): 119-141.

Guntakatta, M., et al. (1984). "Development of a mouse embryo limb bud cell culture system for the estimation of chemical teratogenic potential." Teratogenesis, carcinogenesis, and mutagenesis **4**(4): 349-364.

Hall, B. and T. Miyake (1992). "The membranous skeleton: the role of cell condensations in vertebrate skeletogenesis." Anatomy and embryology **186**(2): 107-124.

Hall, B. K. (2008). Fins into limbs: evolution, development, and transformation, University of Chicago Press.

Hall, B. K. and T. Miyake (2000). "All for one and one for all: condensations and the initiation of skeletal development." Bioessays **22**(2): 138-147.

Han, Y. and V. Lefebvre (2008). "L-Sox5 and Sox6 drive expression of the aggrecan gene in cartilage by securing binding of Sox9 to a far-upstream enhancer." Molecular and cellular biology **28**(16): 4999-5013.

Hayflick, L. (1965). "The limited in vitro lifetime of human diploid cell strains." Experimental cell research **37**(3): 614-636.

Heffer, A. and L. Pick (2013). "Conservation and variation in Hox genes: how insect models pioneered the evo-devo field." Annual review of entomology **58**: 161-179.

Hiscock, T. W., et al. (2017). "On the Formation of Digits and Joints during Limb Development." Developmental cell **41**(5): 459-465.

Hockman, D., et al. (2008). "A second wave of Sonic hedgehog expression during the development of the bat limb." Proceedings of the National Academy of Sciences **105**(44): 16982-16987.

Hockman, D., et al. (2009). "The role of early development in mammalian limb diversification: A descriptive comparison of early limb development between the natal long-fingered bat (Miniopterus natalensis) and the mouse (Mus musculus)." Developmental Dynamics **238**(4): 965-979.

Hoffmann, J., et al. (1982). "DNA methylation affecting the expression of murine leukemia proviruses." Journal of virology **44**(1): 144-157.

Hubbard, T., et al. (2002). "The Ensembl genome database project." Nucleic acids research **30**(1): 38-41.

Hugi, J., et al. (2012). "Heterochronic shifts in the ossification sequences of surface-and subsurface-dwelling skinks are correlated with the degree of limb reduction." Zoology **115**(3): 188-198.

Illing, N., et al. (2002). "Conditionally immortalized clonal cell lines from the mouse olfactory placode differentiate into olfactory receptor neurons." Molecular and Cellular Neuroscience **20**(2): 225-243.

Irfan Maqsood, M., et al. (2013). "Immortality of cell lines: challenges and advantages of establishment." Cell biology international **37**(10): 1038-1045.

Karlsen, T., et al. (2016). "Generation of IL1β-resistant chondrocytes using CRISPR-CAS genome editing." Osteoarthritis and Cartilage **24**: S325.

Kawakami, Y., et al. (1996). "BMP signaling during bone pattern determination in the developing limb." Development **122**(11): 3557-3566.

Kawakami, Y., et al. (2006). "The role of TGFβs and Sox9 during limb chondrogenesis." Current opinion in cell biology **18**(6): 723-729.

Kent, W. J. (2002). "BLAT—the BLAST-like alignment tool." Genome research **12**(4): 656-664.

Kiani, C., et al. (2002). "Structure and function of aggrecan." Cell research **12**(1): 19.

Kim, C.-W., et al. (2016). "Immortalization of human corneal epithelial cells using simian virus 40 large T antigen and cell characterization." Journal of pharmacological and toxicological methods **78**: 52-57.

Kim, D., et al. (2013). "TopHat2: accurate alignment of transcriptomes in the presence of insertions, deletions and gene fusions." Genome biology **14**(4): R36.

King, M.-C. and A. C. Wilson (1975). "Evolution at two levels in humans and chimpanzees."

Kozhemyakina, E., et al. (2015). "A pathway to bone: signaling molecules and transcription factors involved in chondrocyte development and maturation." Development **142**(5): 817-831.

Kretzschmar, K. and H. Clevers (2017). "Wnt/β-catenin signaling in adult mammalian epithelial stem cells." Developmental biology.

Kronenberg, H. M. (2003). "Developmental regulation of the growth plate." Nature **423**(6937): 332.

Kumar, D. and A. B. Lassar (2014). "Fibroblast growth factor maintains chondrogenic potential of limb bud mesenchymal cells by modulating DNMT3A recruitment." Cell reports **8**(5): 1419-1431.

Kunz, T. H. and A. Kurta (1987). Size of bats at birth and maternal investment during pregnancy. Symposia of the Zoological Society of London.

Lefebvre, V., et al. (2001). "L-Sox5, Sox6 and Sox9 control essential steps of the chondrocyte differentiation pathway." Osteoarthritis and Cartilage **9**: S69-S75.

Lefebvre, V. and P. Bhattaram (2010). "Chapter Eight-Vertebrate Skeletogenesis." Current topics in developmental biology **90**: 291-317.

Lefebvre, V. and P. Bhattaram (2016). "SOXC Genes and the Control of Skeletogenesis." Current osteoporosis reports **14**(1): 32-38.

Li, V. S., et al. (2012). "Wnt signaling through inhibition of β-catenin degradation in an intact Axin1 complex." Cell **149**(6): 1245-1256.

Lindblad-Toh, K., et al. (2011). "A high-resolution map of human evolutionary constraint using 29 mammals." Nature **478**(7370): 476.

Lories, R. J., et al. (2013). "To Wnt or not to Wnt: the bone and joint health dilemma." Nature Reviews Rheumatology **9**(6): 328-339.

Love, M. I., et al. (2015). "RNA-Seq workflow: gene-level exploratory analysis and differential expression." F1000Research **4**.

Love, M. I., et al. (2014). "Moderated estimation of fold change and dispersion for RNA-seq data with DESeq2." Genome biology **15**(12): 550.

Mann, R., et al. (1983). "Construction of a retrovirus packaging mutant and its use to produce helper-free defective retrovirus." Cell **33**(1): 153-159.

Marędziak, M., et al. (2014). "The influence of static magnetic fields on canine and equine mesenchymal stem cells derived from adipose tissue." In Vitro Cellular & Developmental Biology-Animal **50**(6): 562-571.

Mariani, F. V. and G. R. Martin (2003). "Deciphering skeletal patterning: clues from the limb." Nature **423**(6937): 319.

Marshall, O. J. (2004). "PerlPrimer: cross-platform, graphical primer design for standard, bisulphite and real-time PCR." Bioinformatics **20**(15): 2471-2472.

Mason, M. K. (2016). Skeletal element elongation and interdigital tissue regression in developing bat limbs: a gene expression analysis, University of Cape Town.

Mason, M. K., et al. (2015). "Retinoic acid-independent expression of Meis2 during autopod patterning in the developing bat and mouse limb." EvoDevo **6**(1): 6.

Mason, M. K., et al. (2010). "Evaluation of maternal features as indicators of asynchronous embryonic development in Miniopterus natalensis." Acta Chiropterologica **12**(1): 161-171.

May, T., et al. (2005). "Establishment of murine cell lines by constitutive and conditional immortalization." Journal of biotechnology **120**(1): 99-110.

Milaire, J. (1965). "Aspects of limb morphogenesis in mammals." Organogenesis: 283-300.

Montero, J. A., et al. (2008). "Activin/TGFβ and BMP crosstalk determines digit chondrogenesis." Developmental biology **321**(2): 343-356.

Myers, P. (2007). "Tandem repeats and morphological variation." Nature Education **1**(1).

Nordin, K. and C. LaBonne (2014). "Sox5 Is a DNA-binding cofactor for BMP R-Smads that directs target specificity during patterning of the early ectoderm." Developmental cell **31**(3): 374-382.

Nusse, R. and H. E. Varmus (1982). "Many tumors induced by the mouse mammary tumor virus contain a provirus integrated in the same region of the host genome." Cell **31**(1): 99-109.

Nüsslein-Volhard, C. and E. Wieschaus (1980). "Mutations affecting segment number and polarity in Drosophila." Nature **287**(5785): 795-801.

Ohbayashi, T., et al. (1999). "Isolation of cDNA, chromosome mapping, and expression of the human TBP-like protein." Biochemical and biophysical research communications **255**(1): 137-142.

Ohuchi, H., et al. (1997). "The mesenchymal factor, FGF10, initiates and maintains the outgrowth of the chick limb bud through interaction with FGF8, an apical ectodermal factor." Development **124**(11): 2235-2244.

Pan, Q., et al. (2008). "Sox9, a key transcription factor of bone morphogenetic protein-2-induced chondrogenesis, is activated through BMP pathway and a CCAAT box in the proximal promoter." Journal of cellular physiology **217**(1): 228-241.

Pennypacker, J. P. and P. F. Goetinck (1976). "Biochemical and ultrastructural studies of collagen and proteochondroitin sulfate in normal and nanomelic cartilage." Developmental biology **50**(1): 35-47.

Petit, F., et al. (2017). "Limb development: a paradigm of gene regulation." Nature Reviews Genetics **18**(4): 245-258.

Pruitt, K. D., et al. (2006). "NCBI reference sequences (RefSeq): a curated non-redundant sequence database of genomes, transcripts and proteins." Nucleic acids research **35**(suppl_1): D61-D65.

Rada-Iglesias, A., et al. (2011). "A unique chromatin signature uncovers early developmental enhancers in humans." Nature **470**(7333): 279-283.

Raspopovic, J., et al. (2014). "Digit patterning is controlled by a Bmp-Sox9-Wnt Turing network modulated by morphogen gradients." Science **345**(6196): 566-570.

Redies, C., et al. (1991). "Differentiation and heterogeneity in T-antigen immortalized precursor cell lines from mouse cerebellum." Journal of neuroscience research **30**(4): 601-615.

Retting, K. N., et al. (2009). "BMP canonical Smad signaling through Smad1 and Smad5 is required for endochondral bone formation." Development **136**(7): 1093-1104.

Reya, T. and H. Clevers (2005). "Wnt signalling in stem cells and cancer." Nature **434**(7035): 843-850.

Richardson, M. K. (1999). "Vertebrate evolution: the developmental origins of adult variation." Bioessays **21**(7): 604-613.

Richardson, M. K., et al. (2009). "Heterochrony in limb evolution: developmental mechanisms and natural selection." Journal of Experimental Zoology Part B: Molecular and Developmental Evolution **312**(6): 639-664.

Riddle, R. D., et al. (1993). "Sonic hedgehog mediates the polarizing activity of the ZPA." Cell **75**(7): 1401-1416.

Rijsewijk, F., et al. (1987). "The Drosophila homology of the mouse mammary oncogene int-1 is identical to the segment polarity gene wingless." Cell **50**(4): 649-657.

Roark, E. F. and K. Greer (1994). "Transforming growth factor-β and bone morphogenetic protein-2 act by distinct mechanisms to promote chick limb cartilage differentiation in vitro." Developmental Dynamics **200**(2): 103-116.

Robinson, J. T., et al. (2011). "Integrative genomics viewer." Nature biotechnology **29**(1): 24-26.

Rodrigues, A. R., et al. (2017). "Integration of Shh and Fgf signaling in controlling Hox gene expression in cultured limb cells." Proceedings of the National Academy of Sciences **114**(12): 3139-3144.

Rodriguez-Esteban, C., et al. (1999). "The T-box genes Tbx4 and Tbx5 regulate limb outgrowth and identity." Nature **398**(6730): 814.

Rooney, P. and C. W. Archer (1992). "The development of the perichondrium in the avian ulna." Journal of anatomy **181**(Pt 3): 393.

Rorabacher, D. B. (1991). "Statistical treatment for rejection of deviant values: critical values of Dixon's" Q" parameter and related subrange ratios at the 95% confidence level." Analytical Chemistry **63**(2): 139-146.

Sears, K. E., et al. (2006). "Development of bat flight: morphologic and molecular evolution of bat wing digits." Proceedings of the National Academy of Sciences **103**(17): 6581-6586.

Seim, I., et al. (2013). "Genome analysis reveals insights into physiology and longevity of the Brandt's bat Myotis brandtii." Nature communications **4**: 2212.

Shi, Y. and J. Massagué (2003). "Mechanisms of TGF-β signaling from cell membrane to the nucleus." Cell **113**(6): 685-700.

Shubin, N. H., et al. (2006). "The pectoral fin of Tiktaalik roseae and the origin of the tetrapod limb." Nature **440**(7085): 764.

Smits, P., et al. (2001). "The transcription factors L-Sox5 and Sox6 are essential for cartilage formation." Developmental cell **1**(2): 277-290.

Sohaskey, M. L., et al. (2008). "JAWS coordinates chondrogenesis and synovial joint positioning." Development **135**(13): 2215-2220.

Solursh, M. (1984). "Ectoderm as a determinant of early tissue pattern in the limb bud." Cell differentiation **15**(1): 17-24.

Steedman, H. (1950). "Alcian blue 8GS: a new stain for mucin." Journal of Cell Science **3**(16): 477-479.

Steimberg, N., et al. (1999). "SV40 large T antigen expression driven by col2a1 regulatory sequences immortalizes articular chondrocytes but does not allow stabilization of type II collagen expression." Experimental cell research **249**(2): 248-259.

Stott, N. S. and C.-M. Chuong (2000). "Retroviral gene transduction in limb bud micromass cultures." Developmental Biology Protocols: Volume I: 509-513.

Stripecke, R. and N. Kasahara (2007). Lentiviral and Retroviral Vector Systems. Gene Therapy for Cancer, Springer**:** 39-71.

Studio, R. (2012). "RStudio: integrated development environment for R." RStudio Inc, Boston, Massachusetts.

Suzuki, T., et al. (2008). "Unique SMAD1/5/8 activity at the phalanx-forming region determines digit identity." Proceedings of the National Academy of Sciences **105**(11): 4185-4190.

Syverton, J. T. and W. F. Scherer (1952). "STUDIES ON THE PROPAGATION IN VITRO OF POLIOMYELITIS VIRUSES: I. VIRAL MULTIPLICATION IN TISSUE CULTURES EMPLOYING MONKEY AND HUMAN TESTICULAR CELLS." The Journal of experimental medicine **96**(4): 355.

Tamura, K., et al. (2011). "MEGA5: molecular evolutionary genetics analysis using maximum likelihood, evolutionary distance, and maximum parsimony methods." Molecular biology and evolution **28**(10): 2731-2739.

Tamura, K., et al. (2008). "The autopod: its formation during limb development." Development, growth & differentiation **50**(s1).

Taylor, S., et al. (2010). "A practical approach to RT-qPCR—publishing data that conform to the MIQE guidelines." Methods **50**(4): S1-S5.

Umansky, R. (1966). "The effect of cell population density on the developmental fate of reaggregating mouse limb bud mesenchyme." Developmental biology **13**(1): 31-56.

Velleman, S. (2000). "The role of the extracellular matrix in skeletal development." Poultry Science **79**(7): 985-989.

Wanek, N., et al. (1989). "A staging system for mouse limb development." Journal of Experimental Zoology Part A: Ecological Genetics and Physiology **249**(1): 41-49.

Wang, Z., et al. (2014). "Unique expression patterns of multiple key genes associated with the evolution of mammalian flight." Proceedings of the Royal Society of London B: Biological Sciences **281**(1783): 20133133.

Wang, Z., et al. (2010). "Digital gene expression tag profiling of bat digits provides robust candidates contributing to wing formation." Bmc Genomics **11**(1): 619.

Weatherbee, S. D., et al. (2006). "Interdigital webbing retention in bat wings illustrates genetic changes underlying amniote limb diversification." Proceedings of the National Academy of Sciences **103**(41): 15103-15107.

Wright, E., et al. (1995). "The Sry-related gene Sox9 is expressed during chondrogenesis in mouse embryos." Nature genetics **9**(1): 15-20.

Yamashita, A., et al. (2015). "Generation of scaffoldless hyaline cartilaginous tissue from human iPSCs." Stem cell reports **4**(3): 404-418.

Yoon, B. S., et al. (2005). "Bmpr1a and Bmpr1b have overlapping functions and are essential for chondrogenesis in vivo." Proceedings of the National Academy of Sciences of the United States of America **102**(14): 5062-5067.

Zang, C., et al. (2009). "A clustering approach for identification of enriched domains from histone modification ChIP-Seq data." Bioinformatics **25**(15): 1952-1958.

Zeller, R., et al. (2009). "Vertebrate limb bud development: moving towards integrative analysis of organogenesis." Nature Reviews Genetics **10**(12): 845-858.

Zheng, Z. and M. J. Cohn (2011). "Developmental basis of sexually dimorphic digit ratios." Proceedings of the National Academy of Sciences **108**(39): 16289-16294.

Zhu, J., et al. (2008). "Uncoupling Sonic hedgehog control of pattern and expansion of the developing limb bud." Developmental cell **14**(4): 624-632.

Zimmermann, B. and M. Thies (1984). "Alterations of lectin binding during chondrogenesis of mouse limb buds." Histochemistry and Cell Biology **81**(4): 353-361.

Zuniga, A. (2015). "Next generation limb development and evolution: old questions, new perspectives." Development **142**(22): 3810-3820.

Supplementary figures

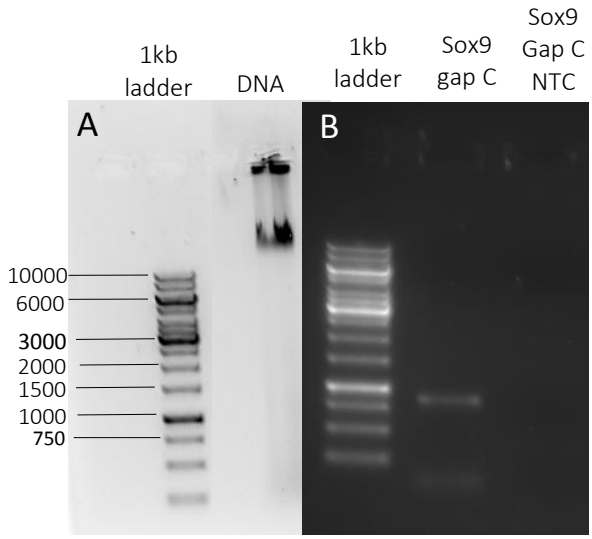

Supplementary figure 2.1: Gel electrophoresis of M. natalensis ***DNA and*** Sox9 ***3rd exon PCR product.*** ***A****: The* M. natalensis *DNA (1.6 µg) was run on a 1% gel at 100V for 30 minutes to produce a single band, suggesting the DNA is intact.* ***B****: The PCR product for the primers designed to fill in missing sequences found in the third exon of* Sox9 *in the* M. natalensis *genome. This amplicon was run on a 1% agarose gel at 80V for 40 minutes. The resulting products size was approximately 900 bp. For each PCR product the "no template control" (NTC) showed no contamination.*

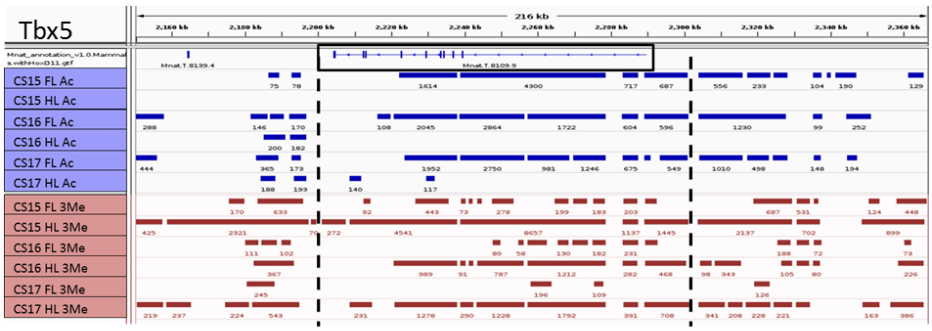

The justification of the positioning of the dashed lines is that the line on the left and right are in the first break in all CHiP tacks that occurs before and after the gene.

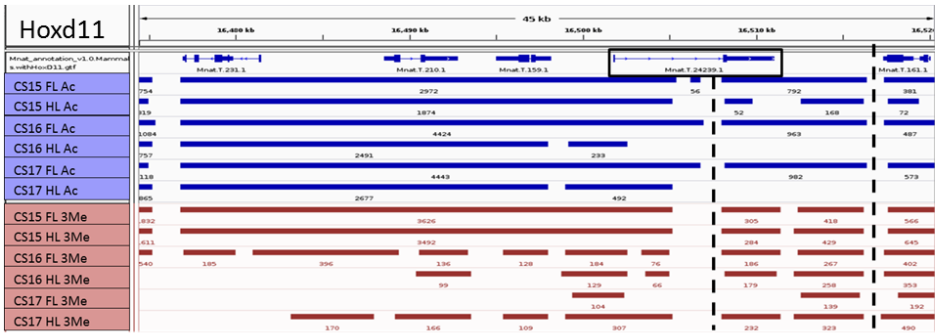

The justification of the positioning of the dashed lines is that the line on the right is in the first break in all CHiP tracks that occurs after the gene. The line on the left is within the gene region however the next gap through all ChIP-seq tracks occurs after three genes to the left of Hoxd11, thus ChiP reads may be due to one or more of the other genes.

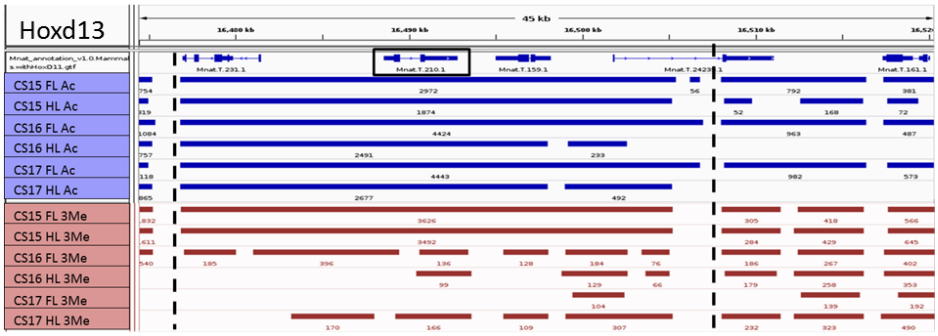

The justification of the positioning of the dashed lines for Hoxd13 is that the line on the left and right are in the first break in all CHiP tracks that occurs before and after the gene. Unfortunately the ChIP tracks cover an extra 2 complete genes, Evx2 and Hoxd12, as well as half of Hoxd11. The two complete genes expression information was thus analysed to see if either of the genes may be influencing the chromatin state of the area.

Supplementary Figure 2.2: ***ChIP site track demarcation for several development genes.*** *Figure continues on next page*

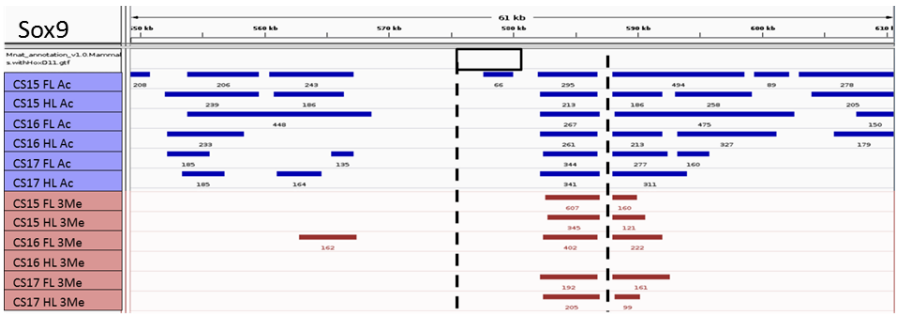

The justification of the positioning of the dashed lines for Sox9 is that the line on the left is straight after the gene and the line on the right in in a clean break close to the start of the gene. Since we know there was a larger region of missing sequencing data in the genome, this may e why ChIP-seq reads did not align within the gene region, except the CS15 FL acetylation data. I thus chose to include ChIP-seq data on the right as, firstly there were no genes close by and secondly this may hint at the open chromatin state in the region.

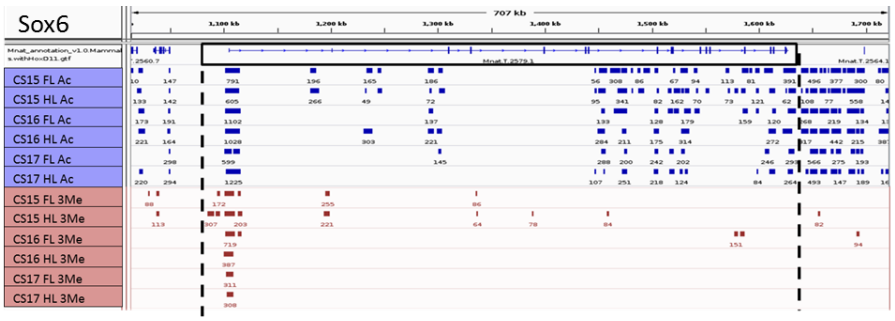

The justification of the positioning of the dashed lines is that the line on the left and right are in the first break in all CHiP tacks that occurs before and after the gene.

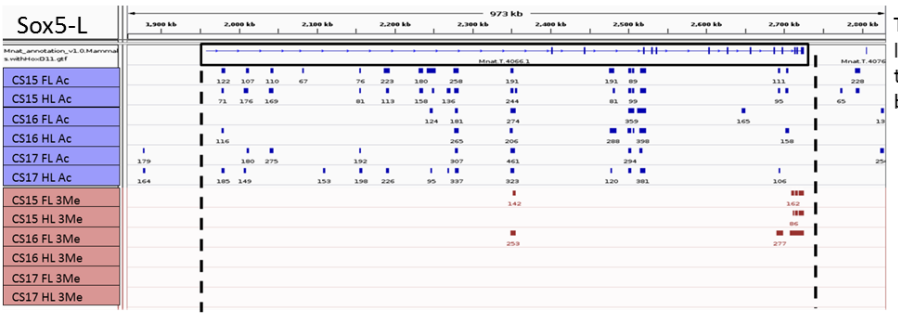

The justification of the positioning of the dashed lines is that the line on the left and right are in the first break in all CHiP tacks that occurs before and after the gene.

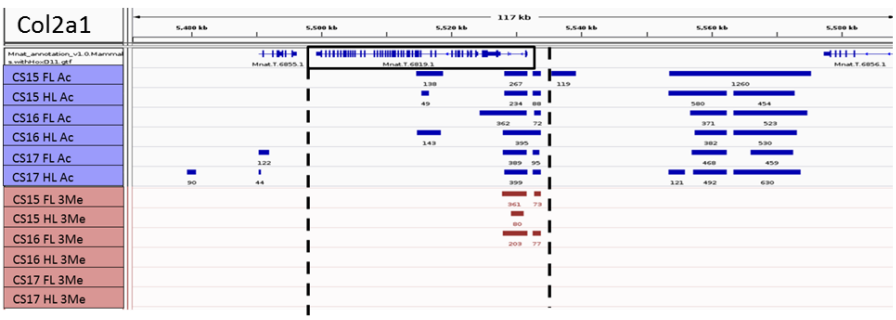

The justification of the positioning of the dashed lines is that the line on the left and right are in the first break in all CHiP tacks that occurs before and after the gene.

Supplementary Figure 2.2: ChIP island inclusion demarcation. *The ChIP sequencing read counts and distribution for H3K27 acetylation (Ac, blue) and H3K27 trimethylation (3Me, red) in FL and HL of CS15, CS16 and CS17* M. natalensis embryos*. The black box indicates the gene of interest and the dashed lines demarcate the ChIP-seq island distribution included in the comparison for said gene ChIP-seq read counts. The justification of the positioning of the dashed lines is described in the right hand panel of each gene.*

Supplementary Table 2.1: Cross-species BLASTn alignment results for Sox9 *mRNA to* M. natalensis *genome. Both the* H. Sapiens *and* M. Musculus Sox9 *mRNA transcripts (query) were aligned to the* M. natalensis *genome (database (Db)). E-values are a measure of the probability of getting the hit in the given database.*

Gene ID	scaffold	Query start	Query end	Db strt	Db end	E value
***H. Sapiens Sox9* to final *M.natalensis* genome**						
gi|568815581:72121020-72126420	chr212	3000	5400	578979	576564	0.0
gi|568815581:72121020-72126420	chr212	470	813	581358	581012	2e-151
gi|568815581:72121020-72126420	chr124	571	813	320138	320383	5e-102
gi|568815581:72121020-72126420	chr322	586	805	1523100	1522875	2e-55
gi|568815581:72121020-72126420	chr322	1696	1808	1521686	1521574	3e-29
gi|568815581:72121020-72126420	chr32	1716	1791	3162618	3162543	5e-22
gi|568815581:72121020-72126420	chr9	682	725	875757	875800	3e-09
gi|568815581:72121020-72126420	chr119	672	784	1757098	1757210	2e-07
***M. Musculus Sox9* to final *M.natalensis* genome**						
gi|372099099:112782210-112787757	chr212	2933	3302	578979	578610	2e-140
gi|372099099:112782210-112787757	chr212	473	824	581358	581007	2e-140
gi|372099099:112782210-112787757	chr212	3658	3937	578278	577999	5e-97
gi|372099099:112782210-112787757	chr212	5219	5544	576916	576564	9e-75
gi|372099099:112782210-112787757	chr212	4670	5008	577401	577095	7e-51
gi|372099099:112782210-112787757	chr124	577	824	320141	320388	7e-101
gi|372099099:112782210-112787757	chr322	589	811	1523100	1522872	5e-52
gi|372099099:112782210-112787757	chr322	1602	1708	1521680	1521574	2e-27
gi|372099099:112782210-112787757	chr32	1616	1691	3162618	3162543	1e-18

Supplementary Table 2.2: Sox9 *and neighbouring genes in* M. musculus*. A list of the closest annotated regions near the* Sox9 l*ocus in* M. musculus*. The last column describes the scaffold that these annotated sequences aligned to in the* M. natalensis *genome*

Gene name/Id	description	Position on chromosome 11 in M. musculus	Scaffolds on the*M. natalensis* genome
Sox9		112782210..112787757	Scaff 212
Gm30562	predicted gene, 30562	112805930-112810575	Scaff 354
Gm11681	predicted gene 11681	12792731-112799008	Scaff 212
BC006965	cDNA sequence	112663927-112711356	Scaff 212 Scaff 619
1700012H19Rik	RIKEN cDNA 1700012H19 gene	112822965-112825128	Scaff 619

Supplementary Table 2.3: Top 10 genes found to be differentially expressed in M. natalensis *FL and HL. Differential expression results performed by Eckalbar et al. (2016) compared to those found in this study which added Sox9 to the genome annotation.*

rank	**Eckalbar et al. 2016**		**This study**	
	Gene	P-adj	Gene	P-adj
1	Tbx4	0	Tbx4	0
2	Hoxd11	4.8E-118	Pitx1	4.61E-125
3	Pitx1	1.8E-113	Tbx5-as	2.63E-113
4	Tbx5-as	2.7E-113	Hoxd11	3.20E-110
5	Hoxd10	2.07E-95	Hoxd10	4.12E-97
6	Tbx18	7.97E-46	Tbx5	1.40E-56
7	Tbx5	9.68E-46	Tbx18	1.62E-45
8	Mnat.G.5624	3.22E-37	Tbx3	4.58E-41
9	Hoxc10	1.17E-36	M.nat.G.5624	3.54E-37
10	Sez6l	1.78E-33	Hoxc10	3.56E-35

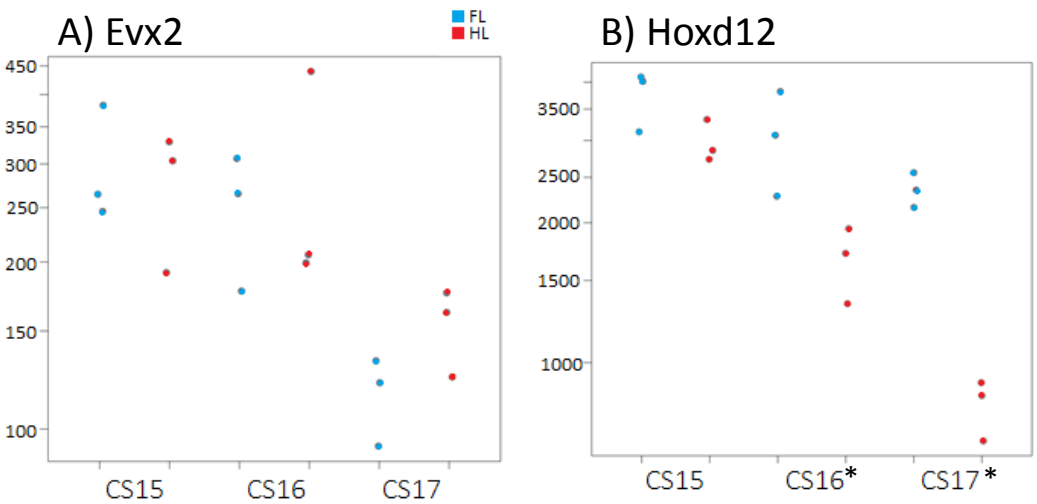

Supplementary Figure 2.3: *Expression analysis of* Hoxd13 *neighbouring genes in* M. natalensis. *The normalised read counts in FL and HL for two neighbouring genes to Hoxd13, Evx2 (A) and Hoxd12 (B), across three consecutive developmental stages. Asterisks show significant difference between FL and HL at a given stage (p-adjusted < 0.01).*

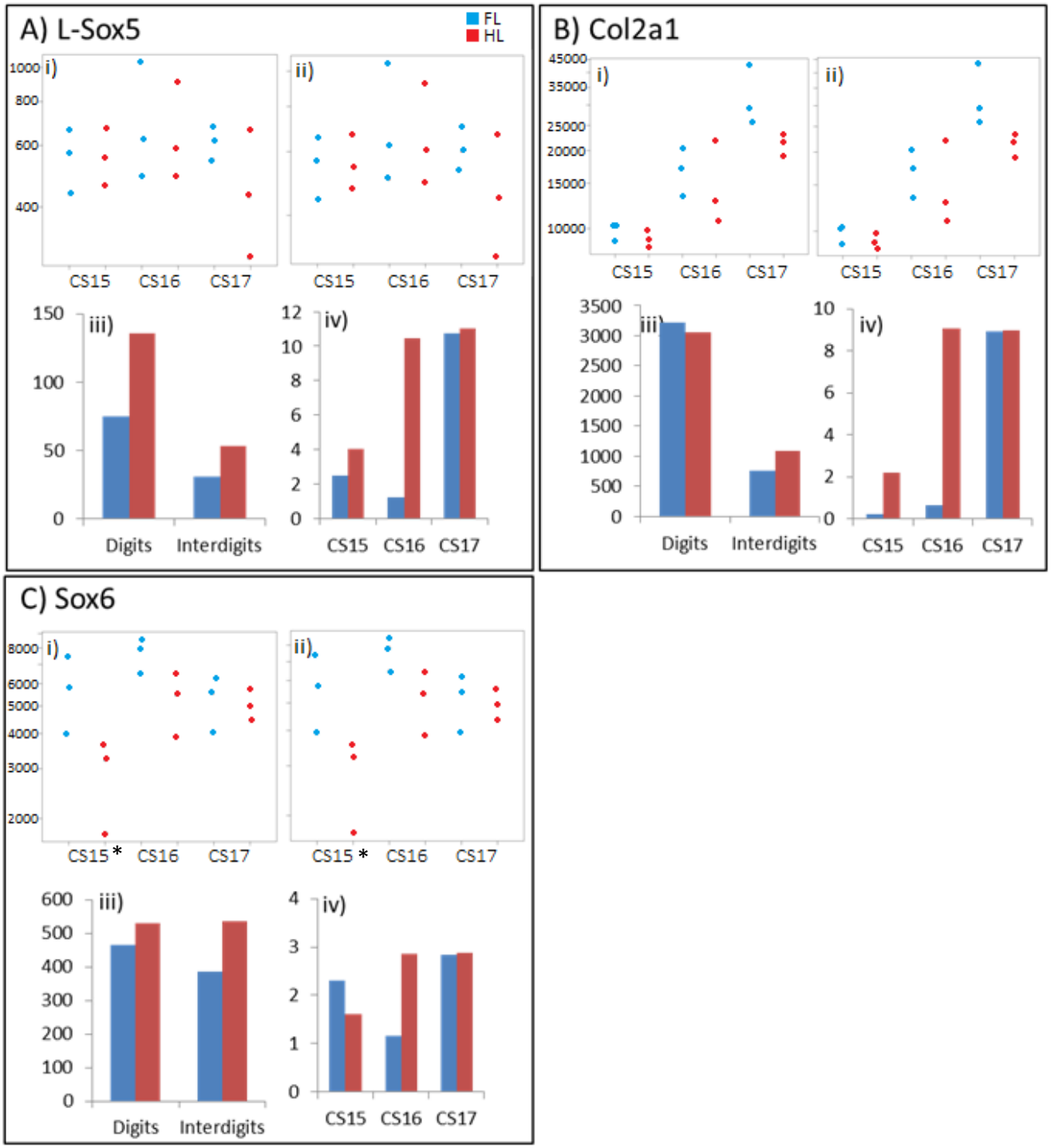

Supplementary Figure 2.4: ***Expression and chromatin modifications of*** Sox9 ***downstream targets*** analysed ***in developing bat limbs.*** *The same four data sets were used to analyse gene expression and chromatin modifications for three* Sox9 *target genes:* L-Sox5 *(A),* Col2a1 *(B) and* Sox6 *(C). The four datasets analysed for each gene are:* ***i)*** *The normalised read counts obtained in this study from FL and HL of three* M. natalensis *embryos per stage during early digit formation.* ***ii)*** *The normalised read counts obtained in Eckalbar et al. (2016) from FL and HL of three* M. natalensis *embryos per stage during digit development. In i) and ii) Asterisks shows significant difference between FL and HL at a given stage (p-adjusted < 0.01).* ***iii)*** *The normalised read counts for FL digital tissue, FL interdigital tissue, HL digital tissue and HL interdigital tissue of* M. schreibersii *embryos during stages of early stages of digit formation.* ***iv)*** *The ChIP-seq read counts over the* respective gene *loci* in M. natalensis *for the same three stages as i) and ii).*

Supplementary Table 3.1: Normalised PNA intensity for all photographed sections. *PNA intensity was normalised in bat and mouse autopod sections by calculating the ratio of green fluorescence (PNA) to blue (Hoechst) across a defined region of interest (the section). Yellow highlighted ratios are the two highest for the biological replicate and the two numbers that were averaged for downstream analysis.*

Bat					Mouse				
Stage	Limb	replicate	section nc	green/blue	Stage	Limb	replicate	section nc	green/blu
CS14	FL	1	6	3.465343	E11.5	FL	1	1	0.260797
CS14	FL	1	7	0.665373	E11.5	FL	1	2	0.12766
CS14	FL	1	8	0.450447	E11.5	FL	1	3	0.123228
CS14	FL	1	10	0.453625	E11.5	FL	2	1	0.243283
CS14	FL	1	11	1.664068	E11.5	FL	2	2	0.26767
CS14	FL	1	12	0.390821	E11.5	FL	3	1	0.439996
CS14	FL	1	13	0.331449	E11.5	FL	3	2	0.39015
CS14	FL	1	14	0.343419	E11.5	FL	3	3	0.490809
CS14	FL	2	1	1.040544	E11.5	FL	3	4	0.283381
CS14	FL	2	2	0.881874	E11.5	HL	1	1	0.088029
CS14	FL	2	3	0.453626	E11.5	HL	1	2	0.09723
CS14	FL	3	2	0.974028	E11.5	HL	1	3	0.129812
CS14	FL	3	3	1.26801	E11.5	HL	1	4	0.100927
CS14	FL	3	4	1.506987	E11.5	HL	2	1	0.077191
CS14	FL	3	5	1.234088	E11.5	HL	3	1	0.109077
CS14	FL	3	6	1.177181	E11.5	HL	3	2	0.138163
CS14	FL	3	7	1.495158	E11.5	HL	3	4	0.214074
CS14	FL	3	8	2.604768	E11.5	HL	3	5	0.206494
CS14	FL	3	9	2.26538	E12.5	FL	1	2	0.217619
CS14	FL	3	10	1.57208	E12.5	FL	2	2	0.107546
CS14	HL	1	1	0.268174	E12.5	FL	2	4	0.08655
CS14	HL	1	2	0.164167	E12.5	FL	2	5	0.137623
CS14	HL	1	3	0.297623	E12.5	FL	2	6	0.170169
CS14	HL	2	2	0.362183	E12.5	FL	2	7	0.371531
CS14	HL	2	5	0.401768	E12.5	FL	2	8	0.275561
CS14	HL	3	1	0.324222	E12.5	FL	3	4	0.149898
CS14	HL	3	2	0.732417	E12.5	FL	3	5	0.298575
CS14	HL	3	3	0.651779	E12.5	FL	3	6	0.268804
CS14	HL	3	4	0.744746	E12.5	HL	1	1	0.291471
CS14	HL	3	5	0.500621	E12.5	HL	1	2	0.436053
CS14	HL	3	6	0.680899	E12.5	HL	1	3	0.261265
CS14	HL	3	7	0.576306	E12.5	HL	1	4	0.275692
CS14	HL	3	8	0.948335	E12.5	HL	1	5	0.346861
CS14	HL	3	9	0.463229	E12.5	HL	3	1	0.136997
CS14	FL	1	2	0.55	E12.5	HL	3	2	0.152557
CS14	FL	1	3	0.94	E12.5	HL	3	3	0.201618
CS15	FL	1	1	1.198146	E12.5	HL	3	4	0.25168
CS15	FL	1	2	1.049215	E12.5	HL	3	5	0.511735
CS15	FL	1	3	1.087062	E12.5	HL	3	6	0.967309
CS15	FL	1	4	0.464486	E12.5	HL	3	7	0.568537

CS15	FL	2	1	0.674184
CS15	FL	2	2	0.989312
CS15	FL	2	3	0.723077
CS15	FL	2	4	1.174428
CS15	FL	2	5	1.622685
CS15	FL	2	6	0.577715
CS15	FL	2	8	0.800851
CS15	FL	2	9	0.441128
CS15	FL	2	10	0.787406
CS15	FL	2	12	0.589152
CS15	HL	1	1	1.283869
CS15	HL	1	2	0.665959
CS15	HL	1	3	0.476504
CS15	HL	1	4	1.342316
CS15	HL	1	5	0.504747
CS15	HL	1	6	0.53747
CS15	HL	1	7	0.646751
CS15	HL	2	1	0.118067
CS15	HL	2	3	0.767953
CS15	HL	2	4	0.200213
CS15	HL	2	5	0.442206
CS15	HL	2	6	0.41898
CS16	FL	1	1	0.429492
CS16	FL	1	3	0.344815
CS16	FL	1	4	0.24366
CS16	FL	1	5	0.276741
CS16	FL	1	6	0.32191
CS16	FL	1	8	0.199499
CS16	FL	1	9	1.268808
CS16	FL	1	10	0.446642
CS16	FL	1	11	0.282624
CS16	FL	1	12	0.224053
CS16	FL	1	13	0.509149
CS16	FL	2	1	0.727808
CS16	FL	2	2	1.06353
CS16	FL	2	3	1.268458
CS16	FL	2	5	1.275633
CS16	FL	2	6	1.482052
CS16	FL	2	7	1.624538
CS16	FL	2	8	1.569941
CS16	FL	2	9	1.670974
CS16	FL	2	10	2.149764
CS16	FL	2	11	1.247913
CS16	FL	2	12	1.115434
CS16	FL	2	14	1.060866
CS16	FL	2	15	1.261463

E13	FL	1	1	0.080486
E13	FL	1	2	0.107372
E13	FL	1	3	0.101798
E13	FL	1	4	0.094638
E13	FL	1	5	0.331225
E13	FL	1	6	0.086429
E13	FL	2	3	0.182928
E13	FL	2	4	0.178971
E13	FL	2	5	0.26365
E13	FL	2	6	0.374828
E13	FL	2	8	0.253695
E13	FL	3	4	0.289192
E13	FL	3	5	0.353
E13	FL	3	6	0.41585
E13	FL	3	7	0.6913
E13	FL	3	8	0.60329
E13	HL	1	1	0.229853
E13	HL	1	3	0.110282
E13	HL	1	4	0.137048
E13	HL	1	5	0.161501
E13	HL	1	7	0.362985
E13	HL	1	8	0.156756
E13	HL	1	9	0.098704
E13	HL	2	1	0.196198
E13	HL	2	2	0.132727
E13	HL	2	3	0.139683
E13	HL	2	4	0.294652
E13	HL	2	8	0.523846
E13	HL	3	1	0.257141
E13	HL	3	2	0.197942

CS16	FL	2	15	1.261463
CS16	FL	3	3	1.395719
CS16	FL	3	4	1.02298
CS16	FL	3	7	1.114115
CS16	FL	3	8	0.609094
CS16	FL	3	12	1.01152
CS16	FL	4	1	1.21445
CS16	FL	4	2	1.059005
CS16	FL	4	4	1.841947
CS16	HL	1	1	0.448245
CS16	HL	1	2	0.470808
CS16	HL	1	3	0.614558
CS16	HL	1	4	0.860879
CS16	HL	1	5	0.571898
CS16	HL	1	6	0.225286
CS16	HL	1	8	0.703553
CS16	HL	1	9	0.419937
CS16	HL	1	10	0.340793
CS16	HL	1	11	0.277068
CS16	HL	1	12	0.286826
CS16	HL	2	2	0.816603
CS16	HL	2	3	1.455563
CS16	HL	2	4	0.816603
CS16	HL	2	5	0.9976
CS16	HL	2	6	1.372891
CS16	HL	2	7	2.158684
CS16	HL	2	8	0.778084
CS16	HL	2	9	0.716304
CS16	HL	2	10	1.010494
CS16	HL	4	1	1.172546
CS16	HL	4	5	0.674469
CS16	HL	4	7	0.847467
CS16	HL	4	9	0.463367

***Supplementary Table 3.2: Digit length in developing autopod of bat and mouse**. The digit length was calculated from PNA stained autopods for each digit (1-5), where possible, for CS16 bat embryos and both E13 and E13.5 mouse embryos. The stage of the mouse is indicated in purple.*

	Bat			Mouse	
	FL	HL	FL	HL	Mouse stage
Digit 1					
BR1	409.18	225.54			
BR2	508	427.82			
BR3	551.61	329.05			
Digit 2					
BR1	665.09	323.48	379.52	352.9	E13
BR2	748.78	439.25	404.11	555.25	E13
BR3	845.04	482.24	562.11	484.33	E13.5_2
BR4			587.94	583.1	E13.5_3
Digit 3					
BR1	919.15	352.54	404.92	502.34	E13
BR2	774.37	562.57	526.33	959.22	E13
BR3	774.12	413.25	622.28	306.32	E13
BR4			491.19	643.17	E13.5
BR5			600.71	497.61	E13.5
Digit 4					
BR1	944.12	359.45	407.78	422.58	E13
BR2	847.19	578.04	509.74	626.84	E13
BR3	690.07	437.13	285.57	217.79	E13
BR4			579.29	366.6	E13.5
Digit 5					
BR1	715.73	249.65	451.2	365.16	E13.5
BR2	735.22	389.38	410.11	338.27	E13.5
BR3	774.94	334.94			

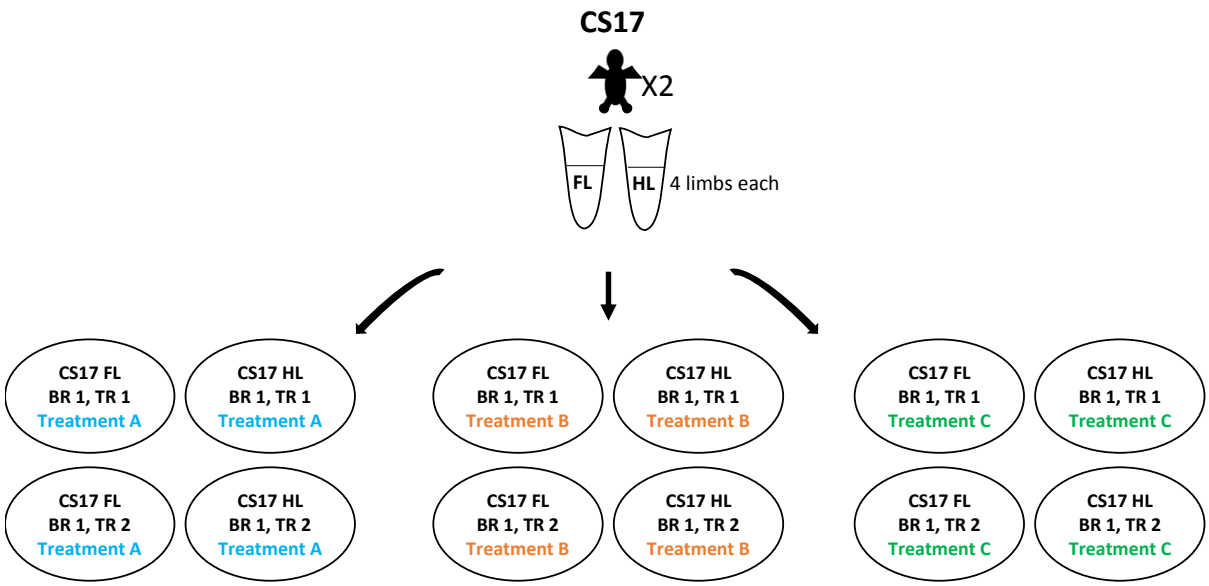

Supplementary Figure 4.1: Plating and treatment plan for immortalisation of embryonic bat limb cells. Each FL and HL biological replicate (BR) was treated as shown with two technical replicate (TR) per treatment. Treatment A: Cells were exposed to SV40 carrying retrovirus for 2 hours after which selection media, containing G418, was used to eliminate untransformed cells. Treatment B: cells were not exposed the virus however the same selection media was used until all cells had died. Treatment C: cells were not exposed to the virus and did not receive selection media, thus allowed to grow as primary cultures.

1:1 HBSS: 0.25% Trypsin

Place at 4°C for 16 hours

Centrifuge at 200g for 5 minutes
Remove 80% of the HBSS: trypsin solution and place tube in 33°C incubator for 20 min

Add 5mls warm DM-10 to inhibit trypisin reaction and disperse limb cells by gently pipetting up and down. Centrifuge at 200 x g for 5 min

Remove DM-10 and washed in HBSS and re-centrifuged at 200 x g for 5 min

Removed HBSS and resuspened in 5mls DM-10

Remove 10ul of suspension into a new tube and add 10ul Trypan blue
Take 10ul of this and count living cells using a haemocytometer

Aliquot enough of the original suspension to plate at $5x10^5$ on 35mm sterile plate. Top up plate to contain 2mls DM-10

Allow cells to settle for 48 hours at 33°C with 5% CO_2

Supplementary figure 4.2: Established protocol for tissue processing and plating bat autopod primary cells. *The protocol has been adapted from Boolay (1999). Several adjustments have been made after optimisations and observations during cell culture experiments using both mouse and bat autopod tissue.*

Supplementary Table 4.1: Efficiencies calculated using standards for various reactions with each primer set.

Primer set	Efficiencies
Tbx4	0.75
Tbx5	0.78
Hoxd11	0.74
Hoxd13	0.79
Tbpl1	0.78

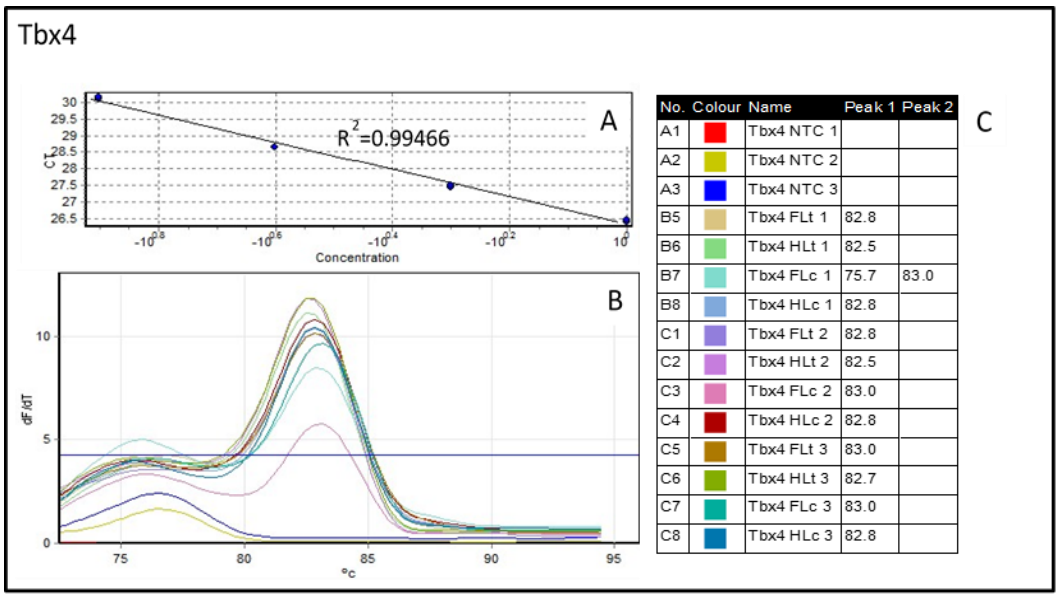

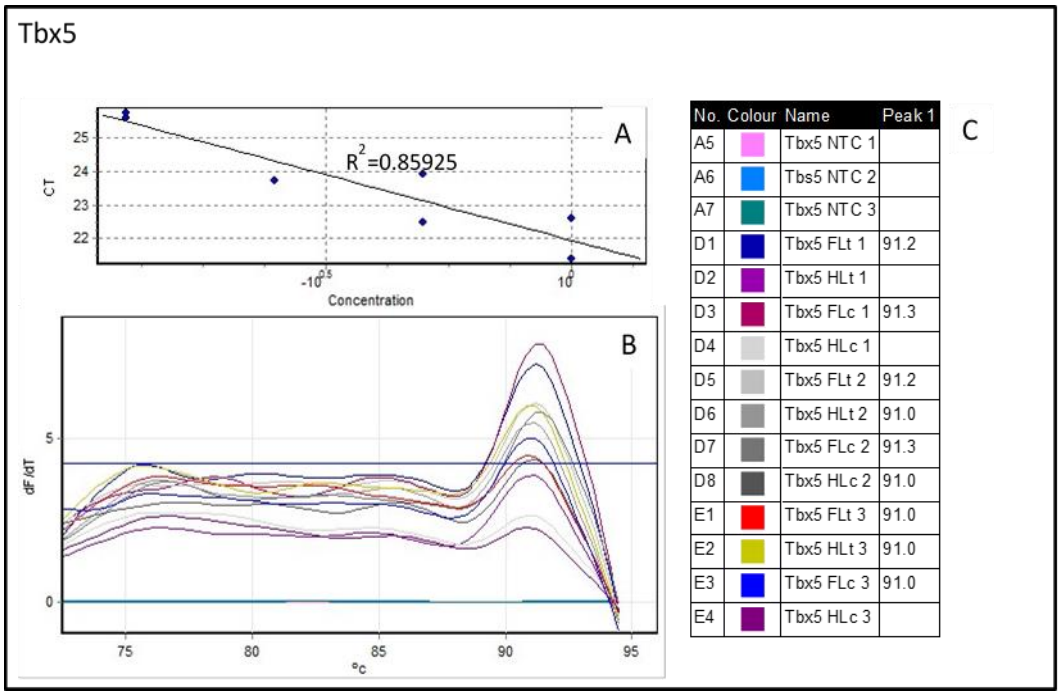

Supplementary figure 4.3: Standard and melt curves of the primer sets used for bat primary cells gene expression*. A) Standard curve after removing outliers, with R2 value reported, B) Melt curve for samples and no template controls (NTC), C) Table of Melt curve peaks and colour key to B.*

Tbpl1

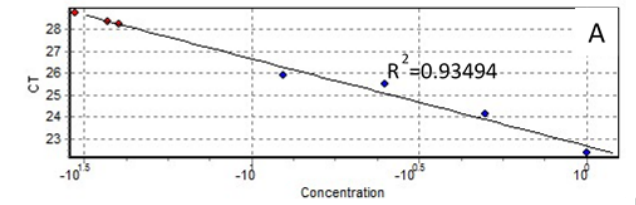

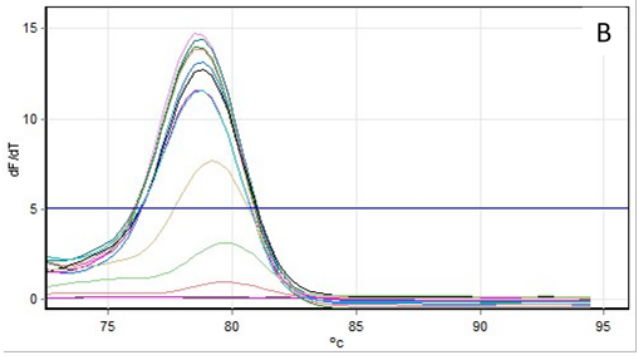

C

No.	Colour	Name	Peak 1
A8		Tbpl NTC 1	
B1		Tbpl NTC 2	
B2		Tbpl NTC 3	
E5		Tbpl FLc 1	78.5
E6		Tbpl HLc 1	78.7
E7		Tbpl FLt 2	78.7
E8		Tbpl HLt 2	78.7
F1		Tbpl FLc 2	78.7
F2		Tbpl HLc 2	78.7
F3		Tbpl FLt 3	78.8
F4		Tbpl HLt 3	78.7
F5		Tbpl FLc 3	79.2
F6		Tbpl HLc 3	

Hoxd11

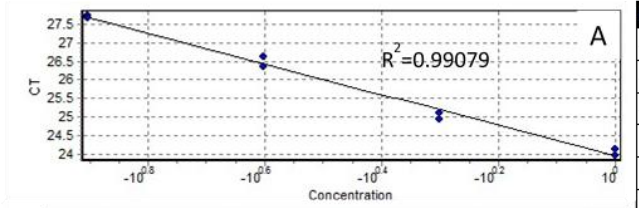

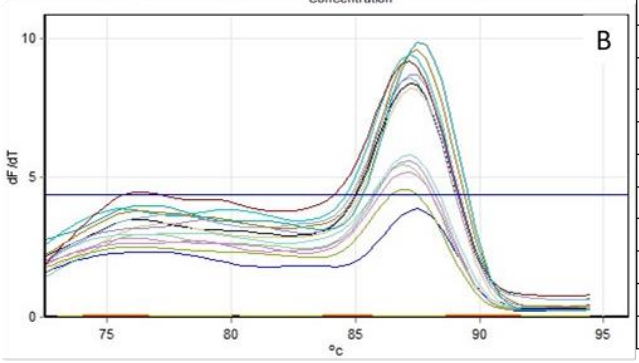

C

No.	Colour	Name	Peak 1	Peak 2
A1		Hoxd11 NTC 1		
A2		Hoxd11 NTC 2		
A3		Hoxd11 NTC 3		
B3		Hoxd11 FLt 1	87.3	
B4		Hoxd11 HLt 1	87.2	
B5		Hoxd11 FLc 1	87.3	
B6		Hoxd11 HLc 1	87.0	
B7		Hoxd11 FLt 2	87.2	
B8		Hoxd11 HLt 2	87.2	
C1		Hoxd11 FLc 2	87.3	
C2		Hoxd11 HLc 2	87.0	
C3		Hoxd11 FLt 3	87.0	
C4		Hoxd11 HLt 3	76.3	87.0
C5		Hoxd11 FLc 3	87.5	
C6		Hoxd11 HLc 3	87.0	
C7		Hoxd13 FLt 1	87.5	

Hoxd13

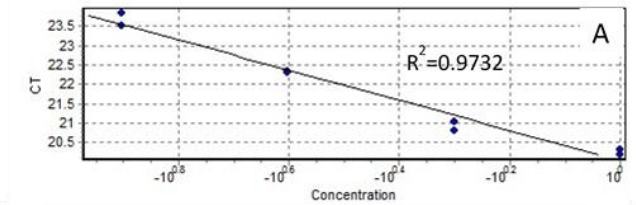

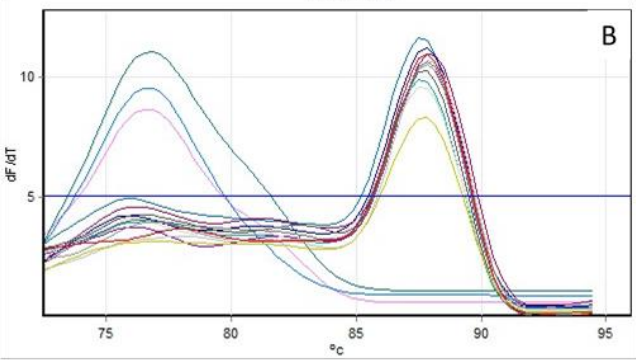

C

No.	Colour	Name	Peak 1
A5		Hoxd13 NTC 1	76.7
A6		Hoxd13 NTC 2	76.7
A7		Hoxd13 NTC 3	76.8
C7		Hoxd13 FLt 1	87.5
C8		Hoxd13 HLt 1	87.5
D1		Hoxd13 FLc 1	87.8
D2		Hoxd13 HLc 1	87.8
D3		Hoxd13 FLt 2	88.0
D4		Hoxd13 HLt 2	87.5
D5		Hoxd13 FLc 2	88.0
D6		Hoxd13 HLc 2	87.8
D7		Hoxd13 FLt 3	87.8
D8		Hoxd13 HLt 3	87.7
E1		Hoxd13 FLc 3	87.8
E2		Hoxd13 HLc 3	87.7

Supplementary Table 4.2: Quantity and purity of RNA extracted cells and tissues in this study. *The A260/A280 ratio measures the protein contamination and RNA is considered pure at a value of 2. The A260/A230 ratio measures general purity and RNA is considered pure at a ratio value of 2 (Wilfinger et al. 1997).*

	Amount (µg)	A260/A280	A260/A230
Immortalised mouse HL cells	50.01	2.05	2.28
E13.5 mouse FL tissue	6.56	2.1	2.14
E13.5 mouse HL tissue	10.57	2.12	2.18
FL bat primary cells	3.62	1.97	2.08
HL bat primary cells	2.45	1.96	2.02

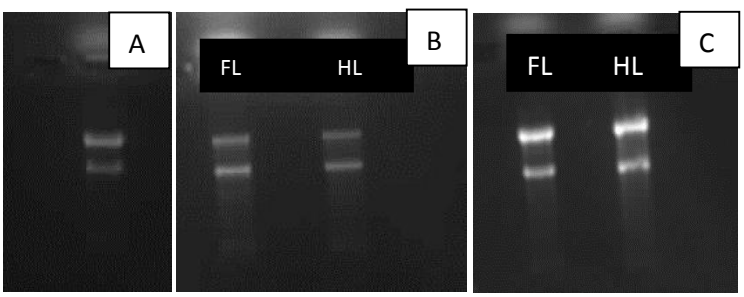

Supplementary figure 4.4: Quality of RNA extracted from bat and mouse limbs: *The RNA was extracted and 1 µg was run on a RNA gel for mouse samples while 500ng was run for bat samples. A) Immortalised embryonic mouse HL cell RNA, B) FL and HL mouse tissue RNA extracted from pooled E13.5 embryos stored in RNAlater. C) FL and HL bat primary cell RNA. The gel electrophoresis shows two distinct bands, the 28S sub unit (top band) and 18S sub unit (bottom band), which are in abundant in every cell. The quality of the RNA extraction is confirmed to be high as the two bands are distinct. Degraded RNA would form a smear rather than distinct bands.*